SKB

TECHNICAL REPORT 93-14

Simulation of the European ice sheet through the last glacial cycle and prediction of future glaciation

G S Boulton, A Payne

Department of Geology and Geophysics, Edinburgh University, Grant Institute, Edinburgh, United Kingdom

December 1992

SVENSK KÄRNBRÄNSLEHANTERING AB
SWEDISH NUCLEAR FUEL AND WASTE MANAGEMENT CO

BOX 5864 S-102 40 STOCKHOLM
TEL. 08-665 28 00 TELEX 13108 SKB
TELEFAX 08-661 57 19

SIMULATION OF THE EUROPEAN ICE SHEET THROUGH THE LAST GLACIAL CYCLE AND PREDICTION OF FUTURE GLACIATION

G S Boulton, A Payne

Department of Geology and Geophysics, Edinburgh University, Grant Institute, Edinburgh, United Kingdom

December 1992

SIMULATION OF THE EUROPEAN ICE SHEET THROUGH THE LAST GLACIAL CYCLE AND PREDICTION OF FUTURE GLACIATION

By

G.S.Boulton and A.Payne

Department of Geology and Geophysics
Edinburgh University
Grant Institute
Kings Buildings
Edinburgh EH9 3JW

1992

Keywords: Glaciation, future glaciations, climate change, Milankovitch, Weichselian, ice-sheet, modelling, permafrost, glacial geology

CONTENTS

ABSTRACT (ENGLISH)

Global climates of the recent past appear to correlate with patterns of variation in the earths orbit round the sun. As such orbital changes can be predicted into the future, it is argued that the pattern of natural long-term future change can also be estimated. From this, future trends of glaciation can be inferred.

The physical and mathematical basis of a time-dependent, thermo-mechanically coupled, three dimensional ice sheet model is described. The model is driven by changes in the equilibrium line altitude (ELA) on its surface. This causes flexure of the underlying lithosphere.The model is tuned to the maximum extension of the last (Weichselian) ice sheet and driven by an ELA fluctuation which reflects the NE Atlantic sea surface temperature fluctuation pattern during the last glacial cycle in such a way that the model reproduces the ice sheet margin at the glacial maximum. The distribution of internal ice sheet velocity, temperature, basal melting rate and subglacial permafrost penetration are all computed.

The model is then tested against its predictions of the areal pattern of ice sheet expansion and decay, the pattern of crustal flexure and relative sea level change, and the distribution of till produced by the last European ice sheet.

The tested model is then driven by predictions of future climate change to produce simulations of future ice sheet glaciation in northern Europe.

ABSTRACT (SWEDISH)

Studier av storskaliga klimatvariationer, som glaciationer med mellanliggande värmeperioder, visar att det finns ett samband mellan dessa och variationer i jordens läge i förhållande till solen. Eftersom man kan beräkna framtida variationer av jordens bana kan man därför även dra slutsatser om framtida klimatvariationer förutsatt att man vet hur sambandet fungerar.

Denna rapport beskriver ovannämnda samband med hjälp av en tidsberoende, termomekaniskt kopplad 3D modell av en inlandsis. Drivande i modellen är variationer i jämviktslinjen (eng. ELA=equilibrium line altitude) som i sin tur medför nedtryckning av underliggande lithosfär. Modellen har avstämts mot den senaste inlandsisen (Weichsel) dels genom att variera jämviktslinjen enligt de variationer i havsytans temperatur som har bestämts från nordöstra Atlanten för denna tidsperiod, dels genom att avstämma modellen mot inlandsisens maximala utsträckning. Utifrån dessa förutsättningar, samt kända termiska egenskaper hos den Skandinaviska berggrunden, beräknar modellen inlandsisens tjocklek och rörelsemönster, variationer i luft och is temperatur, produktion av smältvatten vid isbotten och permafrostens mäktighet under och utanför istäcket.

Modellens resultat har därefter testas mot kända uppgifter om hur den senaste inlandsisen växte till och avsmälte, hur berggrunden nedtrycktes, hur stora de relativa havsnivåförändringar var och hur moränen har fördelat sig.

Den testade modellen har därefter använts för att simulera framtida glaciationer.

SUMMARY

The patterns of past global climate change have been shown to correlate with variations in the intensity of solar radiation reaching the earth as a consequence of variations in the earth's orbit around the sun. It is therefore concluded that these orbital variations are the pace-makers of climatic change on earth. Moreover orbital variations can be reconstructed in the past and predicted into the future as they depend only on the gravitational relationships between the planets, which are predictable using Newtonian mechanics. As a consequence, the correlations between orbital variations and global change can be used to predict the pattern of future "natural" global change. In evaluating the consequences of global change for a particular waste repository, we need to know the local component of global change. To do this, we investigate the correlation between records of past global change and past local records in order to be able to predict local changes from the prediction of future global changes.

Ice sheets are made up of the simplest material, ice, which covers a large part of the Earth's surface. The ice sheets of Greenland and Antarctica at the present day have predictable surface profiles, internal thermal regimes and patterns of flow which reflect the relatively simple and predictable flow properties of the ice which makes it up. We therefore suppose that the European and North American ice sheets of the recent past can be reconstructed using understanding of the same physical laws and theories. A mathematical model of ice sheet behaviour has therefore been developed. It is driven by changes in the elevation of the permanent snowline on its surface and by air temperature. The ice sheet acts as a conveyor belt to transport ice which accumulates at a high elevation on its surface to a low elevation, where it melts. The rate at which this occurs depends on the flow properties of ice, which are known. It also depends on the temperature of the ice. Flow of the ice also transports cold ice from a high elevation to a low elevation, and therefore changes the distribution of internal temperature. An ice

sheet is thus a coupled thermo-mechanical system, and the numerical model developed below describes and predicts its behaviour when driven by given atmospheric conditions (temperature and equilibrium line altitude (ELA)), and for an earth's surface of given form and given mechanical properties which determine how the surface will flex when an ice sheet grows and decays on it.

The last glacial period lasted from about 120,000 years ago to about 10,000 years ago, during which a large ice sheet grew and decayed over Europe. The history of ice sheet fluctuation during this last glacial cycle is more or less well known. Ice sheet fluctuations were driven by climate fluctuations for which we believe the reconstructions of sea-surface temperature (SST) in the N.E. Atlantic, derived from studies of the geology of ocean cores, is the best proxy record. The trend through time of sea surface temperature in this region is likely to reflect both the temperature and precipitation trends in N.W. Europe, which in turn drove past ice sheet fluctuation. We therefore derive an ELA function for the last glacial cycle which bears a simple mathematical relationship to trends of N.E. Atlantic SST and thus sea surface air temperature (SLAT) which drives the ice sheet model so that it produces a pattern of ice sheet fluctuation which agrees with the geological evidence of fluctuation.

The relationship is established between the N.E. Atlantic sea level air temperature (SLAT) record and the equilibrium line altitude (ELA) required to drive the ice sheet in the way that geological evidence suggests it varied through the last glacial cycle.

The ice sheet model is driven by the ELA function established for the last glacial cycle. The model reconstructs ice sheet thickness, ice sheet temperature distribution, including basal temperature, basal melting pattern and velocity distribution. Some tests were undertaken to establish the sensitivity of the basal temperature/melting distribution, and the distribution of permafrost below and beyond the ice sheet to variations in the assumptions used about surface

temperature. It was found that the reconstruction was relatively insensitive to these assumptions, and that a robust prediction of the model is of a very broad zone of basal melting between a narrow terminal frozen zone and a few 10s of kilometres in width, and a zone freezing beneath the ice divide.

The ice sheet model has been "tuned" so that it reproduces the pattern of fluctuation of the ice sheet during the last glacial cycle in Europe. It was tested against the precise areal pattern of expansion and decay of the ice sheet; the pattern of erosion and deposition generated by the ice sheet in the southern Baltic and adjacent areas of Poland/Germany; the pattern of lithosphere flexure, and therefore of post-glacial relative sea-level change.

Calculations of future Milankovitch-variations are used to calculate future climate, including future N.E. Atlantic SSTs. These are then used to compute future ELA variations and future ice sheet variations, including basal temperatures, melting rates, etc. The probability of sites at different distances from the initial ice divide being glaciated at given future times is estimated. We believe that within the limitations of present knowledge, the ice sheet model is able to satisfactorily simulate the behaviour of the last ice sheet in Europe. Provided therefore that we are able to generate a climate forcing function for the future, we should be able to predict future ice sheet behaviour.

..... ***** .....

1 SIMULATION OF FUTURE GLACIATION AND ITS EFFECTS.

The patterns of past global climate change have been shown to correlate with variations in the intensity of solar radiation reaching the earth as a consequence of variations in the earth's orbit around the sun. It is therefore concluded that these orbital variations are the pace-makers of climatic change on earth. Moreover orbital variations can be reconstructed in the past and predicted into the future as they depend only on the gravitational relationships between the planets, which are predictable using Newtonian mechanics. As a consequence, the correlations between orbital variations and global change can be used to predict the pattern of future "natural" global change. In evaluating the consequences of global change for a particular waste repository, we need to know the local component of global change. To do this, we investigate the correlation between records of past global change and past local records in order to be able to predict local changes from the prediction of future global changes.

..... ***** .....

The purpose of this report is to establish and apply a methodology to predict the course of climate over the next 100, 000 years in Sweden. Our evidence of the climate of the last million years suggests, by extrapolation, that this would normally be dominated by a cold, glacial and permafrost climate, very different from that of the present day. It is therefore important to concentrate on those processes in a glacial environment which are most likely to influence the integrity of an underground waste repository and dispersal from it. The processes most likely to be of importance are loading by glaciers, freezing by permafrost, and meltwater flow beneath both glaciers and permafrost.

Scientific theories are at their best when they make precise predictions about real phenomena, which are unlikely to arise by chance and which can be unambiguously tested against that reality. Developing a theory which attempts to predict the distant future seems therefore to offer little prospect of generating a satisfactory test. We believe, however, that a way in which theories that attempt to predict the distant future can be tested, and possibly the only way, is against the geological record of the past. We must reverse the sense of Hutton's famous dictum that "the present is the key to the past", and argue that the past is the key to the future. Hutton's axiom first assumed however that explanation of the past should firstly be based upon understanding of present processes. We must make a similar proviso, that the processes which we consider are "natural processes", in the sense that we assume that the human race will not make a major intervention in the operation of the natural system so as to steer its course. This may of course now be happening through an enhanced greenhouse effect brought on by burning of fossil fuel since the industrial revolution. Nonetheless, though it may soon be possible to include such human intervention in a theory such as that presented here, we shall certainly not be able to devlop a methodology for a human-influenced future if we cannot first develop one for a "natural" future.

Over the last 3/4 million years, the earth has been known to undergo a repetitive tempo of climatic change (Imbrie et al, 1984) characterised by the growth and decay of large ice sheets associated with major changes in all parts of the earth's surface environment (figure 1.1). The dominant frequencies of change, are at 100ka, 40ka and 20ka. These correlate well with changes in the intensity of solar radiation received by the earth over the same period (Hays et al, 1976) as a consequence of changes in the earth's orbit around the sun which can be calculated by Newtonian mechanics (Milankovitch, 1941; Berger, 1978). These orbital changes are regarded therefore as the "pacemakers" of the Late Cenozoic ice age (Hays et al, 1976). As the orbital changes can be predicted into the future we can thus use the correlation between past insolation simulations and past global changes to infer future global changes from calculations of future insolation (Berger, et al, 1981; Kukla et al, 1981).

However we seek to predict something much more specific than future global change. We are interested in future glaciation in Europe, and more precisely an

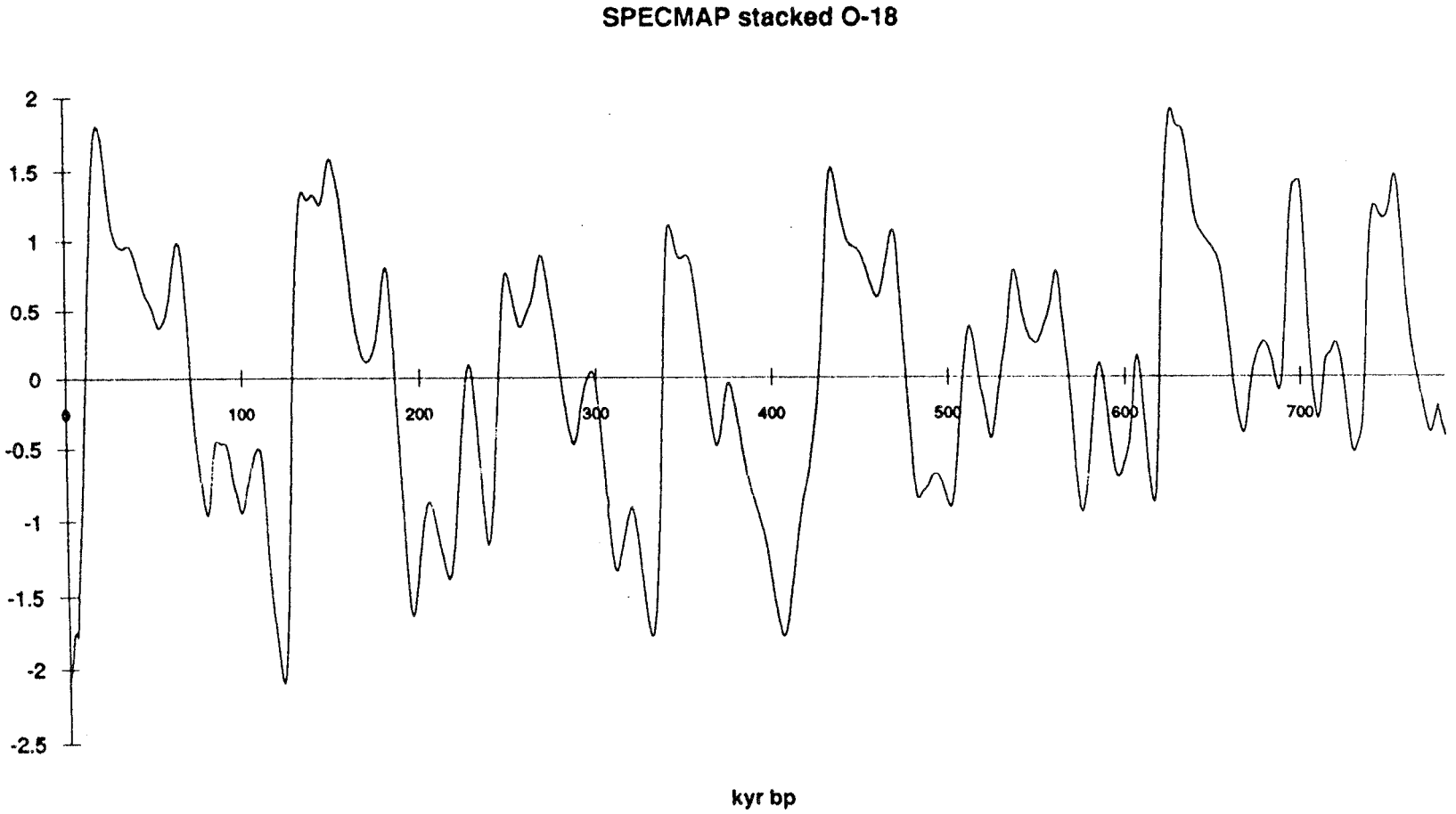

Figure 1.1 Generalised palaeoclimate curve for the last 0.75million years produced by the SPECMAP group (Imbrie et al,1984).

estimation of subglacial conditions such as zones of freezing, zones of melting, the rate of melting and the depth and extent of permafrost beyond any future glaciers.

Figure 1.2 shows an estimation of the mean oxygen isotope composition of the oceans since the last interglacial period (Labeyrie, et al, 1987). This change is believed to be a direct reflection of ice sheet volume changes and therefore of changes in ocean level. However this primarily reflects growth and decay of an ice sheet in North America which had a volume of about 30 million cu km at its maximum extent, whereas the Scandinavian ice sheet only had a volume of about 7 million cu km (Denton & Hughes, 1981). We cannot unfortunately assume that the European ice sheet showed a volumetric fluctuation that was simply proportional to the changes shown in Figure 1.2, as the European ice sheet was less thermally stable than the North American ice sheet and developed later and decayed earlier. There are now proxy climatic records from the NW European area which show the regional pattern of climate fluctuation through the last glacial cycle (Guiot, et al., 1989, figure 1.3; Labeyrie, pers. comm. figure 1.4). If we are able to correlate these regional patterns of climate change through the last cycle either with the global (SPECMAP) curve and thence with Milankovitch fluctuations or directly with fluctuations, we can use calculations of future Milankovitch insolation changes to produce a prediction of local European climate. Moreover, there is now increasing stratigraphic evidence of the pattern of ice sheet fluctuation in Europe during the last glacial cycle (Mangerud, 1991; Lundqvist, 1986). We believe that the best index of the climate which drove these fluctuations is given by the sea surface temperatures calculated for the north-east Atlantic from down-core microfaunal assemblages (Labeyrie, pers. comm.). Temperatures at the sea surface in the north-east Atlantic are likely to give a good index of both temperature and precipitation trends which determined mass balance over the north-west European ice sheet. We then assume that the north-east Atlantic sea surface temperatures (SSTs) give the trend of equilibrium line altitude (ELA) changes over the ice sheet and use a model of an ice sheet to establish a correlation between sea surface temperature and ELA which will cause the ice sheet to behave as stratigraphic evidence suggest it did through the last glacial cycle. This correlation function is then used to derive a future ELA change from a prediction of future sea surface temperatures and the future ELA change is used to drive the future ice sheet.

The structure of this procedure is illustrated in figure 1.5. It involves four steps:

- Calculation of a correlation function between Milankovitch and N.E. Atlantic SSTs.

- Calculation of the transfer function needed between N.E. Atlantic SSTs and equilibrium line altitude (ELA) which permits the ice sheet model to produce a simulation of ice sheet fluctuation which matches the geological evidence of fluctuation.

- Computation of future N.E. Atlantic SSTs from a computed future Milankovitch insolation change and the correlation function between past Milankovitch changes and past SSTs.

- Computation of future ice sheet behaviour from the computed future SSTs and the correlation function between past SSTs and snowline elevation.

The model, whether in past or future mode, also computes temperatures within the ice and in the underlying lithosphere and in the lithosphere beyond the ice sheet margin, thus enabling the extent of subglacial and proglacial permafrost to be estimated (figure 1.6). It gives the history of ice loading and the rate of basal melting. All these are important criteria in the evaluation of repository sites.

The model must also be tested. This is done (figure 1.6) in this interim model by using output from the model as input into a sub-routine which computes the thickness distribution of till resulting from the glacial cycle, and one which computes the flexural response of the lithosphere to loading, and therefore the pattern of relative sea level at any site after deglaciation. These predictions for the last glacial cycle are compared with the actual till thickness distribution and the relative sea level record. In subsequent elaboration of the model, further geological constraints and tests will be used (figure 1.6).

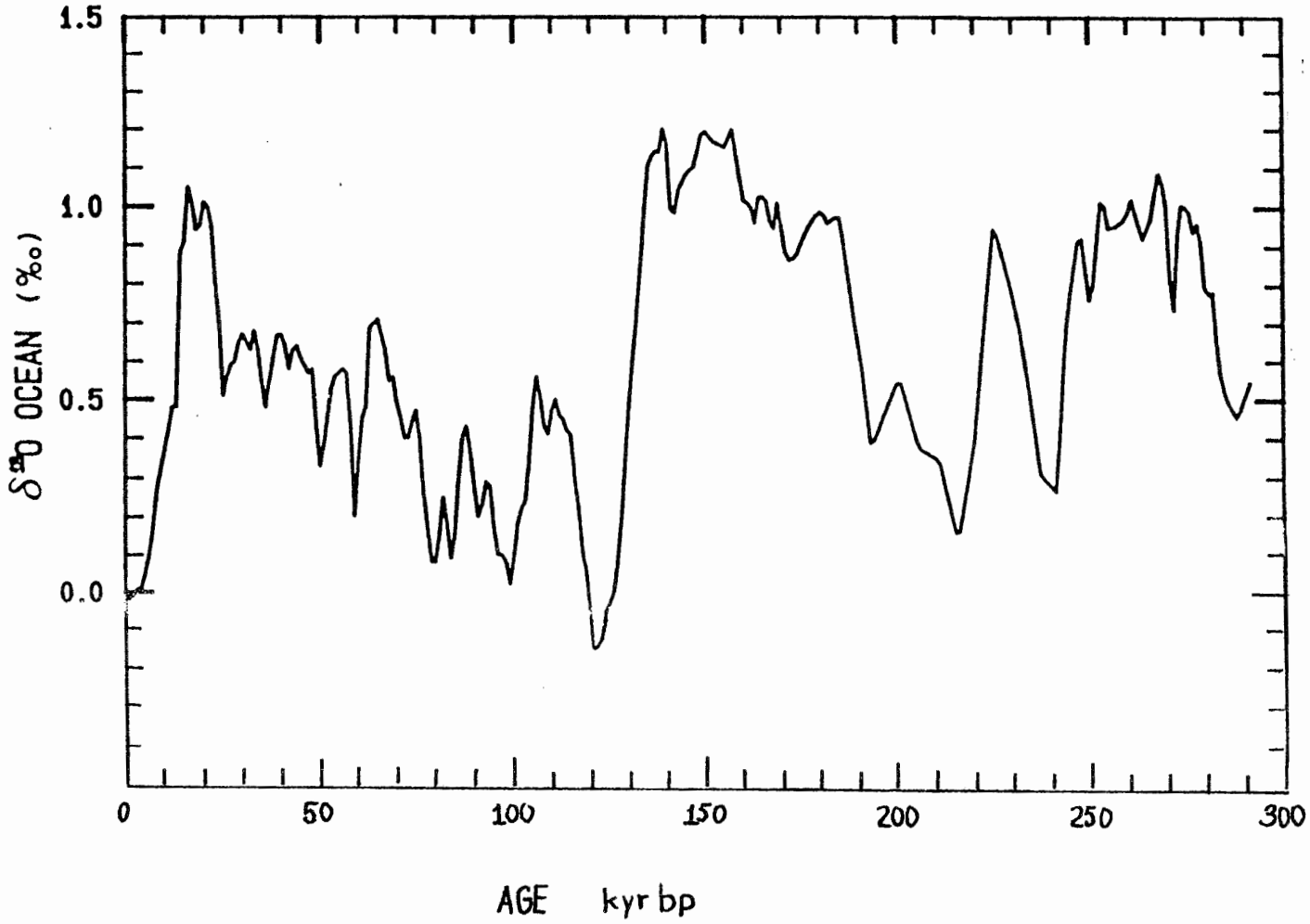

Figure 1.2 Mean isotopic composition of the oceans through the last two glacial cycles (Labeyrie et al., 1987; Martinson et al., 1987) This is largely an an index of global ice volume change.

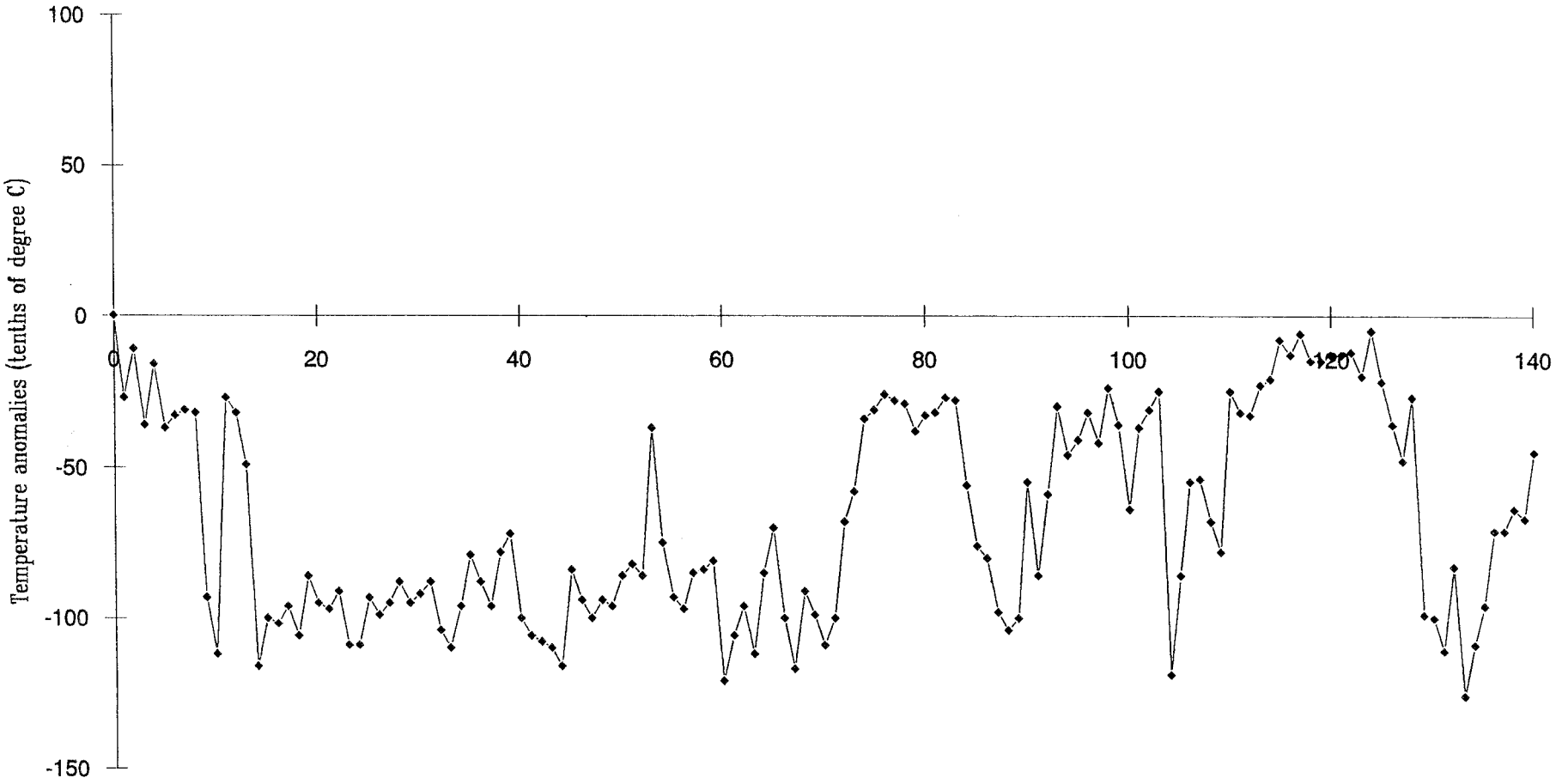

Figure 1.3 Mean annual temperature at Les Echets (France) through the last glacial cycle. The horizontal scale is in thousands of years before present. (Personal communication from J. Guiot).

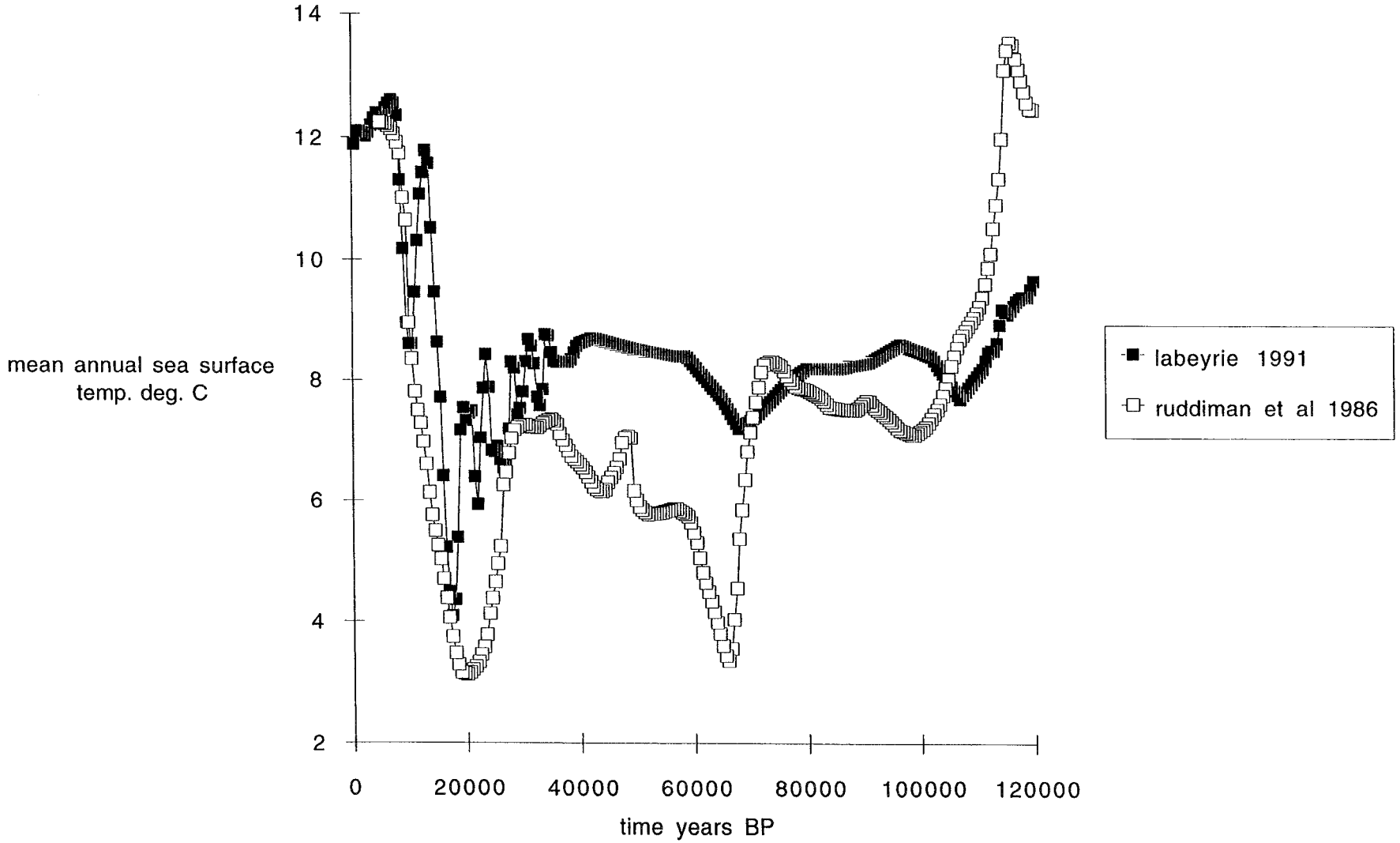

Figure 1.4 Mean annual sea surface temperatures (SSTs) from the NE Atlantic during the last Glacial cycle.

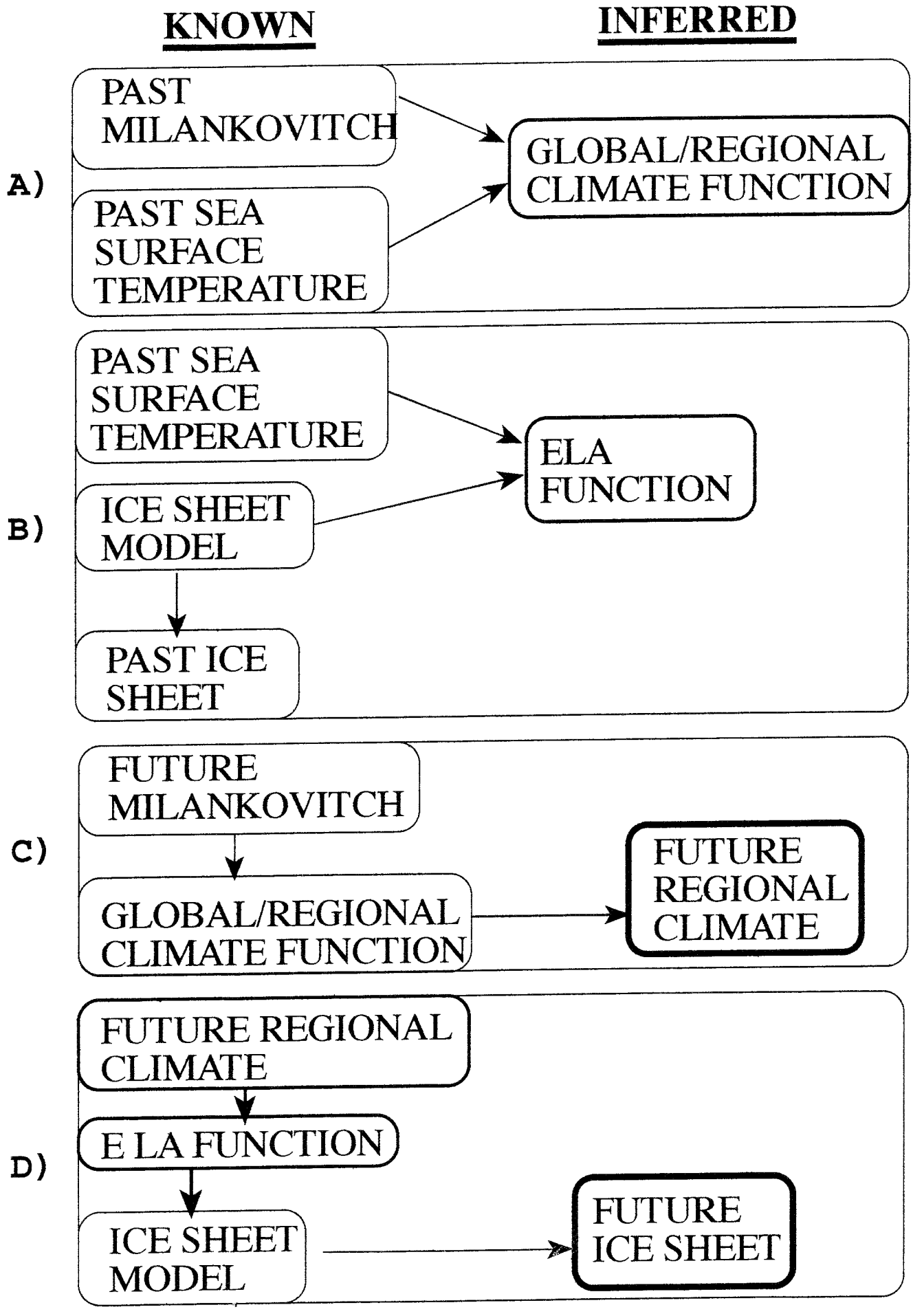

Figure 1.5 Structure of the modelling exercise.

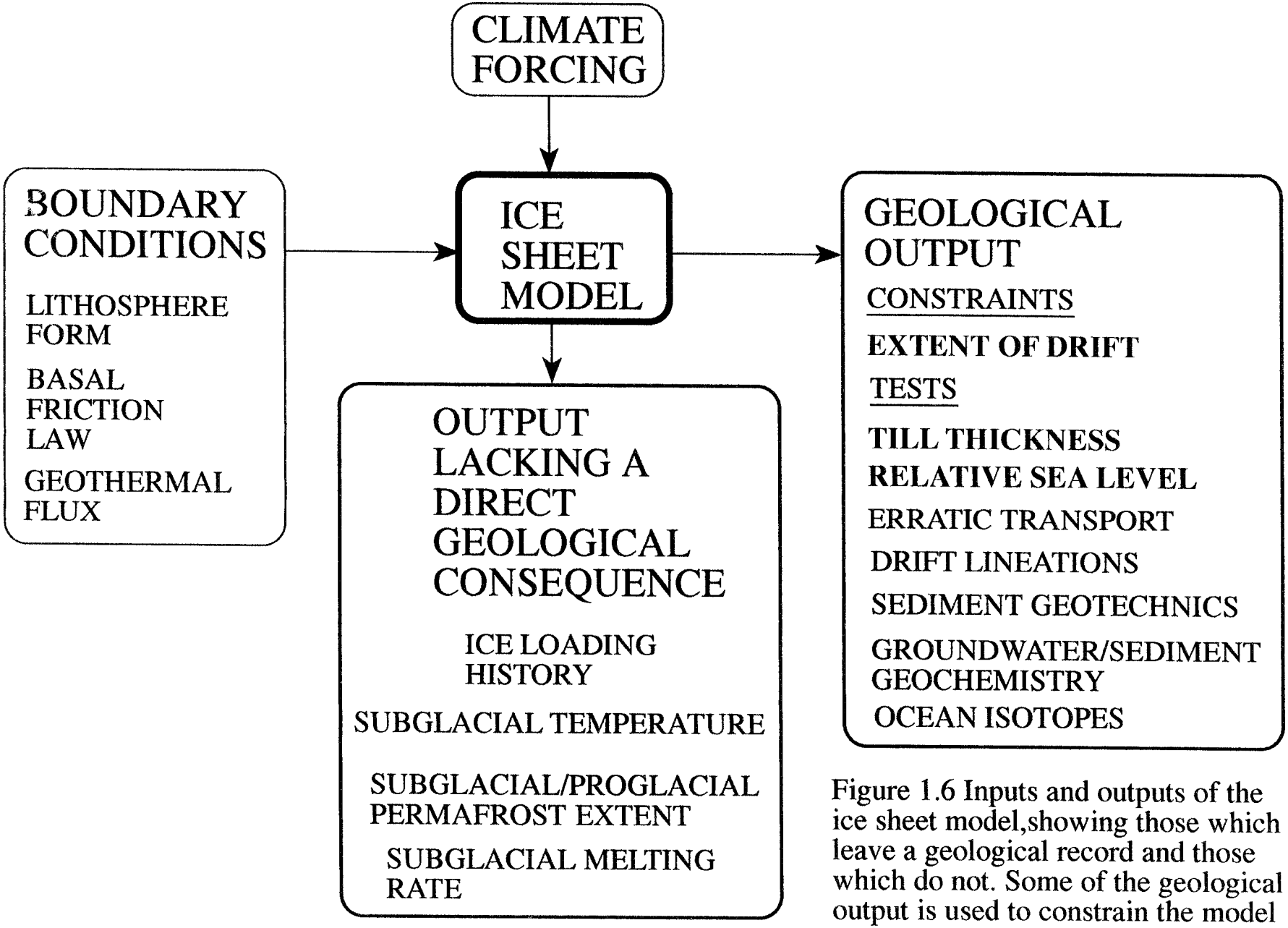

Figure 1.6 Inputs and outputs of the ice sheet model,showing those which leave a geological record and those which do not. Some of the geological output is used to constrain the model and some used to test it.

2 THE ICE SHEET MODEL.

Ice sheets are made up of the simplest material, ice, which covers a large part of the Earth's surface. The ice sheets of Greenland and Antarctica at the present day have predictable surface profiles, internal thermal regimes and patterns of flow which reflect the relatively simple and predictable flow properties of the ice which makes it up. We therefore suppose that the European and North American ice sheets of the recent past can be reconstructed using understanding of the same physical laws and theories. A mathematical model of ice sheet behaviour has therefore been developed. It is driven by changes in the elevation of the permanent snowline on its surface and by air temperature. The ice sheet acts as a conveyor belt to transport ice which accumulates at a high elevation on its surface to a low elevation, where it melts. The rate at which this occurs depends on the flow properties of ice, which are known. It also depends on the temperature of the ice. Flow of the ice also transports cold ice from a high elevation to a low elevation, and therefore changes the distribution of internal temperature. An ice sheet is thus a coupled thermo-mechanical system, and the numerical model developed below describes and predicts its behaviour when driven by given atmospheric conditions (temperature and equilibrum line altitude (ELA)), and for an earth's surface of given form and given mechanical properties which determine how the surface will flex when an ice sheet grows and decays on it.

..... ***** .....

2.1 SUMMARY OF ICE SHEET MODEL.

This chapter outlines the development of the ice sheet model used in the study. The model considers a 1620 km flowline running from southern Norway to central

Poland, and can follow the evolution of ice sheet form, velocity and temperature through time along this flowline.

The two dimensional distributions of ice velocity and temperature within the ice sheet are explicitly modelled. The former is calculated assuming that ice flow is by deformation only and that shear stresses dominate the ice sheet's stress field. The distribution of temperature within the ice sheet evolves as the result of advection, diffusion and heating by deformation. The ice sheet's velocity and temperature fields interact through the dependence of strain rate on temperature. When ice reaches its pressure melting point the excess heat energy is used to calculate a basal melt rate. The evolution of temperature within the bedrock underlying the ice sheet can also be modelled. This evolution is coupled to that of temperature within the ice sheet via the geothermal heat flux at the ice/bedrock interface. This part of the model can also be used to follow the evolution of permafrost depth. The underlying bedrock also interacts with the ice sheet via isostasy. The effect of ice loading on bedrock depression is modelled using a diffusion equation.

The model is driven by variations in the equilibrium line altitude (ELA) and the sea level air temperature (SLAT). Mass balance (the difference between snow accumulation and ice ablation rates) is specified as a function of the difference between ELA and ice sheet surface elevation, while air temperature is calculated using a constant lapse rate.

The sea level air temperature (SLAT) is required as a means of determining the mean annual temperature on the ice sheet surface which determines the temperature of the snow accumulating on the ice sheet, which in turn is used to determine the temperature distribution within the ice sheet. SLAT is the temperature of the air, and is not the same as sea-surface temperature (SST) which is the temperature of the water. It will fluctuate with a pattern similar to SST, but will have a different magnitude. Equation 4.2 gives the relationship between SST and SLAT. From the SLAT, ice sheet surface temperature is calculated by using an appropriate lapse rate (vertical temperature gradient) over an ice sheet surface.

The equations comprising the model are solved using various finite difference techniques. The horizontal grid spacing of the model is 20 km and the time step is 5 years.

This chapter is divided into three sections. The first details the physics used in the model and gives the basic equations on which it is based. The second gives the various boundary conditions needed to complete the model. The final section gives details of the numerical techniques used to solve the model's equations.

2.2 THE PHYSICAL BASIS OF THE ICE SHEET MODEL.

This discussion will be divided into five sections, each dealing with a separate component of the model. These sections are:

- ice sheet form;
- internal velocity field of the ice sheet;
- internal temperature field of the ice sheet;
- temperature field in the underlying bedrock;
- isostatic response of the underlying bedrock.

The overall behaviour of the model is controlled by the interactions between these components (Figure 2.1). The following sections outline the physics incorporated in each component of the model, give the basic equations used and indicate their limitations. The geometry used in the model is shown in Figure 2.2 and a summary of the symbols is supplied in Table 2.1. (see appendix)

2.2.1 Ice sheet form.

The complex three dimensional form of an ice sheet is best described by the distribution of ice thickness (H) over the horizontal extent of the ice sheet. It is a function of time (H(x, t)) because the form of the ice sheet may change through time.

The modelling problem is to estimate this function H(x,t) (where t is time, x the horizontal coordinate) and this is done using the continuity equation of ice thickness (Mahaffy 1976):

$$\frac{\partial H}{\partial t} = -\frac{\partial}{\partial x}(\bar{u}\,H) + b \qquad (2.1)$$

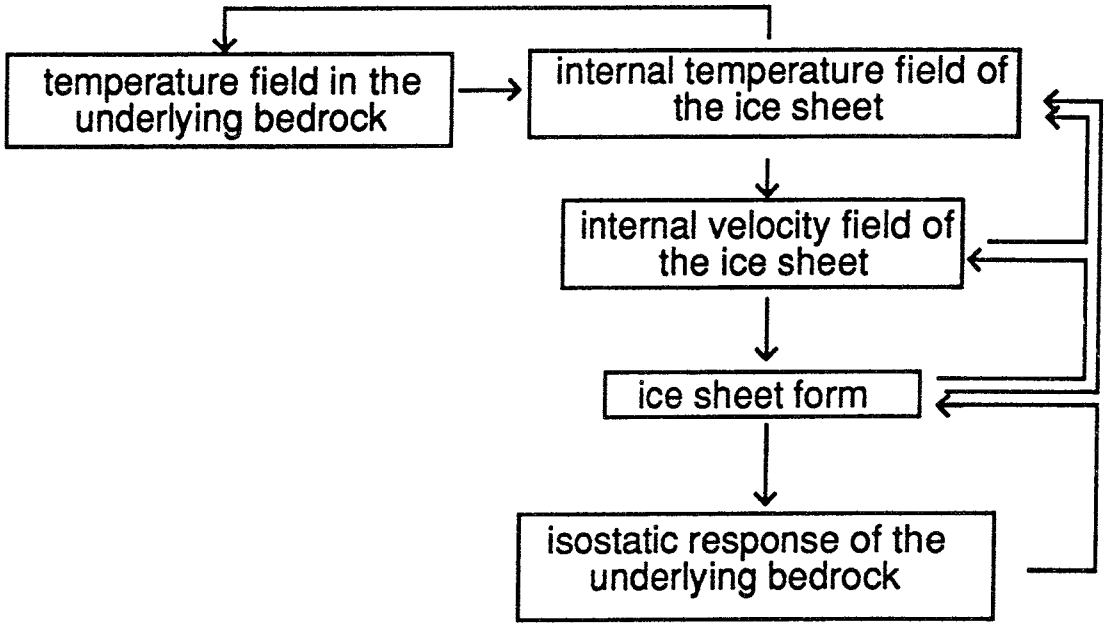

Figure 2.1 The interaction between various components of the ice sheet system.

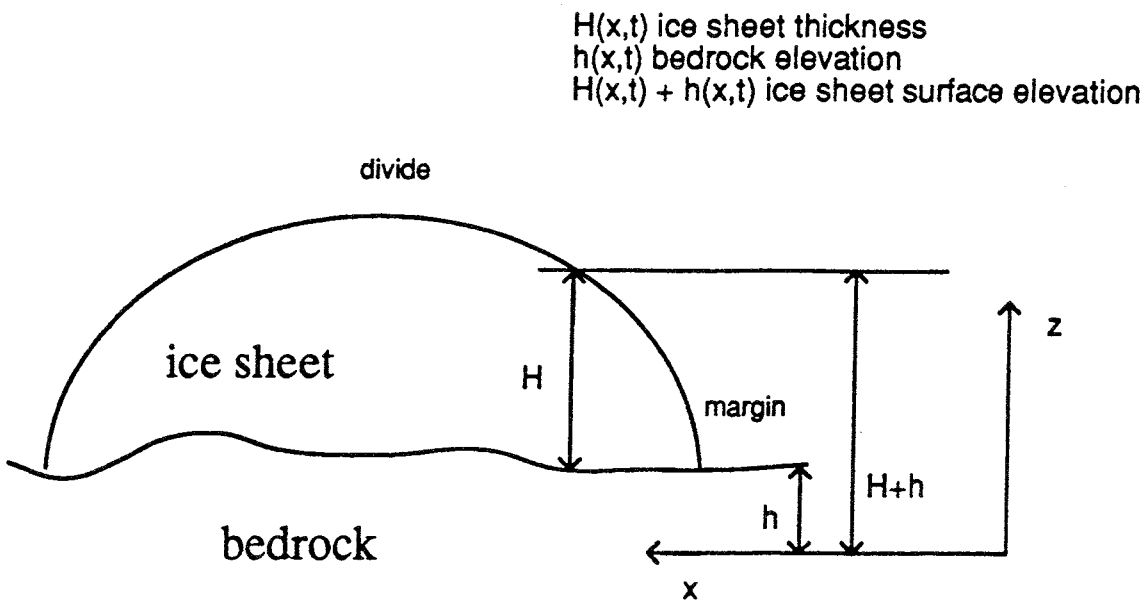

Figure 2.2 The geometry used in the model.

The rate of ice thickness change at any point is a function of the local mass balance (b(x,t)) and the local convergence/divergence of horizontal flow within the ice sheet. This latter term is found from the horizontal variation of ice discharge, itself the product of local ice thickness and vertically-averaged horizontal ice velocity ($\bar{u}(x,t)$).

The time evolution of form is found by integrating equation (2.1) forward through time at each point in the model domain. In order to do this both mass balance and vertically-averaged horizontal ice velocity need to be known at each point. The next section discusses the theory used to obtain $\bar{u}$, while the estimation of b is given in (2.3.1).

It is important to note the contrast between the two terms. The convergence/divergence term merely acts to redistribute ice within the ice sheet, allowing horizontal expansion (but not contraction) and vertical thickening or thinning by flow alone. In contrast, the mass balance term adds ice to or takes ice away from the ice sheet system. Changes in overall volume can only, therefore, arise through changes in mass balance.

2.2.2 Internal velocity field of the ice sheet.

The problem of finding the velocity of ice within an ice sheet is amenable to the techniques of continuum mechanics (for instance Turcotte and Schubert 1982). This section outlines the basic assumptions used in a general theory of ice flow. Details of the derivation are available in Lliboutry (1987) and Paterson (1981). It involves two stages. The first is the estimation of the stress field within the ice mass and the second is the relation of this stress field to a strain rate (and hence to a velocity field).

Ice flow is typically very slow and seldom reaches velocities greater than 1000 m $year^{-1}$ in ice sheets. The accelerations involved are therefore insignificant. This implies that the forces within an ice mass must be in balance, both locally and over the ice mass as a whole. In particular, the weight of overlying ice must be balanced by stresses within the ice mass.

The stress field within an ice mass of known geometry may be calculated using this and two other simplifying assumptions (Nye 1959):

- horizontal stress gradients are insignificant; and
- the pressure distribution within an ice mass is everywhere hydrostatic.

The first of these assumptions stems from the aspect ratio of ice sheets: horizontal extent is typically 100 to 1000 times greater than vertical extent (thickness). It is supported theoretically by Budd (1970) and Budd and Jenssen (1975) but may not be true near the margin, where large horizontal stress gradients exist. The other assumption states that the only significant longitudinal (horizontal) stress component is that associated with the weight of overlying ice. It may not be true at ice divides, where significant longitudinal stresses exist.

Using these assumptions one can say that ice flows in simple shear and that the only significant stress within the ice mass is the horizontal shear stress (τ_{xz}, where z is the vertical coordinate). Its magnitude is:

$$\tau_{xz} = -\rho_i g (H + h - z) \frac{\partial}{\partial x}(H + h) \qquad (2.2)$$

where h is bedrock elevation, g is the acceleration due to gravity and ρ_i is the density of ice. Its direction is parallel to ice sheet surface slope.

The second stage in the derivation is to relate this stress field to deformation within the ice mass. The key to this is Glen's flow law for ice (Glen 1955). This is an emperical relationship which gives ice deformation (strain rate) as a cubic function of stress. The proportionality factor within this law varies by several orders of magnitude, and depends on factors such as ice temperature and impurity content.

Given the simplified stress environment described above and the assumption that horizontal rates of change are insignificant compared to vertical ones, then an expression for horizontal velocity (u(x,z,t)) anywhere within the ice mass can be found:

$$u = -2(\rho_i g)^n \left|\frac{\partial(H+h)}{\partial x}\right|^{n-1} \left(\frac{\partial(H+h)}{\partial x}\right) \int_h^z A(T)\,(H+h-z)^n dz + u_h \qquad (2.3)$$

where n is a power (usually 3) used in Glen's flow law, A is the proportionality factor in Glen's flow law, T is ice temperature and u_h is velocity at the ice/bedrock interface (here assumed to be zero as explained below).

The proportionality factor (A) is determined from ice temperature corrected for variation in the pressure melting point (T^*). An Arrhenius equation is used (Paterson and Budd 1982):

$$A = a\exp\left\{\frac{-Q}{RT^*}\right\} \qquad (2.4)$$

where Q is the activation energy for ice creep, R is the gas constant and a is a multiplier.

In this analysis horizontal velocity is determined by ice thickness (H(x)) and ice sheet surface slope, which are both dependent on the local form of the ice sheet. There is therefore the potential for feedback to develop in the evolution of ice sheet form, because changes in form depend on the internal velocity distribution and vice versa. Expression (2.3) can be vertically integrated to provide the $\bar{u}$ required in the ice sheet form evolution equation (2.1).

Horizontal velocity also depends on ice temperature through the proportionality factor in Glen's flow law ($A(T^*)$). The ice sheet's internal temperature field must therefore be included in the model in order to allow A to be calculated. This will be discussed in the next section.

The above analysis only considers ice flow via deformation. Ice flow can also occur via the differential movement of an ice sheet over its bed, either through some form of sliding over a rigid bed (Weertman, 1979) or through the deformation of the underlying sediment (Boulton and Jones 1979). At present neither process is incorporated in the model because a generally applicable, quantitative theory (of the type used to model internal deformation) is not yet available. The consequences of this omission may not be too serious for two reasons. First, the potential for

enhanced basal flow only exists where melt water is present at the ice/bed interface (Boulton and Hindmarsh 1987, Bindschadler 1983) and this may be limited to the outer margin of the ice sheet (Sugden 1977). Second, the coupling between ice sheet form and internal velocity mentioned above implies that the omission of enhanced basal flow will be compensated by an increase in ice flow via internal deformation. However, the omission of a mechanism for enhanced basal flow is a major shortcoming in the present model because these mechanisms undoubtedly increase the potential for rapid change in real ice sheets. It is aimed to include basal deformation in future versions of the model.

At present the analysis of internal ice velocity covers only the horizontal component. However, the vertical component may also be important because it plays a part in the advection of temperature changes through an ice sheet (see the next section). Vertical velocity (w(x,z,t)) can be found from the calculated horizontal velocity field by invoking the conservation of mass:

$$w = -\int_{h}^{z} \frac{\partial u}{\partial x} dz + w_h \qquad (2.5)$$

w(x,z,t) can be found by integrating this equation from the bed to the ice sheet surface. This requires an estimate of vertical velocity at the bed ($w_h(x,t)$), which in the absence sliding is:

$$w_h = \frac{\partial h}{\partial t} - S \qquad (2.6)$$

where S is basal melt rate, the calculation of which is outlined in the next section.

2.2.3 Internal temperature field of the ice sheet.

A knowledge of the changing internal temperature field of the ice sheet is required because of the dependence of ice flow on temperature (equation 2.4). The basis for the temperature model is the conservation of energy:

$$\frac{\partial T}{\partial t} = \frac{k_i}{\rho_i c_i} \frac{\partial^2 T}{\partial z^2} - u\frac{\partial T}{\partial x} - w\frac{\partial T}{\partial z} + \frac{g}{c_i}(H+h-z)\frac{\partial u}{\partial z}\frac{\partial}{\partial x}(H+h) \qquad (2.7)$$

where c_i is the specific heat capacity of ice and k_i is the thermal conductivity of ice. Put simply this equation states that changes of ice temperature at a point can be brought about by:

- vertical diffusion (conduction) through the ice mass; horizontal diffusion is ignored because the temperature gradients involved are several orders of magnitude smaller than the vertical temperature gradient;

- advection in both the horizontal and the vertical; this is why w(x,z,t) had to be calculated in the previous section; and

- the strain heating produced by differential deformation rates within the ice mass.

The first two terms act to redistribute temperature within the ice sheet. Advection is important because it brings colder, near-surface ice down into the body of the ice sheet, thereby cooling the ice mass as a whole. The third term represents a source of heat within the ice mass. This term leads to a feedback between ice flow and temperature. Faster flowing ice is deforming more than slower flowing ice, and so produces greater amounts of heat via strain. This tends to warm faster flowing ice relative to slower flowing ice. The dependence of ice deformation on ice temperature means that this warmer ice may then flow still faster, allowing a positive feedback to develop (Clarke and others 1977). This feedback is countered by the fact that the faster flowing ice increases the rate of cold ice advection, which opposes the warming inherent in strain heating (Huybrechts and Oerlemans 1988).

A second source of stability within the temperature model is the production of melt water. The melting point of ice is affected by the pressure acting on the ice:

$$\dot{T} = -\phi\,\rho_i g(H+h-z) \qquad (2.8)$$

where ϕ is a constant.

When ice temperature exceeds this pressure melting point then melting can occur. The amount of melting is dependent on the excess heat available (Budd and others 1971):

$$S = \frac{k_i}{L\rho_i}\left(\frac{\partial T}{\partial z}_c - \frac{\partial T}{\partial z}_b\right) \qquad (2.9)$$

where the subscripts c and b refer to the temperature gradient after and before the correction for pressure melting has been made, and L is the latent heat capacity of ice. This equation converts the excess heat available into a depth of melt water.

In order to integrate equation (2.7) forward through time two boundary conditions are needed. These reflect the conditions at the ice sheet surface and at the ice/bed interface. The former depends on mean annual temperatures and will be discussed in section (2.3.2). The latter is more complex and is treated in two distinctly different ways in this report. An introduction to the role of ice/bed boundary condition is given here and further modelling details supplied in the next section. The boundary condition relies on the flow of heat from bedrock to ice (or vice versa). This is referred to as the geothermal heat flux. Results will be presented for the case of a constant geothermal heat flux and for the case where the temperature evolution in the bedrock is allowed to interact with that of the ice sheet. In the second case geothermal heat flux is not a constant.

In general the warmest ice within an ice sheet occurs near the bed at a position closer to the margin than to the divide. This location is favoured because:

- cold ice advection is at a minimum;

- strain rates are largest near the bed and towards the margin, so strain heating is largest here; and

- the geothermal heat flux supplies an extra source of heat.

Warmer ice is more likely to reach pressure melting point and melting is therefore concentrated at the ice/bed interface. The first two factors in the above list have already been discussed. The geothermal heat flux (G) can be evaluated as:

$$G = k_r \frac{\partial T_r}{\partial z} \qquad (2.10)$$

where subscript r refers vales for rock; T_r refers to bedrock temperature and k_r refers to the thermal conductivity of rock.

If the vertical gradient of temperature within the underlying bedrock is assumed constant at 0.013 $^{o}C\ m^{-1}$ then the basal ice is subject to a flux of 42 $mW\ m^{-2}$ (based on Haenel 1980). This flux of heat can also be used to melt ice when it is at pressure melting point. At the base of an ice sheet the first two terms of equation (2.9) reflect the difference in the flux of heat supplied from the bedrock and the flux conducted away through the ice sheet.

The case where the vertical gradient of temperature within the underlying bedrock can vary with both time and depth is discussed in the next section.

2.2.4 Temperature field in the underlying bedrock.

The geothermal heat flux is determined by the vertical temperature gradient within the bedrock underlying the ice sheet. If the distribution of temperature within the bedrock is changed then the geothermal heat flux must also change. The growth of an ice sheet will cause bedrock temperatures to change because the escape of heat from the earth's surface will be hindered. The ice sheet will, in fact, insulate the bedrock immediately underlying it and cause local warming, which in turn will reduce the local geothermal heat flux. The removal of the ice sheet allows the renewed escape of heat and the increase of the geothermal heat flux.

This process can be modelled by extending the model's temperature calculations down into the bedrock. Work by Ritz (1987) indicates that the top 2 km of bedrock can be considered active, in the sense that its temperature evolution interacts with that of the ice sheet.

The processes governing heat flow within the bedrock are modelled in a simpler way than those governing heat flow within ice sheets. In fact the vertical diffusion

term is the only significant one, giving the equation for evolving bedrock temperature ($T_r(x,z,t)$) as:

$$\frac{\partial T_r}{\partial t} = \frac{k_r}{\rho_m c_r} \frac{\partial^2 T_r}{\partial z^2} \qquad (2.11)$$

where c_r is the specific heat capacity of ice and ρ_m is the density of rock material.

Horizontal diffusion is omitted because vertical temperature gradients are expected to be several orders of magnitude greater than the horizontal ones. Some advection may occur because of the circulation of groundwater. However, the majority of the area is underlain by crystalline basement rock and an extensive groundwater circulation is unlikely.

Equation (2.11) also represents a first order approximation to the evolution of permafrost in the area. The depth of permafrost is given by the depth of the 0°C isotherm. The model is a first order approximation because it only considers the sensible heat budget of the bedrock and does not include associated latent heat fluxes. However, a complex model utilising the theory of mixtures (such as that attempted by Kelly and others 1990) is beyond the scope of this study and is probably more detailed than the scanty palaeo-climatological data justifies.

The ice sheet model used in this study was run in two different modes:

- using a constant geothermal heat flux; and

- using time dependent bedrock temperature modelling to find the geothermal heat flux.

In the former mode a specified geothermal heat flux is applied as a boundary condition to the ice/bed interface. In the latter mode equations (2.7) and (2.11) are integrated forward through time together. The temperature at the ice/bed interface in this case is allowed to evolve through the interplay of bedrock and ice temperatures distributions. In this mode the specified geothermal heat flux is applied as a boundary condition at the base of the active bedrock layer.

2.2.5 Isostatic response of the underlying bedrock.

The presence of an ice sheet imposes an additional load on the underlying bedrock. The bedrock can be divided into two regions, which respond to the loading in very different ways. The upper 35 km is called the lithosphere. Its response to loading is similar to that of an elastic plate (Turcotte and Schubert 1982). The load on a point is supported not only at the point but by the surrounding area. This leads to downwarping beneath the loading and to upwarping in surrounding areas. This latter feature is called a forebulge. The second region is called the asthenosphere and forms a deep zone underlying the lithosphere. Its response to loading is by viscous flow (Oerlemans and van der Veen 1984). The extent of this flow is controlled by the mass of the overlying ice sheet, so that eventually the mass of asthenospheric material which has flowed away from the loading will equal the ice sheet's mass. Thus, at equilibrium, there is a bedrock depression equal to the local ice thickness multiplied by the ratio of the asthenosphere's density to ice density (approximately 0.27).

The most important feature of asthenospheric compensation is the large period of time required before an equilibrium is reached. This is a reflection of the very high viscosity of the asthenosphere. It has two effects. First, the equilibrium depression under an ice loading is seldom attained because the residence time of an ice sheet is of the same order of magnitude as the time required for an equilibrium to be established (Mörner 1971). Second, the asthenospheric material moving away from an area of ice loading does so very slowly and this can result in the transient upwarping of areas immediately adjacent to the ice sheet (Walcott 1970). This leads to the formation of a forebulge, which has a different origin and behaviour than the forebulge produced by the elastic lithosphere.

The isostasy model used in this study includes only the asthenospheric flow part of the above description. This is because the effects of the lithosphere's rigidity are felt mainly in the adjacent, forebulge areas. Modelling work which includes both processes indicates that within the area covered by ice the effect of the lithosphere's rigidity is minimal (Oerlemans and van der Veen 1984). Since this study is primarily concerned with what happens in the ice covered areas, the omission of lithospheric effects seems justified. A diffusion equation can be used to model the effect of asthenospheric flow on bedrock elevation (h(x,t)):

$$\frac{\partial h}{\partial t} = D_a \frac{\partial^2}{\partial x^2}\left(h - h_o + \frac{\rho_i}{\rho_m} H \right) \qquad (2.12)$$

where D_a is the diffusivity of the asthenosphere and $h_O(x)$ is the relaxed bedrock elevation.

This equation allows bedrock elevation to change as consequence of the balance between the buoyancy of the lithosphere (the difference between relaxed and current bedrock elevation) and the imposed load (as a bedrock height equivalent). The rate at which an equilibrium is approached depends on the numerical value of the viscosity. A value of 100 km^{-2} $years^{-1}$ implies that 22.5 kyears are needed before equilibrium is established (Huybrechts 1986).

2.3 BOUNDARY CONDITIONS.

The model described in section (2.2) can only be used if the appropriate boundary conditions can be found for the period of interest. These boundary conditions fall into four categories:

- mass balance;
- thermal;
- topographic and isostatic; and
- marine.

The mass balance and thermal boundary conditions are expected to change through time with the changing glacial/interglacial climate. The time series data on which this variation is based are discussed in chapters 3 and 4.

2.3.1 Mass balance boundary conditions.

An estimate of mass balance variation is needed to allow the integration of the ice thickness continuity equation forward through time (equation 2.1). Mass balance in this context refers to the annual difference between the depths of accumulated snow and melted ice/firn at a point. This quantity is positive when a surplus of snow remains at the end of a year and negative when there is a net deficit. It will vary both with position and time as the regional climate changes.

The underlying physics causing this variation are extremely complex and only partially understood. To model accumulation and ablation changes fully is beyond the scope of this project. An emperical approach is commonly used to obtain a first estimate of the mass balance distribution.. Central to this approach is the use of the equilibrium line altitude (ELA), which is the plane within the atmosphere above which net accumulation occurs and below which net ablation occurs. The variation of mass balance with altitude around the ELA has a distinctive form, found by many researchers on glaciers and ice sheets the world over (for compilations see Budd and Smith 1981 and Boulton and others 1984).

This form is illustrated in Figure 2.3. It provides a convenient method of parameterizing mass balance in the model. Mass balance has this particular relationship with altitude for the following reasons:

- the flat portion of the curve reflects the situation where all of the accumulated snow remains at the end of a year (no ablation);

- the portion of the curve between this area and the ELA reflects the gradual increase in ablation towards the ELA, however accumulation still predominates; and

- the portion of the curve below the ELA has ablation predominating and increasing rapidly with decreasing altitude.

This implies that accumulation is everywhere constant and that ablation has a non-linear, inverse relationship to altitude. Work in Greenland by Braithwaite (1981) relates the latter point to the increasing air temperatures and, more specifically, to

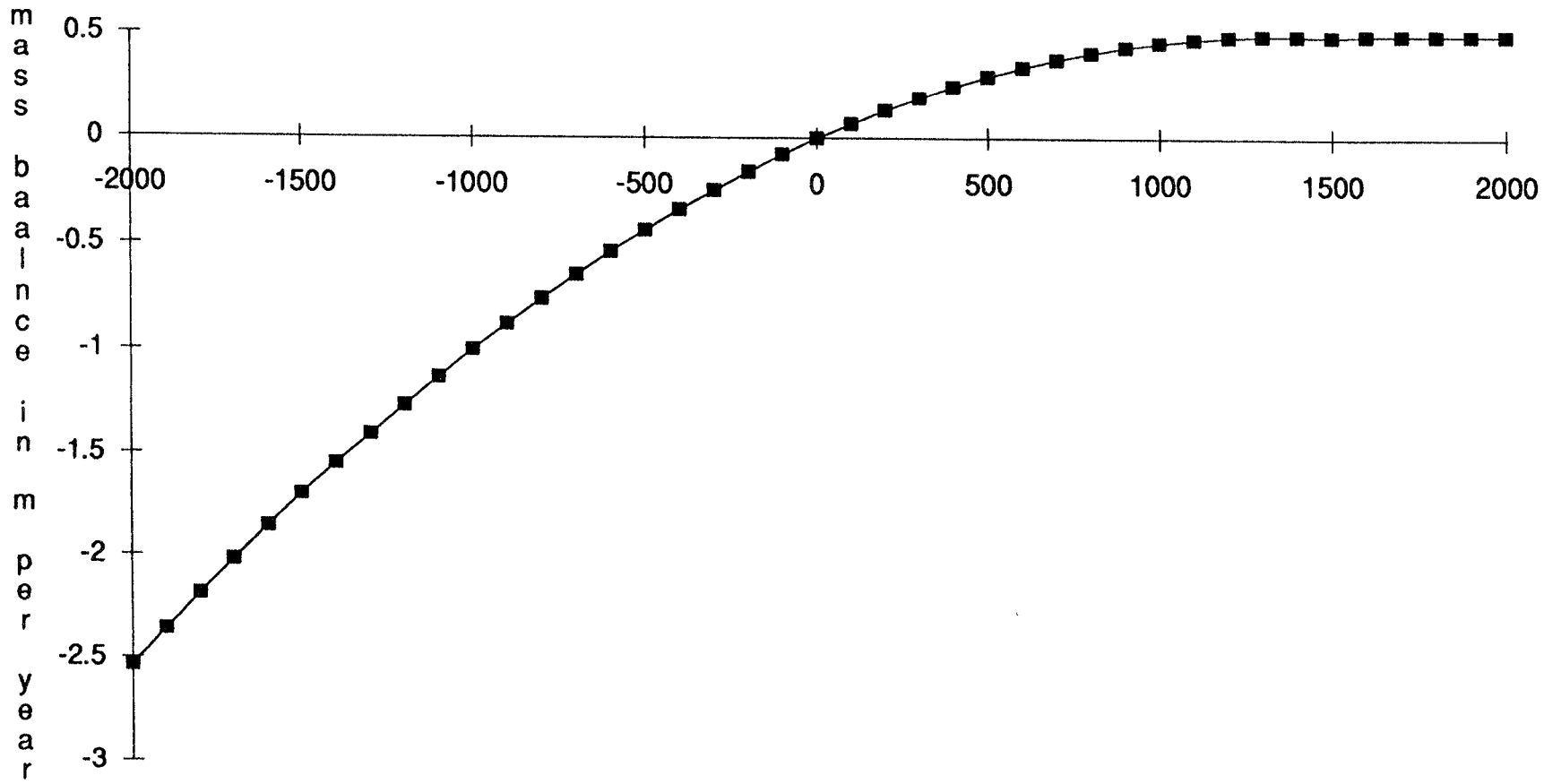

Figure 2.3 The relationship between mass balance and elevation used in the model.

the near exponential increase in the number of days per year with temperatures above 0 ^{o}C at lower altitudes.

The equation used to obtain mass balance is :

$$b = \begin{cases} \alpha(H+h-\lambda) - \beta(H+h-\lambda)^2 & \text{if } H+h-\lambda < 2000\text{m} \\ b_{max} & \text{if } H+h-\lambda \geq 2000\text{m} \end{cases} \qquad (2.13)$$

where b_{max} is the maximum allowed positive mass balance, λ is equilibrium line altitude and α and β are constants.

This is easily incorporated into the model because ice sheet surface elevation is already known from the ice thickness continuity equation (2.1). This equation was successfully used by Oerlemans (1981) in a study of the growth rate of the former Fennoscandian ice sheet. Its use requires a knowledge of the ELA and how it varies with distance and through time.

Equation (2.13) falls within the series of mass balance - altitude curves identified by Boulton and others (1984). This set of curves reflect varying mass balance gradients. Maritime areas have steep mass balance gradients and high rates of both accumulation and ablation, while continental areas have flatter mass balance gradients where accumulation and ablation rates are always low.

The use of equation(2.13) implies that the degree of continentality does not vary across the model flowline or through time. This is done to simplify the overall behaviour of the model, in terms of the ice sheet's contraction and expansion. The main aim of the modelling work is to evaluate the temperature and flow regime within the ice sheet. The omission of changing mass balance gradients is therefore only a problem if this significantly affects the ice flow/temperature regime. Sensitivity analysis of the model's predictions using mass balance curves with varying degrees on continentality indicates that flow and temperature where not particularly dependent on mass balance gradient.

The form of equation (2.13) immediately introduces a new feedback into the model. The coupling of ice thickness evolution to mass balance in the continuity equation (equation 2.1) and the relation of mass balance to ice sheet surface elevation

(equation 2.13) implies that a thickening ice sheet will experience progressively greater positive mass balances and its thickening rate will accelerate through time. This is indeed a very strong feedback, which is only partially compensated in equation (2.1) by the flux divergence/convergence term. The latter will tend to reduce the rate of thickening at a point by increasing the outflow of ice from that point. It is to be expected that ice sheet growth and decay rates will be very sensitive to changes in mass balance and imposed ELA.

2.3.2 Thermal boundary conditions.

Two boundary conditions are required before the continuity equation for ice temperature (equation 4) can be integrated through time. The first of these, the geothermal heat flux, has been discussed in sections (2.2.3) and (2.2.4). In different versions of the model it is either applied directly to the ice/bed interface or to the base of the 2 km thick slab of bedrock underlying the ice sheet, depending on whether bedrock temperature evolution is modelled or not. In either case a value of 42 mW m^{-2} is used.

The second boundary condition is applied to the ice sheet surface, and is the surface air temperature. This differs from the lower boundary condition because it represents the fixed value which the temperature at the upper boundary condition should take. The lower boundary condition is, of course, a flux term and is related to the flow of heat across that boundary. Surface air temperature (T_a) is found from:

$$T_a = T_{sl} - \psi(H+h) \qquad (2.14)$$

where ψ is the lapse rate and T_{sl} is the air temperature at sea level.

When ice is not present, this boundary condition is applied to the top of the modelled bedrock slab. In this event a correction is made between air temperature and the temperature of the ground surface. Following Boulton and others (1989) it is assumed that the temperature of the ground surface is uniformly 3 ^{o}C warmer than the appropriate air temperature. This effect is found arctic Canada today and reflects the different energy balances of the near surface air and the ground surface.

The lapse rate used in the model is 10 $^{o}C\ km^{-1}$ (Orvig 1970), which is typical of the rates observed over present day ice sheets. The sea level air temperature provides the model forcing and is a function of time alone. Its derivation from records of past climate and its use in the model are discussed in chapters 3 and 4 respectively.

2.3.3 Topographic and isostatic boundary conditions.

A representation of the bedrock elevation along the flowline is required for three reasons:

- the mass balance and air temperature calculations use ice sheet surface elevation;
- the ice velocity calculation uses ice sheet surface slope as a input; and
- the marine boundary condition uses a bathymetric limit on ice sheet extent.

These are the principal reasons for not using a simple flat topography. Points (a) and (b) are only important when ice sheet thickness is small, during initial growth and final decay. This is because the great thickness of ice present during most of the ice sheet's existence masks most of the initial topographic variation. Point (c), however, operates during the complete sequence of growth and decay.

The flowline selected for the model is shown in Figure 2.4. It runs roughly North-West to South-East from Kristiansund in southern Norway, across Lake Vänern in southern Sweden, through the southern Baltic to central Poland. It covers a total of 1740 km, of which 160 km is below -500 m in the Atlantic Ocean. This flowline was selected because it contains an area of known ice sheet initiation (the Jotunheimen area) and the sites of interest to the study in southern Sweden. Its close proximity to the Skagerrak raises doubts as to whether the actual Fennoscandian ice sheet used this flowline throughout all of the last glaciation. It seems likely that during at least some of this time flow would have been deflected towards the West by the operation of a Skagerrak ice stream. This type of spatially

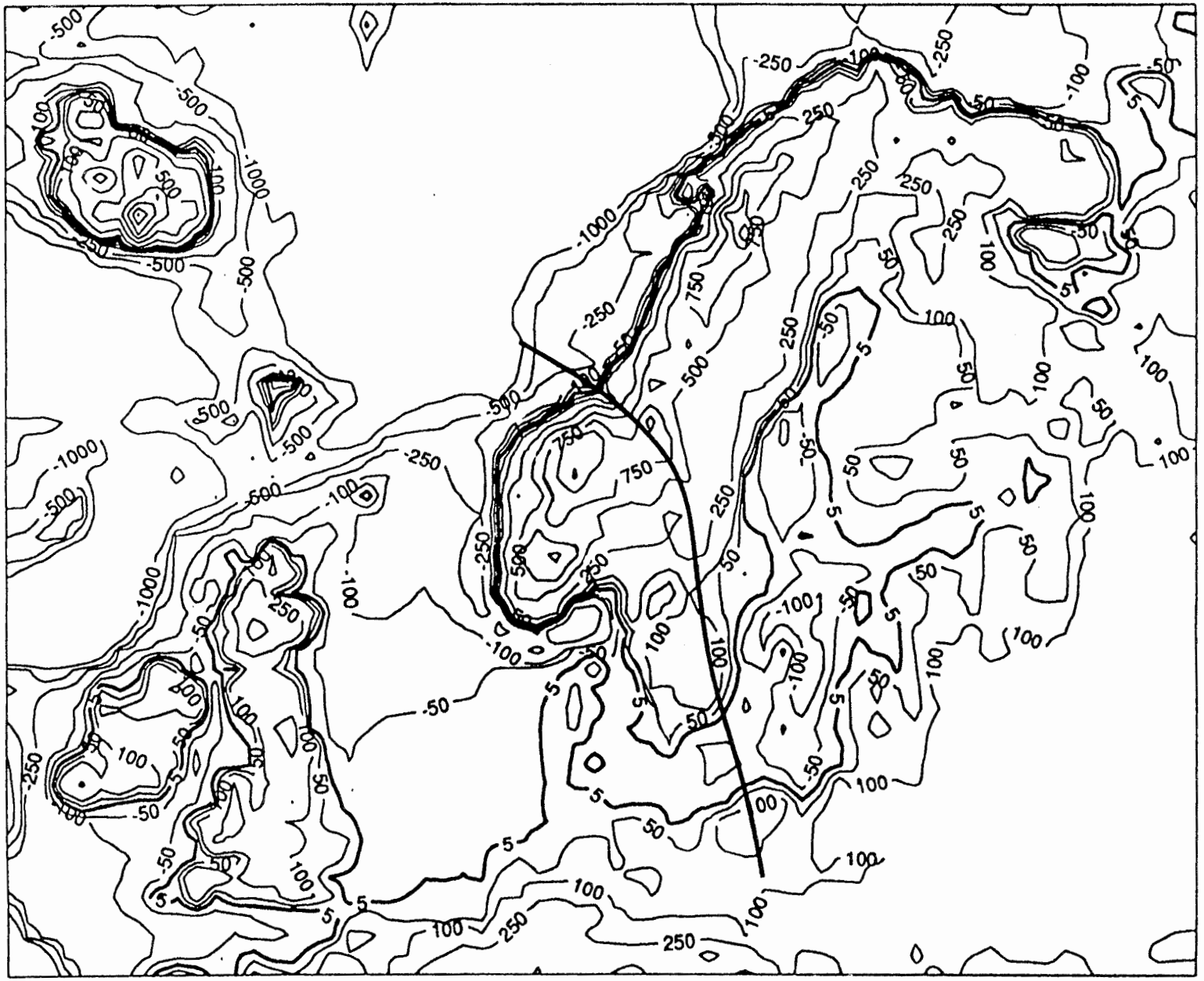

Figure 2.4 Contoured map of the topography of North West Europe showing the position of the flowline used in this study.

shifting flow pattern cannot be modelled by the two dimensional flowline model that is used in this study. However, the flowline model will give a good indication of the overall sequence of events affecting southern Sweden in terms of key ice sheet variables such as ice flow, temperature and thickness.

The topographic data used for the flowline was interpolated from a spatial topographic data set, which covers all of Europe. This data was compiled from the U.S. Navy 10' x 10' global orography dataset; has a Lambert conformal conic projection and a 20 x 20 km grid resolution.

A relaxed topography is required in the isostatic model (equation 2.12). This represents the topography along the flowline after the recovery (uplift) from ice sheet loading is complete. The difference between this relaxed topography and the topography at any time during a model run can therefore be used as a measure of the buoyancy of the bedrock. The present day topography along the flowline is used as the relaxed topography. The errors incorporated by doing this are probably small for two reasons. First, although southern Sweden is still rising in response to the removal of ice loading, the rate of uplift is relatively slow compared to past rates (0.5 mm/year on average, Ekman 1991) indicating that this area may already be near isostatic equilibrium. Second, variations in ice loading are expected to be both large (in excess of 2 km) and rapid (deglaciation occurred within 10 kyears, Boulton and others 1985). Errors in the buoyancy calculation (relaxed minus current bedrock elevation) of equation (2.12) are therefore minor in comparison to the fluctuations occurring in the ice load term, and a good estimate of the rate of isostatic response can therefore be expected.

2.3.4 Marine boundary conditions.

The discussion of the physical basis of the ice sheet model (section 2.2) is strictly applicable only to ice which rests on bedrock (grounded ice). This is always the case when ice sheets form and flow over dry land. However, an ice sheet can also flow into the ocean. In this case the ice sheet may locally cease to be grounded and start to float. The physics of flow so far discussed cease to apply. This is because the discussion in section (2.2) assumes a large shear stress acting at the ice sheet base. When the ice starts to float, this shear stress is lost. The stress regime

within the ice sheet ceases to be shear dominated and becomes dominated by longitudinal stresses (Herterich 1987). The complex transition between the two stress regimes occurs near the grounding line and has been discussed by many authors, including Van der Veen (1987), Alley and Whillans (1984) and Muszynski and Birchfield (1987).

This study is principally concerned with the behaviour of the ice sheet far from the ocean. A very simple scheme is therefore used at the marine/floating boundary. The western side of the flowline extends over the continental shelf. Reconstructions of the Fennoscandian ice sheet based on geological evidence indicate that the marine margin of the ice sheet never extended past the continental shelf (Lehman and others 1991). The most likely scenario is that the western margin ended in a short shelf of floating ice. This situation is incorporated into the model by allowing the ice sheet to extend into water depths of up to -500 m depth but no further. This effectively ties the western margin to the continental shelf. Any ice flow past this point is assumed to be lost by the calving of ice bergs. A boundary condition of this type is often used in numerical models of large, predominantly land based ice sheets (eg Oerlemans 1981).

2.4 NUMERICAL METHODS USED IN THE MODEL.

The numerical methods used to solve the equations discussed in sections (2.2) and (2.3) are outlined here. The techniques used are all of the finite difference type and can be divided into three sections:

- horizontal operations;
- vertical operations; and
- temperature calculations.

The first section concerns the solution of the ice thickness continuity and isostatic diffusion equations by the Crank-Nicholson technique. The second section is involved with the introduction of a flexible computational grid in the vertical. The calculation of horizontal and vertical velocity is outlined here. Finally, the solution

of the temperature continuity equation is outlined along with the incorporation of the various boundary conditions into the model. A summary of the flow of information within the model is given in Figure 2.5.

2.4.1 Horizontal operations used in the numerical model.

Both the ice thickness continuity and the isostasy equations (2.1 and 2.12 respectively) are diffusion equations relating a time derivative of some quantity (ice thickness or bedrock elevation) to the second derivative of the same quantity. The difference between the two is that the isostasy equation is linear, while the ice thickness continuity equation is non-linear and has a diffusivity which varies in both space and time.

The ice thickness continuity equation (2.1) and the equation for horizontal velocity (2.3) can be recast into a diffusion equation form by:

- finding the vertically averaged horizontal velocity from (2.3) by integration through ice thickness;
- substituting vertically averaged horizontal velocity in (2.1); and
- using a diffusivity term in (2.1).

$$\frac{\partial H}{\partial t} = -\frac{\partial}{\partial x}\left(D\frac{\partial (H+h)}{\partial x} \right) + b \qquad (2.15)$$

The result is an ice sheet diffusion equation with non-linear diffusivity (D):

$$D = -2(\rho_i g)^n \left| \frac{\partial (H+h)}{\partial x} \right|^{n-1} \int_h^{H+h} \int_h^z A(T)\,(H+h-z)^n dz\, dz + u_h \qquad (2.16)$$

Both this equation and the isostatic diffusion equation:

$$\frac{\partial h}{\partial t} = D_a \frac{\partial^2}{\partial x^2}\left(h - h_o + \frac{\rho_i}{\rho_m} H \right) \qquad (2.17)$$

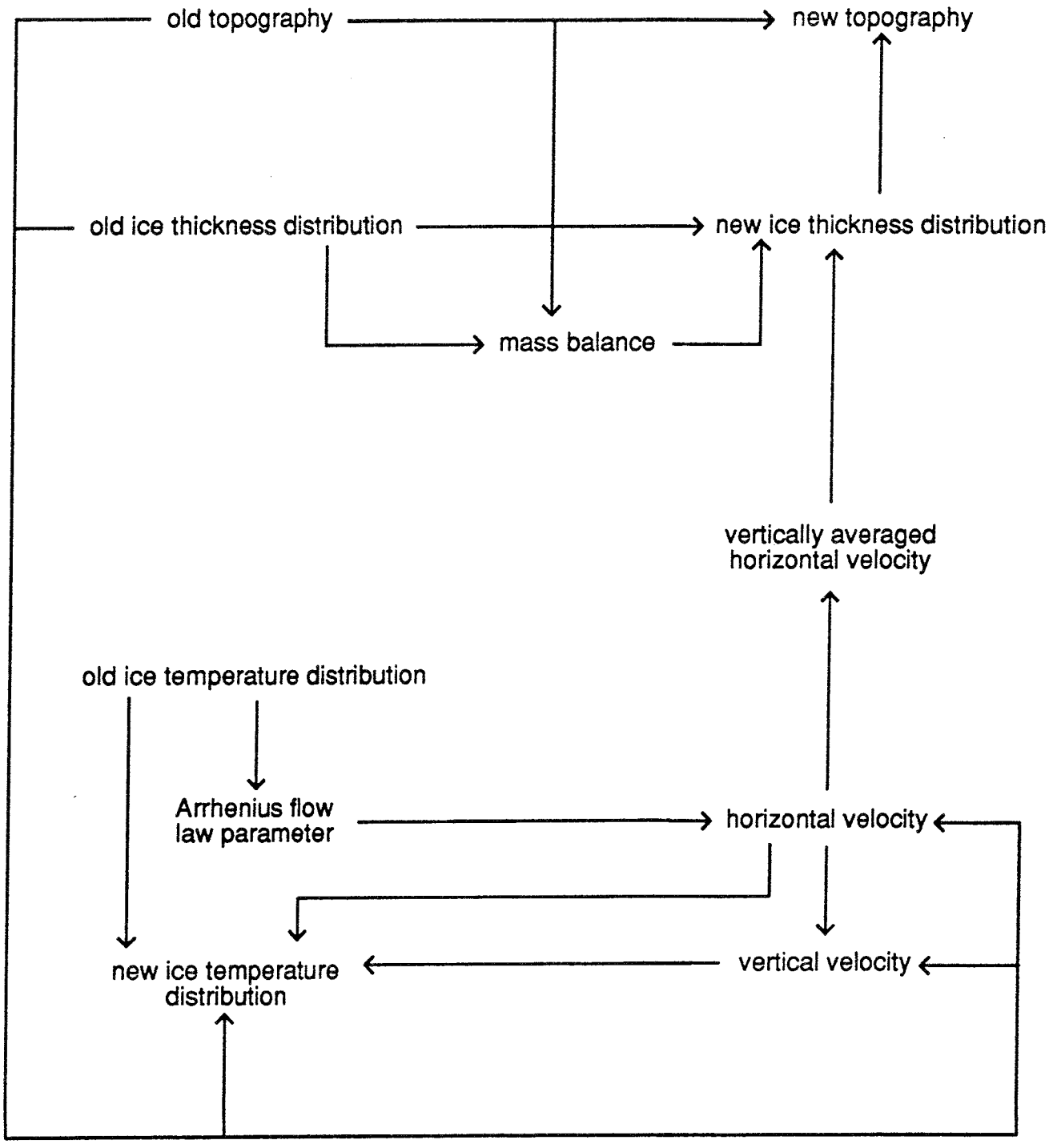

Figure 2.5 The flow of information in the model.

can now be solved numerically using the same technique.

The Crank-Nicholson implicit finite difference scheme is used (see Smith 1985). This is of the 'forward in time and centred in space' type. The horizontal derivatives are approximated by the average of their values at times t and t + dt. The resultant tridiagonal matrices are solved using Gaussian elimination (see Press and others 1989). The solution of equation (2.17) is a simple matter using this scheme. The solution of (2.15) is, however, slightly more involved.

The stability of the Crank-Nicholson scheme can be improved when dealing with non-linear, flux type equations (such as 2.15) by calculating the fluxes on a staggered grid (Patankar 1980). This is done in the model by determining the quantity $D\,\partial(H+h) / \partial x$ at points half way between grid points, using the values of D,H and h at the adjacent grid points. The second horizontal derivative is then found half way between adjacent staggered grid points. This location corresponds to a grid point on the original net. The values of H used in these calculations are the average of those at t and dt, while the values of D and h are only those at time t. The diffusivity is found using values of H, h and T at time t only.

This scheme combines the stability of the fully implicit method and the ease of programming of the fully explicit method. A fully implicit method would involve a far more complex elimination procedure than the Gaussian one used here. While a fully explicit scheme would require very small time steps in order to remain stable.

This scheme proved satisfactory when used with a horizontal grid spacing of 20 km and a time step of 5 years. Larger time steps at this horizontal grid spacing proved unstable.

2.4.2 Vertical operations used in the numerical model.

The calculation of velocity and temperature is based on vertical methods. The numerical grid used in the vertical is not fixed in space (as the horizontal grid is) but varies with local ice thickness Vertical grid points are located relative to the ice sheet surface and the ice/bedrock interface elevation:

$$\xi = \frac{H + h - z}{H} \qquad (2.18)$$

In the model used in this study eleven vertical grid points are used at 0.00, 0.15, 0.30, 0.45, 0.60, 0.75, 0.83, 0.90, 0.95, 0.98 and 1.00. The first point is located at the ice sheet surface and the last at the ice/bedrock interface. This scheme was first devised by Haltiner (1971) for use in atmospheric global circulation models and was introduced into ice sheet modelling by Jenssen (1977). It complicates the equations given in section (2.2) but has the advantage that the computational effort can be concentrated in the basal layers of the ice sheet, where most variation occurs. The scheme also simplifies the use of the calculation of ice sheet boundary conditions because a grid point always falls on the boundary, he continual thickening and thinning of the ice would otherwise mean that some grid points would fall outside of the model domain.

The use of a flexible vertical coordinate necessitates the incorporation of correction factors for integration and differentiation because a vertical grid point now has an apparent vertical velocity:

$$\int_h^z F(z)\,dz = -H\int_1^\xi F(\xi)\,d\xi \qquad (2.19)$$

$$\left(\frac{\partial F}{\partial x}\right)_z = \left(\frac{\partial F}{\partial x}\right)_\xi + \frac{1}{H}\frac{\partial F}{\partial \xi}\left\{\frac{\partial H}{\partial x}(1-\xi) + \frac{\partial h}{\partial x}\right\} \qquad (2.20)$$

$$\left(\frac{\partial F}{\partial t}\right)_z = \left(\frac{\partial F}{\partial t}\right)_\xi + \frac{1}{H}\frac{\partial F}{\partial \xi}\left\{\frac{\partial H}{\partial t}(1-\xi) + \frac{\partial h}{\partial t}\right\} \qquad (2.21)$$

$$\left(\frac{\partial F}{\partial z}\right) = -\frac{1}{H}\left(\frac{\partial F}{\partial \xi}\right) \qquad (2.22)$$

These expressions are substituted for the integrations and differentiations used in the equations of section (2.2).

Horizontal velocity (u(x,z,t)) requires a numerical integration of the Glen flow law parameter (A(T)) through ice thickness. This is easily done once the correction factor (2.19) has been applied. This numerical integration is necessary because the variation of temperature (which directly determines the value of the flow law

parameter) through ice thickness is not known analytically. A second numerical integration is required in the calculation of the vertically averaged horizontal velocity ($\bar{u}((x,))$ because the variation of horizontal velocity through ice thickness is not known analytically. Again the correction factor in equation 2.19) must be applied. The vertically averaged horizontal velocity can now be used in the ice continuity calculation described above. The use of a staggered grid for the ice continuity calculation means that a similarly staggered grid must be used in the velocity calculations if the two are to be compatible. Thus horizontal velocity is found on the staggered grid using values of H, h and T at the two adjacent original grid points. The velocity at the original grid points is then interpolated from the values known on the staggered grid.

The calculation of vertical velocity (w(x,z,t)) requires the numerical integration of the horizontal derivative of horizontal velocity (u(x,z,t)) Correction factors (2.20) and (2.19) therefore have to be applied, the first to correct for horizontal variation in the grid point's vertical location and the second because of the numerical integration. The horizontal differentiation is performed using the velocities calculated on the staggered grid, as described above.

2.4.3 Temperature calculation in the numerical model.

The ice temperature continuity equation (2.7) is also solved using finite differences. However, it must first be adapted to the flexible vertical coordinate system discussed above. The time, vertical space and horizontal space derivatives are expanded according to equations (2.20) to (2.22).

The numerical scheme employed is a composite one. The equation is integrated forward in time. Vertical temperature derivatives are calculated at time t + dt, while the horizontal ones are calculated at time t. The scheme is thus implicit in the vertical and explicit in the horizontal. The resultant tridiagonal matrices can be solved using Gaussian elimination. This concentration on the vertical is warranted because temperature gradients in the vertical are several orders of magnitude steeper than those in the horizontal. The vertical grid spacing is also far smaller than the horizontal grid spacing. The vertical derivatives of horizontal velocity required in the strain heating term are found at time t.

The temperature continuity equation involves advection in the horizontal and the vertical directions. Both terms are calculated using an upwind scheme (Patankar 1980). This is a common approach is advection modelling and tends to be stabler than the usual 'centred in space' differencing. Upwind differencing means that temperature derivatives at a point are calculated using the temperature values at the point and at the point immediately upstream in the local velocity field. The upwind scheme in the vertical must consider the vertical velocity relative to the apparent velocity of the grid point discussed in (2.4.2). The diffusion and strain heating terms can be calculated using 'centred in space' differencing.

The bedrock temperature continuity equation (2.11) is far simpler to solve. The vertical diffusion term is incorporated using centred differences and solved at time t + dt, as are the vertical temperature terms in the ice. The calculation is simplified because the vertical grid within the bedrock is fixed in space and because no advection terms are present.

Finally, the boundary conditions should be included in the finite difference scheme. The calculations at the upper boundary are straight forward and simply require that the ice temperature at the ice sheet surface is set equal to the prevailing air temperature. At the basal boundary the majority of the above correction terms (2.19 to 2.22) become zero. The actual calculations performed at the ice/bedrock interface depend on whether the temperature evolution of the underlying bedrock is being modelled or not. If not then the basal boundary condition (equation 2.10) is used to provide the vertical temperature gradient which is needed for the diffusion and advection terms. The advection term uses velocity relative to the bed (which itself may be rising or sinking), which is simply the current basal melt rate (equation 2.9).

If the temperature evolution of the bedrock is being modelled then the basal boundary condition (equation 2.10) is applied to the base of the modelled bedrock slab. The calculations at the ice/bedrock interface proceed in much the same way as above, except that the vertical temperature gradient is now found internally as a function of the varying ice and bedrock temperature fields.

3 PAST CLIMATE AND ICE SHEET HISTORY.

The last glacial period lasted from about 120,000 years ago to about 10,000 years ago, during which a large ice sheet grew and decayed over Europe. The history of ice sheet fluctuation during this last glacial cycle is more or less well known. Ice sheet fluctuations were driven by climate fluctuations for which we believe the reconstructions of sea-surface temperature (SST) in the N.E. Atlantic, derived from studies of the geology of ocean cores, is the best proxy record. The trend through time of sea surface temperature in this region is likely to reflect both the temperature and precipitation trends in N.W. Europe, which in turn drove past ice sheet fluctuation. We therefore derive an ELA function for the last glacial cycle which bears a simple mathematical relationship to trends of N.E. Atlantic SST and thus sea surface air temperature (SLAT) which drives the ice sheet model so that it produces a pattern of ice sheet fluctuation which agrees with the geological evidence of fluctuation.

..... ***** .....

As explained in Chapter 1, the sea surface temperature record of the Weichsalian glacial cycle from the N.E. Atlantic (Rockall Plateau) is used as a proxy indicator of those areas of regional climate which would be most important in influencing behaviour of an ice sheet over north-west Europe. We have used the record provided by Labeyrie.

As has been discussed in Chapter 1, a relationship is sought between ELA and the SST record from the Rockall Plateau which would drive an ice sheet in N.W. Europe to behave as geological evidence suggests it did. Thus this evidence of ice sheet fluctuations is not part of the model output, but part of the input parameterisation of the model.

We have used summaries by Lundqvist (1986) and Mangerud (1991) to reconstruct the behaviour of the ice sheet prior to its Weichselian maximum, unpublished data from Rodnicki (1991) to determine the date of advance to and retreat from the outer maximum and the evidence of Boulton et al (1985) for the pattern and tempo of decay. Although there is still some considerable uncertainty, the approximate positions of the ice sheet margins in Europe are shown in figure 03.1 for the Late Weichselian maximum (18ka); the mid-Weichselian interstadial at 55 ka; an early Weichselian stadial at 110 ka. These reconstructions are broadly compatible with the evidence of shifting Weichselian flow directions presented by Kleman (1990) and Hirvas (1981) and by the Nordkalott project.

Accepting the reconstruction in figure 3.1 as a reasonable approximation, it is possible to identify transects from the western continental shelf of Norway across the ice divide to the east and thence to the south-south-east in northern Poland in the two dimensional behaviour of the ice sheet in plan, can be represented through time along a one dimensional transect. Although it is clear that the flow direction will have crossed this line of transect from time to time, we suggest that the angular divergence was not likely to have been large, except in the southern Baltic, where Baltic "ice streams" might have developed from time to time.

Our extrapolation of the geological evidence ice sheet fluctuation onto this transect is shown in figure 3.2.

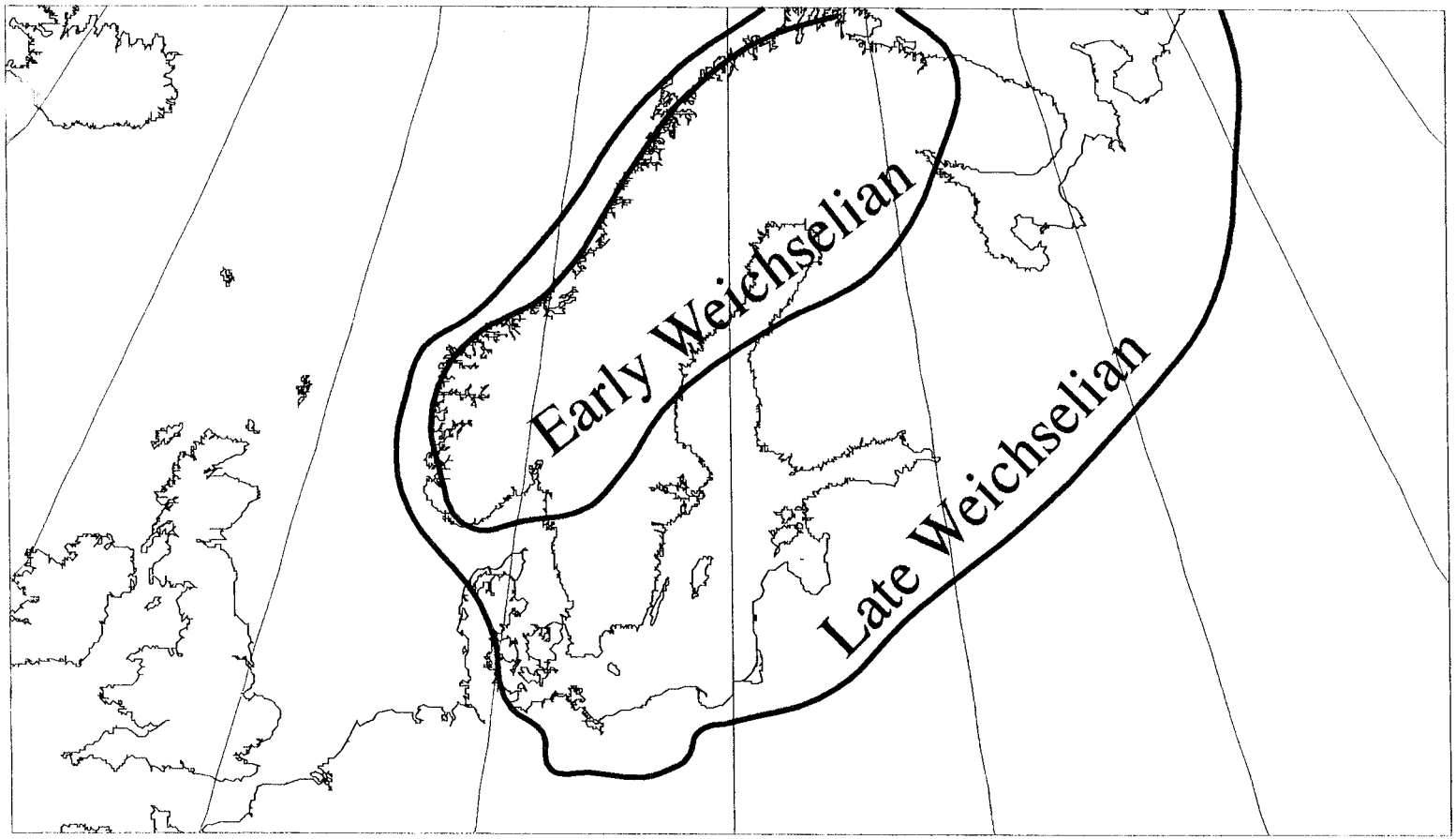

Figure 3.1 Early and Late Weichselian maximal ice sheet marginal positions

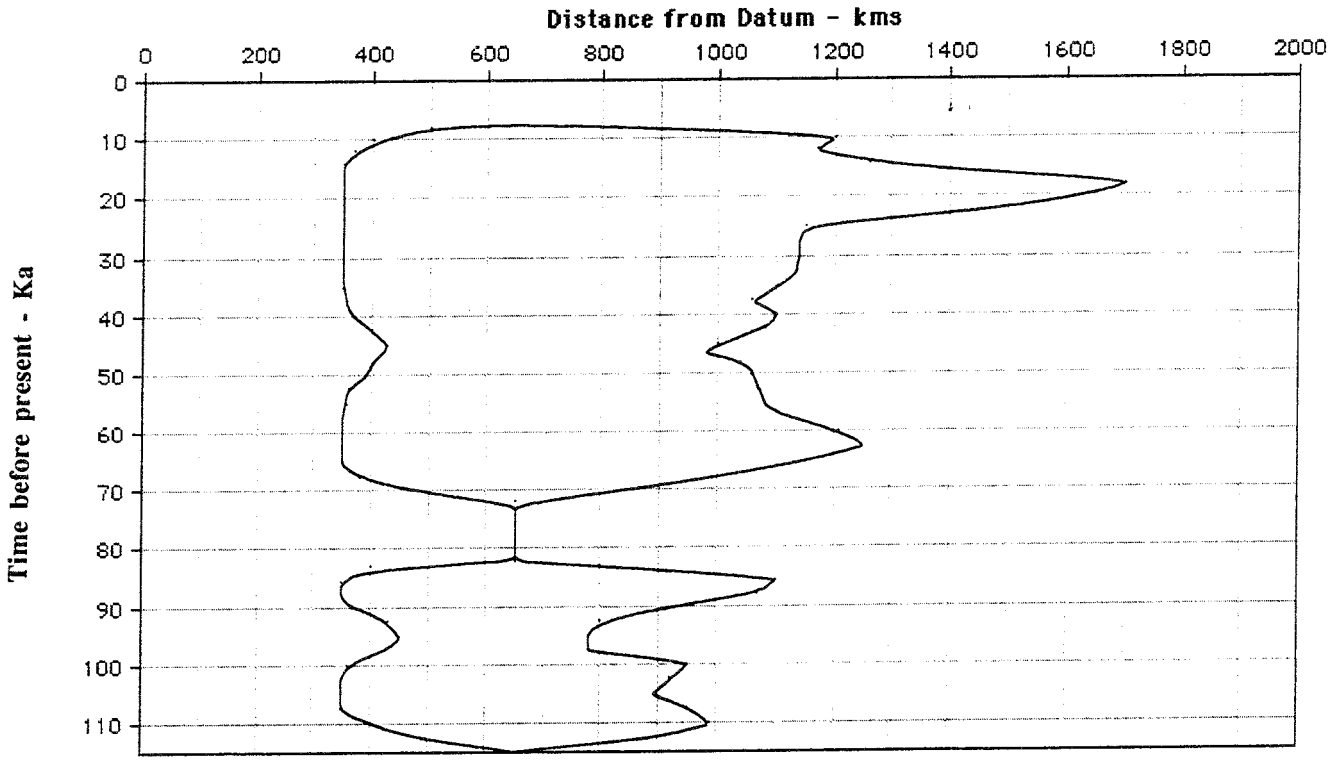

Figure 3.2 Postulated temporal fluctuation of the European ice sheet along the line of transect during the last glacial cycle

4 DRIVING THE MODEL USING CLIMATE DATA.

The relationship is established between the N.E. Atlantic sea level air temperature (SLAT) record and the equilibrium line altitude (ELA) required to drive the ice sheet in the way that geological evidence suggests it varied through the last glacial cycle.

..... ***** .....

4.1 SUMMARY OF THE MODEL'S DRIVING FUNCTIONS.

This chapter is concerned with the way in which the climate data described in Chapter 3 are used in the model. The Rockall trough Weichselian sea surface temperature record is the key data in this context. It is used to obtain time series of both equilibrium line altitude and sea level air temperature for the 120 kyears of the model simulation. This indirect approach is necessary because of the lack of temperature and precipitation estimates for Weichselian Scandinavia. Equilibrium line altitude is needed in the model to drive the mass balance variation, that is the net difference between snow accumulation and ice ablation (section 2.3.1). While sea level air temperature is needed to drive the ice sheet surface air temperature calculations (section 2.3.2).

Linear relationships are defined which allow the creation of the necessary time series. The form of these curves depends wholly on the form of the Rockall trough data. However, the amplitude of the curves is controlled by the value of the parameters used in the transfer functions. In case of the sea level air temperature, two time series are produced with minimum temperatures of -10 and -5 ^{o}C (at 18 kyears BP) respectively. The amplitude of the equilibrium line altitude time series is tuned so that the maximum extent of the modelled ice sheet agrees with the Weichselian maximum extent known from the area's Quaternary geology.

4.2 THE RATIONALE USED IN DRIVING THE MODELLED EQUILIBRIUM LINE ALTITUDE.

Previous modelling studies of the late Quaternary, mid-latitude ice sheets reveal that these ice sheets were unlikely to have ever been in equilibrium with their environment (Budd and Smith 1981 and Oerlemans 1981). The principal reason for this is the slow response time associated with ice sheet form changes. This response time is of the same magnitude as the typical wavelength of the variations in the environmental phenomena driving the ice sheet. In particular, the variation of both insolation at high latitudes (Berger 1978) and North Atlantic sea surface temperature (Ruddiman and others 1986) is strong at wavelengths shorter than the ice sheet response time. This implies that the maximum ice sheet extents known from the Quaternary geological record reflect not long term equilibria but short term standstills between phases of growth and decay. The relevance of this argument to the present study is in the way that the climate data outlined in chapter 3 is used, especially the relationship between the Rockall trough sea surface temperature record and the variations in equilibrium line altitude used to drive the model.

Viewed in this context, the maximum extent of the Weichselian ice sheet in Europe is simply the size to which the ice sheet had time to grow to before climatic conditions ameliorated sufficiently to initiate decay. There is nothing intrinsically important about this size. Initial experiments with the model used an equilibrium line altitude which was constant through time. They confirmed that an ice sheet the size of the Weichselian maximum had no particular significance in terms of an equilibrium with the model driving variable. The span of the modelled ice sheet grew unrealistically large when realistic equilibrium line altitudes were employed. This is because the residence time of the modelled ice sheet was too long and the ice sheet therefore grew past the Weichselian maximum extent. The growth rate of the modelled ice sheet at this time is extremely rapid (mostly because of the strong mass balance feedback mentioned in (2.3.1)) and the length of time for which it occupies the Weichselian maximum extent is therefore brief. The problem is to get the model to behave in such a way that the modelled maximum extent is similar to that known from the area's Quaternary geology. This is clearly a dynamic problem and relates to both the growth rate of the ice sheet and its residence time. The model can only therefore be calibrated to the Weichselian maximum extent if both the growth rate and the residence time are closely constrained.

Specifically the problem is to find a method of making the time series input to the model (the Rockall trough sea surface temperature record) compatible with the known Weichselian maximum extent (the estimates of Boulton and others 1985 are used). The Weichselian maximum extent is the strongest evidence available for the calibration of the model. Estimates of the variation of extent through the Weichselian are available as a secondary means of calibration (eg Lundqvist and Mangerud 1981) and will be discussed in Chapter 5. The method chosen was to tune the relationship between the equilibrium line altitude (used in the model to drive the ice sheet's growth and decay) and the sea surface temperature time series input so that a reasonable Weichselian maximum extent was produced at 18 kyears BP. The details of this tuning are outlined in section (4.3).

This methodology has an important implication for the results of the study. The predicted maximum extent of the Weichselian ice sheet and the timing of that maximum can no longer be regarded as output from the model. This is because this information has been used as input to the model by way of the tuned relationship between sea surface temperature and equilibrium line altitude. This is in line with the aim of the study, which is to predict and understand the changing flow and temperature patterns within the ice sheet. If the aim where truly to predict and understand the size and timing of the Weichselian maximum then a global climate model would be required in addition to the ice sheet model already used in this study.

4.3 THE RELATIONSHIP BETWEEN SEA SURFACE TEMPERATURE AND EQUILIBRIUM LINE ALTITUDE.

The present day equilibrium line altitude over Scandinavia is modelled using a parameterization developed by Oerlemans (1981) based on data from Charlesworth (1957). The present day equilibrium line altitude was modelled using a plane inclined to the South and East The projection of the flowline used in this study on to this plane gives an equilibrium line altitude which slopes down from 2597 m over central Poland to 1095 m over southern Norway.

This equilibrium line altitude is moved up or down during the course of a model run to simulate the changing climate though a glacial/interglacial cycle. The amount by which the equilibrium line altitude is depressed is related to the difference between the present day and the former sea surface temperatures in the Rockall trough area. The present day sea surface temperature is 12 ^{o}C. The relationship assumed in the model is a linear one which is the simplest one possible. Thus:

$$\Delta\lambda = f_1.(SST - 12.0) \qquad (4.1)$$

where f_1 is a constant, Dλ equilibrium line is the depression and SST is the sea surface temperature.

The Rockall trough data described in Chapter 3 provides a time series of sea surface temperature through the 120 kyears of the Weichselian. Equation (4.1) can be used with this data to derive an equilibrium line depression time series to drive the ice sheet model. The value of f_1 in equation (4.1) can be used to vary the amplitude of this equilibrium line depression time series. This value is therefore crucial in determining the behaviour of the overall model and the maximum size to which the modelled ice sheet grows to during its Weichselian simulation. It is the value of f_1 which is tuned as described in section (4.2). A value of 88.4 m $^{o}C^{-1}$ was found to produce a reasonable Weichselian maximum extent at 18 kyears BP of 1500 km. This value controls the amplitude of the equilibrium line depression forcing curve but the form of this curve comes directly from the form of the sea surface temperature time series. Figure 4.1 shows the equilibrium line depression forcing curve used to obtain the results described in Chapter 5.

4.4 THE RELATIONSHIP BETWEEN SEA SURFACE TEMPERATURE AND SEA LEVEL AIR TEMPERATURE.

Air temperature forms the second boundary condition whose variation drives the model. Very little data relating to Weichselian air temperatures exists in Scandinavia, mostly because of the presence of the ice sheet The variation of sea surface temperature in the Rockall trough core is therefore assumed to have affected the sea level air temperature in Scandinavia. Surface temperatures are then derived using a constant lapse rate. A linear relationship is again assumed:

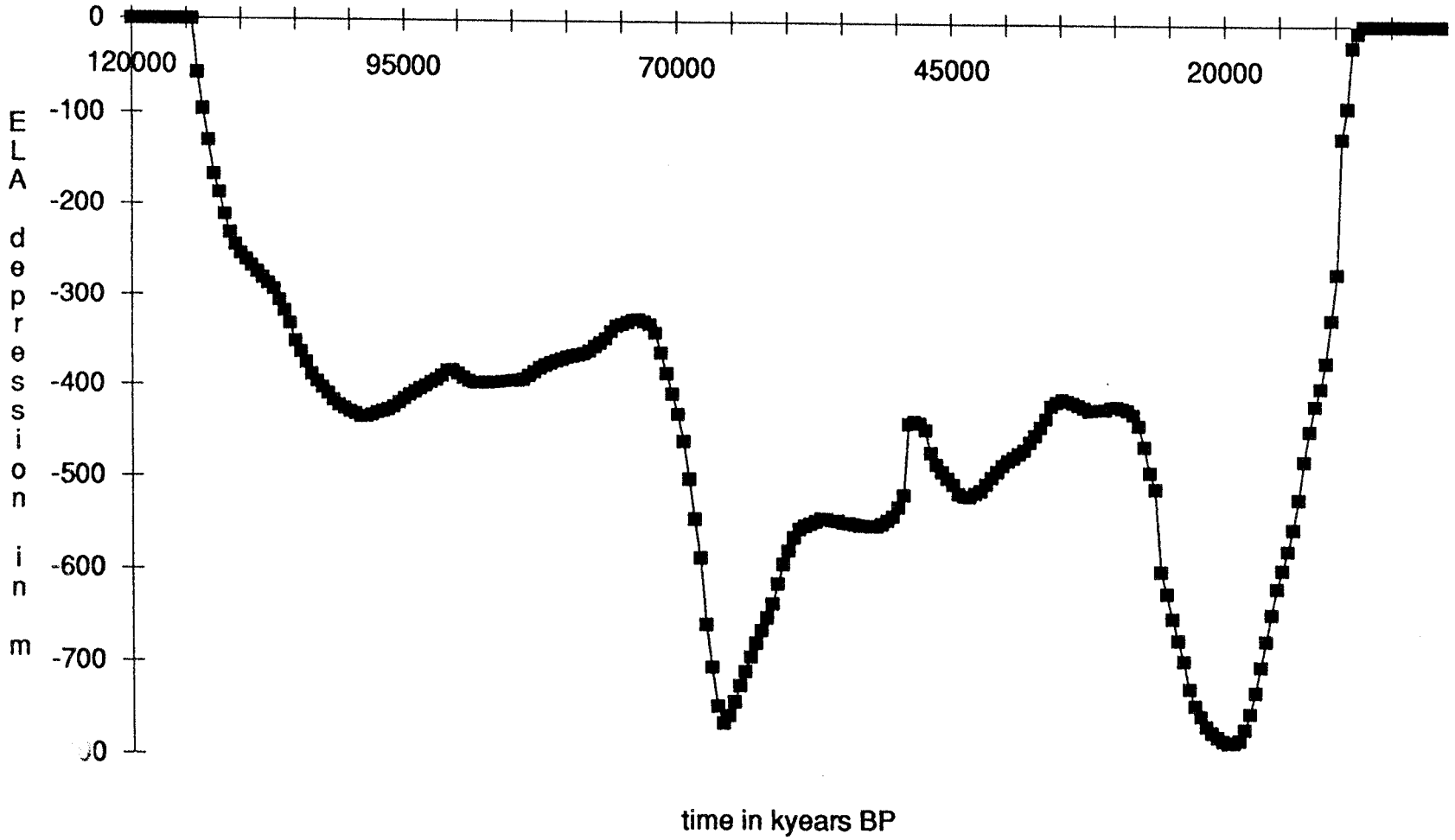

Figure 4.1 The equilibrium line depression time series used to force the model.

$$SLAT = f_2 + f_3.(SST - 12.0) \qquad (4.2)$$

where f_2 and f_3 are constants, and SLAT is sea level air temperature.

The values of f_2 and f_3 control the amplitude of the sea level air temperature time series. Two time series were developed because of the uncertainty about air temperatures during the Weichselian. One time series was scaled so that the minimum temperature (at 18 kyears BP) was -10°C, while the second was scaled to give a minimum temperature of -5°C . The sea level air temperature was not varied along the flowline because no data is available from which to estimate such variations in the past. The present day sea level air temperature in Scandinavia was taken as a uniform 6 °C (on the basis of data in Wallen 1970). The form of the sea level air temperature is a again a reflection of the Rockall trough sea surface temperature record. The two curves are shown in Figure 4.2. Air temperature data provided by Lundqvist (pers. comm.) for Stockholm and Östersund at 100 kyears BP fall between the values on the -5 and -10 °C time series, providing some justification for their use.

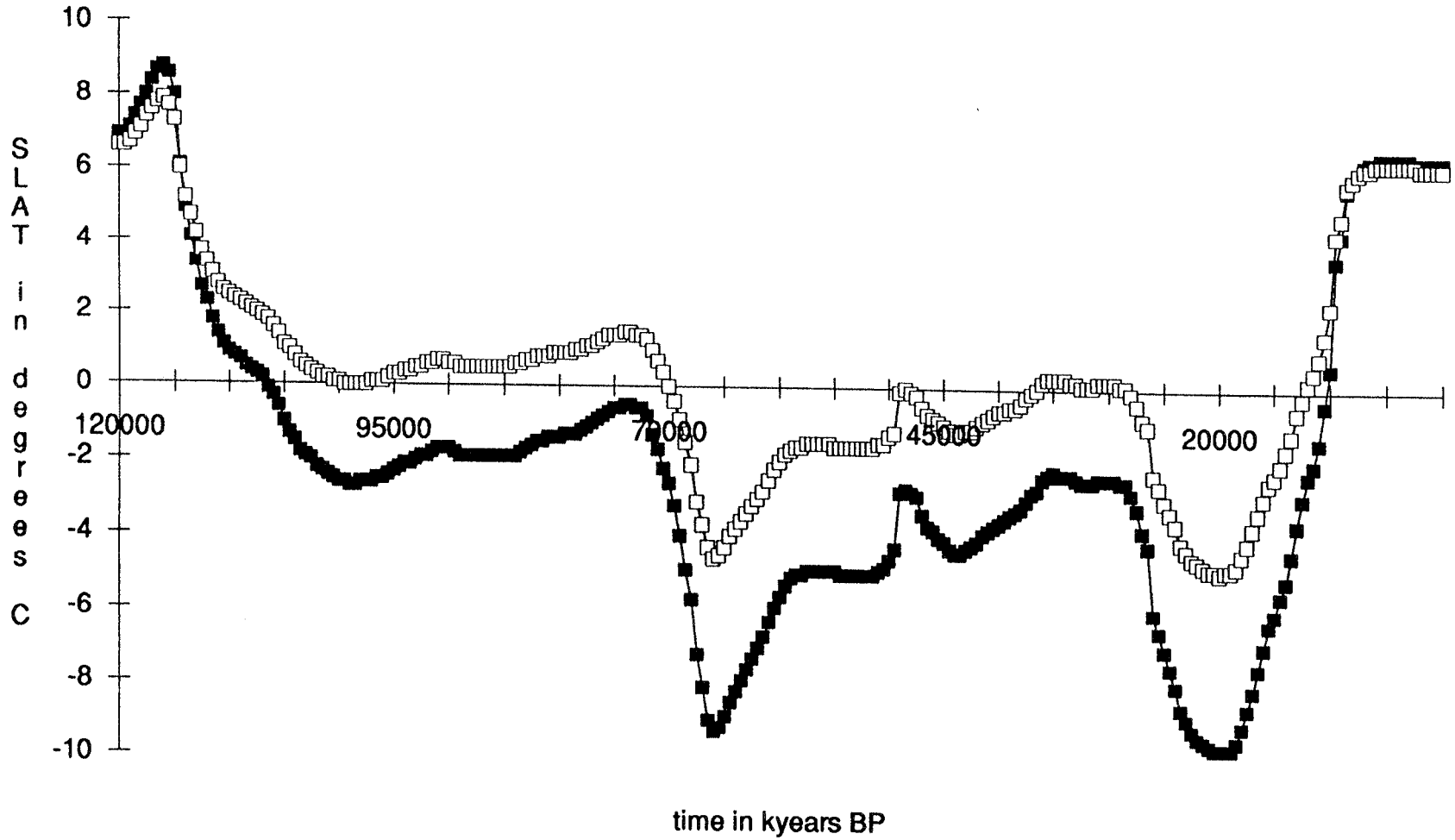

Figure 4.2 The sea level air temperature curves used to force the model. The open squares show the series with a -5°C sea level mean annual temperature at the glacial maximum, the black squares show the series with a -10°C sea level mean annual temperature at the glacial maximum.

5 THE APPLICATION OF THE MODEL TO THE WEICHSELIAN GLACIATION.

The ice sheet model is driven by the ELA function established for the last glacial cycle. The model reconstructs ice sheet thickness, ice sheet temperature distribution, including basal temperature, basal melting pattern and velocity distribution. Some tests were undertaken to establish the sensitivity of the basal temperature/melting distribution, and the distribution of permafrost below and beyond the ice sheet to variations in the assumptions used about surface temperature. It was found that the reconstruction was relatively insensitive to these assumptions, and that a robust prediction of the model is of a very broad zone of basal melting between a narrow terminal frozen zone and a few 10s of kilometres in width, and a zone freezing beneath the ice divide.

..... ***** .....

5.1 SUMMARY OF WEICHSELIAN RESULTS.

This chapter presents the results of the Weichselian simulation. These are presented in two types of figure. The first is the time-space diagram, which shows the distribution of a particular ice sheet variable along the model flowline and its variation through time. The second is a cross-section through the Weichselian maximum ice sheet. Results are given for ice sheet thickness, surface elevation, temperature, basal melt rate, velocity, geothermal heat flux and permafrost depth.

The results from two sets of model runs are presented. The first set uses the model without bedrock temperature calculations, while the second set includes bedrock temperature evolution. Each set in turn comprises two runs using the different sea level air temperature time series described in section (4.4).

The prediction is of a series of three ice sheet maxima, which increase in their span from 420 km at 90 kyears BP, to 1100 km at 40 kyears BP, and finally to 1540 km at 12 kyears BP. All four model runs predict similar patterns of thickness, velocity and temperature variation. Features worthy of particular note are:

- the maximum predicted thickness of 2500 m is reached at 12 kyears BP;

- it is only during the final (12 kyears BP) maximum that significant divide migration occurs; this is to a position 260 km East of the original divide over the Jotunheimen mountains;

- there is a broad outer band of basal ice at pressure melting point during all of the ice sheet's history;

- vertically averaged horizontal velocity never exceeds 120 m $year^{-1}$; and

- permafrost may reach a maximum depth of 413 m outside of the ice-covered area, inside of this area permafrost only occurs near the divide.

5.2 THE FORMAT OF THE RESULTS.

Two particular types of figure are presented. The first is the time-space diagram. This plots the distribution of a particular variable along the modelled flowline and its evolution through time.

The x-axis of these plots refers to distance along the flowline in km. This axis runs from the continental slope off of Norway (0 km) to central Poland (1700 km). Along the flowline lie: Kristiansund at 270 km; the Jotunheimen mountains at 408 km; Oslo at 706 km; Jönköping at 978 km; and the island of Bornholm at 1224 km.

The y-axis refers to time in kyears It runs from 120 kyears before the present (BP) at the top of each figure to 0 kyears BP (ie the present) at the bottom. Within the plot, the time-space domain of the ice sheet is shown in the heavy line. Within this domain the time-space distribution of the appropriate ice sheet variable is

contoured. The variables chosen for display are: ice thickness (H, in m); ice sheet surface elevation (H + h, in m); the vertical mean of horizontal velocity ($\bar{u}$, n m year^{-1}); basal ice temperature uncorrected for pressure melting point variation (T, in ^{o}C); and the basal melt rate (S, in mm year^{-1}).

The second type of figure presented is a cross-section through the maximum ice sheet. This shows the distribution of a variable throughout the ice sheet at a particular time. The x-axis of these plots is once again distance along the flowline, running from the continental shelf on the left to central Poland on the right (approximately 1600 km). The y-axis refers to vertical elevation and runs from -850 m to 2800 m. These figures therefore have a vertical exaggeration of approximately 1:206. Two variables are plotted on these cross-sections. The first is ice temperature (T, in ^{o}C), uncorrected for pressure melting point variation. This is presented as a contour plot. The second is ice velocity (in m year^{-1}), which is plotted as a vector field. Both the horizontal and vertical components of velocity (u and w respectively) are shown in these plots. The horizontal velocity is several orders of magnitude larger than the vertical velocity. The length of a particular arrow is therefore made proportional only to the horizontal velocity at the point. The direction in which the arrow points reflects the relative importance of the horizontal and vertical components of velocity. This requires that vertical motion is exaggerated, and the exaggeration factor used is the same as that of the ice sheet form (1:206).

5.3 RESULTS FROM THE MODEL WITHOUT BEDROCK TEMPERATURE CALCULATIONS.

The results in this section were obtained using the ice sheet model described in chapter 2 without the calculation of temperature within the underlying bedrock, instead a constant geothermal heat flux was applied to the ice/bedrock interface. The results from two model runs will be described. These runs use different air temperature forcing (as outlined in section 4.4), which reach minimum sea level air temperatures of -5 ^{o}C and -10 ^{o}C respectively. Figures showing various aspects of the model's predictions are listed in Table 5.1.

Table 5.1 Figures relating to the results of the model without temperature calculation in the underlying bedrock.

Figure	Type of plot	Variable plotted (units)	Forcing
5.1	time-space	thickness (m)	-5 ^{o}C
5.2	time-space	thickness (m)	-10 ^{o}C
5.3	time-space	ice sheet surface elevation (m)	-5 ^{o}C
5.4	time-space	ice sheet surface elevation (m)	-10 ^{o}C
5.5	time-space	basal ice temperature (^{o}C)	-5 ^{o}C
5.6	time-space	basal ice temperature (^{o}C)	-10 ^{o}C
5.7	time-space	basal melt rate (mm year^{-1})	-5 ^{o}C
5.8	time-space	basal melt rate (mm year^{-1})	-10 ^{o}C
5.9	cross-section	ice temperature (^{o}C)	-5 ^{o}C
5.10	cross-section	ice temperature (^{o}C)	-10 ^{o}C
5.11	time-space	vertically averaged horizontal ice velocity (m year^{-1})	-5 ^{o}C
5.12	time-space	vertically averaged horizontal ice velocity (m year^{-1})	-10 ^{o}C
5.13	cross-section	ice velocity (m year^{-1})	-5 ^{o}C
5.14	cross-section	ice velocity (m year^{-1})	-10 ^{o}C

Figures 5.1 and 5.2 show the predicted variation of ice sheet thickness during the Weichselian. The patterns produced using the two sea level air temperature time series are very similar. Three maxima are predicted, at 90, 40 and 12 kyears BP. These are associated with three phases in the equilibrium line depression time series used to drive the model (Figure 4.1).

The first maximum is relatively small (a span of 420 km) and corresponds to the initial equilibrium line altitude lowering of 410 m. The near stationary equilibrium line altitude during the period 105 to 80 kyear BP is associated with ice thicknesses which vary little through time. The period of falling equilibrium line altitude at 70 kyears BP initiates sustained growth lasting 30 kyears.

The maximum extent at 40 kyears BP is 1100 km and is reached some 35 kyears after the maximum equilibrium line depression. This delay is a measure of the strength of the feedback between mass balance and ice sheet thickness (see section 4.3). Although the equilibrium line altitude is rising during most of this period, growth is sustained because a sufficient amount of the ice sheet is above the

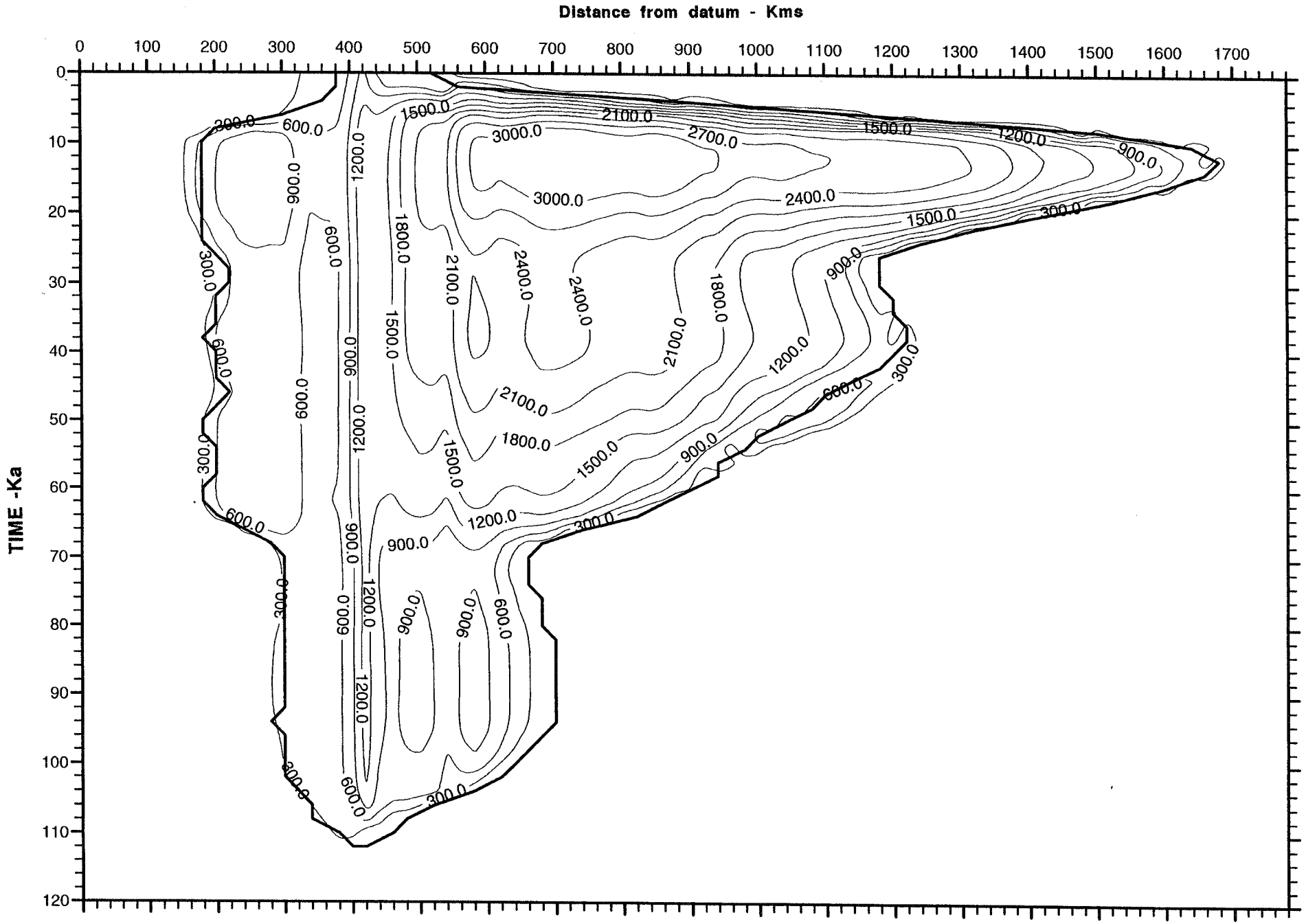

Figure 5.1 Time distance diagram showing predicted variation of thickness (m) during the last glacial cycle (Weichselian) along the standard transect from the western Norwegian continental shelf to northern Poland using the -5^{0}C air temperature time series and without bedrock temperature calculations.

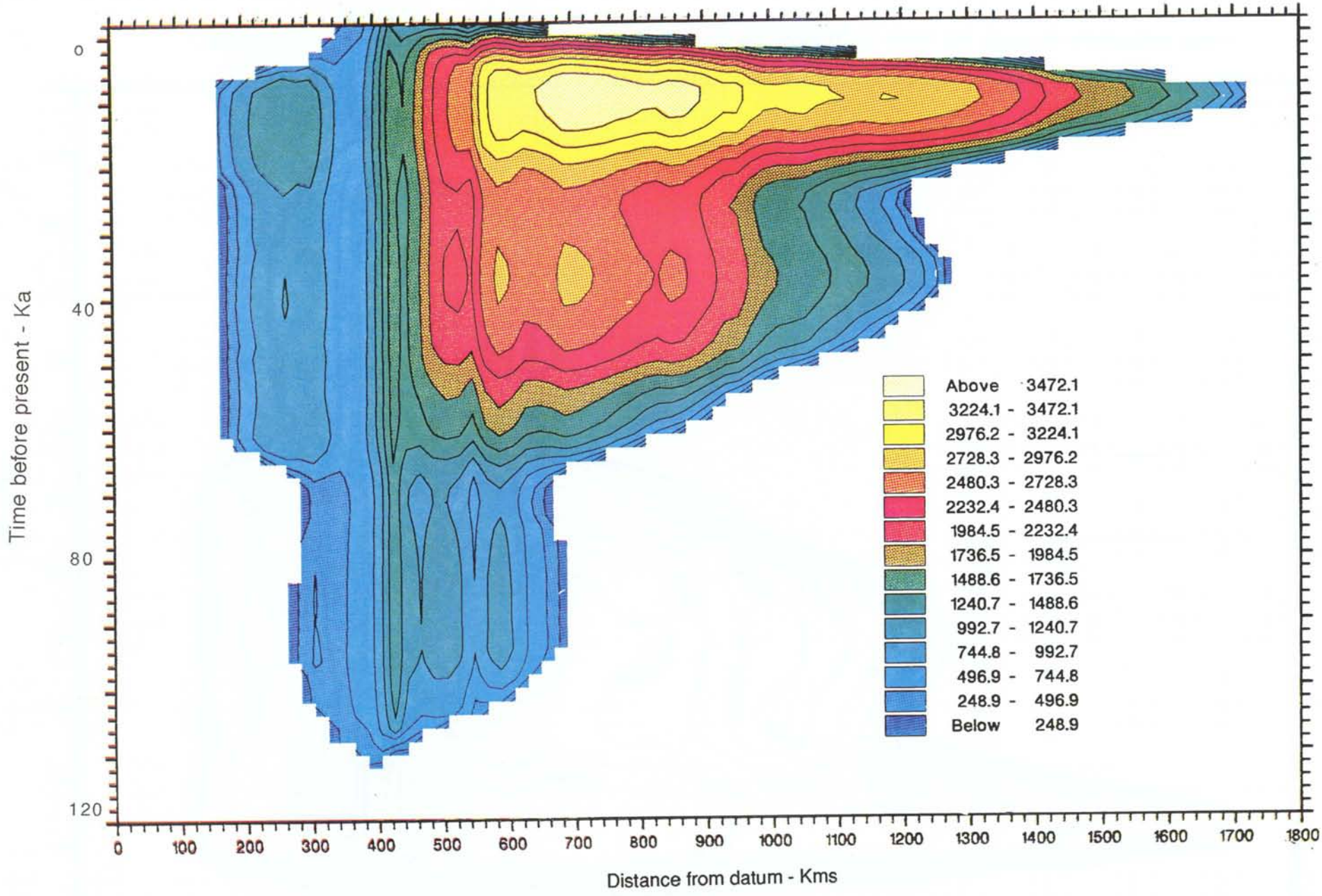

Figure 5.1a W-E TRANSECT EUROPEAN ICE SHEET -THICKNESS- m

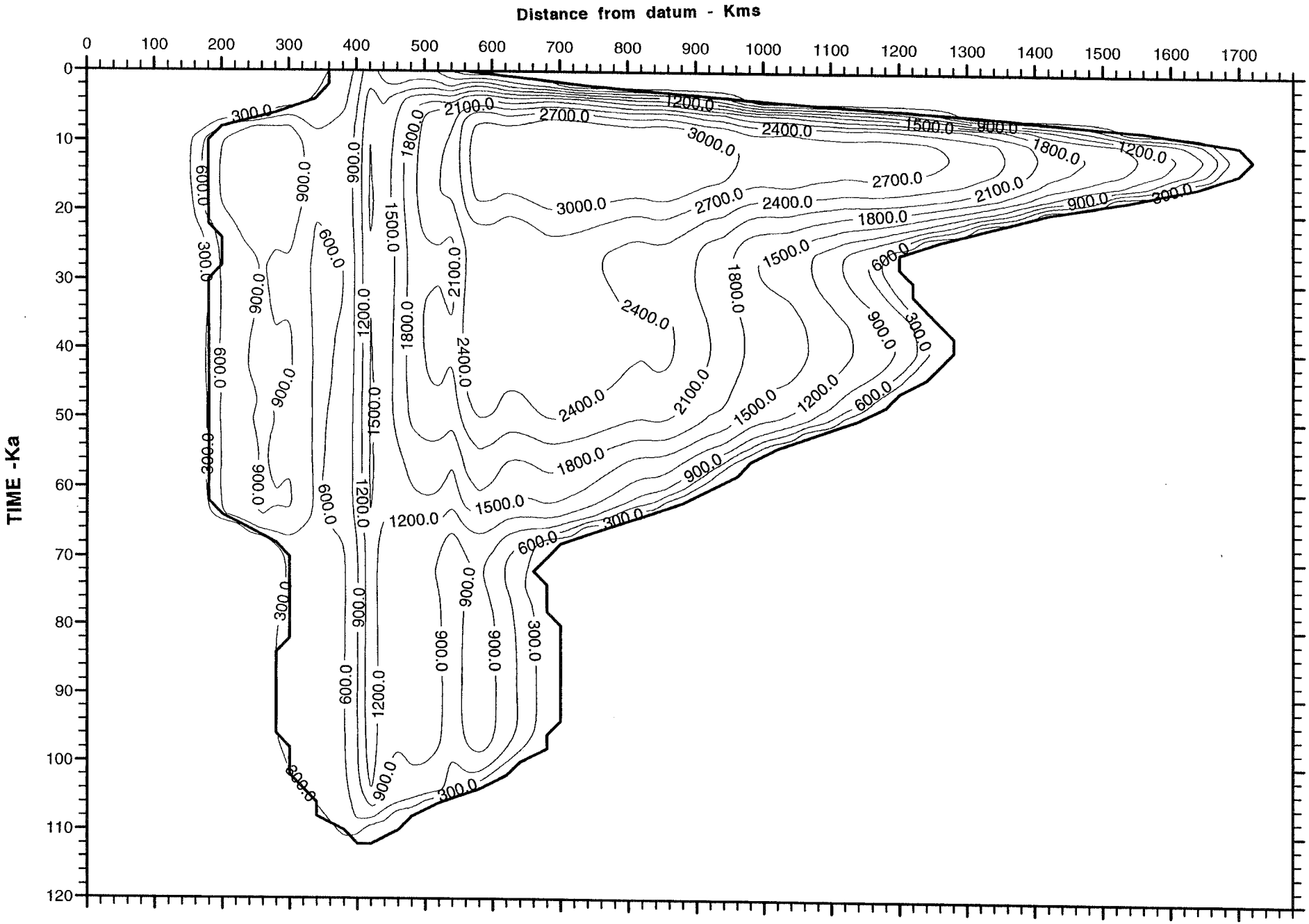

Figure 5.2 **Predicted variation of thickness (m) during the Weichselian using the -10°C air temperature time series and without bedrock temperature calculations.**

equilibrium line altitude. This growth is only reversed when the equilibrium line depression falls below 420 m.

The final phase of growth starts at 26 kyears BP and corresponds to a rapid fall in the equilibrium line altitude. The Weichselian maximum is achieved some 14 kyears afterwards and has a span of 1540 km. This maximum is larger (140%) than the previous maximum but is achieved by much the same size of equilibrium line depression. This is because the volume of ice at the start of the final growth phase is far larger than at the start of the previous growth phase.

The maximum ice thicknesses occur during this final maximum and are in excess of 3200 m. The two runs differ slightly because of their different air temperature forcing. The colder run tends to have cooler ice temperatures (as described latter), ice flow is therefore more sluggish and greater thicknesses of ice build up. The slight difference between the two predicted thickness distributions is thus a consequence of the coupling between ice temperature, flow and thickness (see section 2.2.3).

The behaviour of the western margin is constrained by the marine boundary condition used in the model (section 2.3.4); the margin is held at the continental slope. The eastern margin is, n contrast, free to expand because the Baltic Sea is shallower than the crucial 500 m used as the ice sheet cut off point. The dynamics discussed below therefore centre on the advance and retreat of the eastern sector of the ice sheet.

Figures 5.3 and 5.4 show the corresponding evolution of the ice sheet surface elevation. Again the slight differences between the two runs reflect the coupling between temperature and flow, producing thicker ice with a higher surface altitude in the cooler run. It is interesting to note that this extra thickness of ice is not fully accommodated by increased bedrock lowering via isostasy. This is because of the longer time scales over which the isostasy diffusion equation operates (equation 2.12) and illustrates the fact that the predicted bedrock depression at the Weichselian maximum is not in equilibrium with the ice loading.

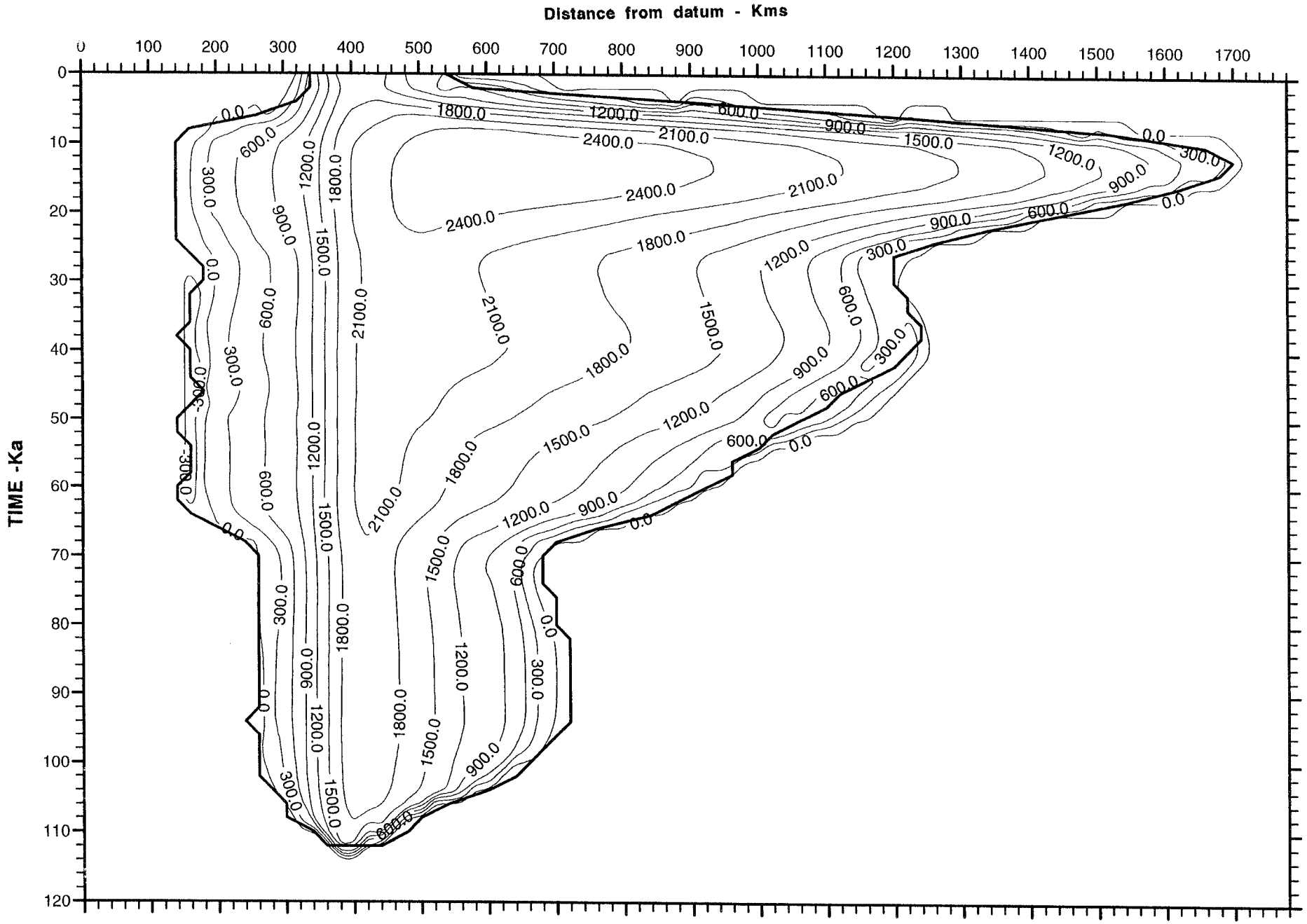

Figure 5.3 **Predicted variation of surface elevation (m) during the Weichselian using the -5°C air temperature time series and without bedrock temperature calculations.**

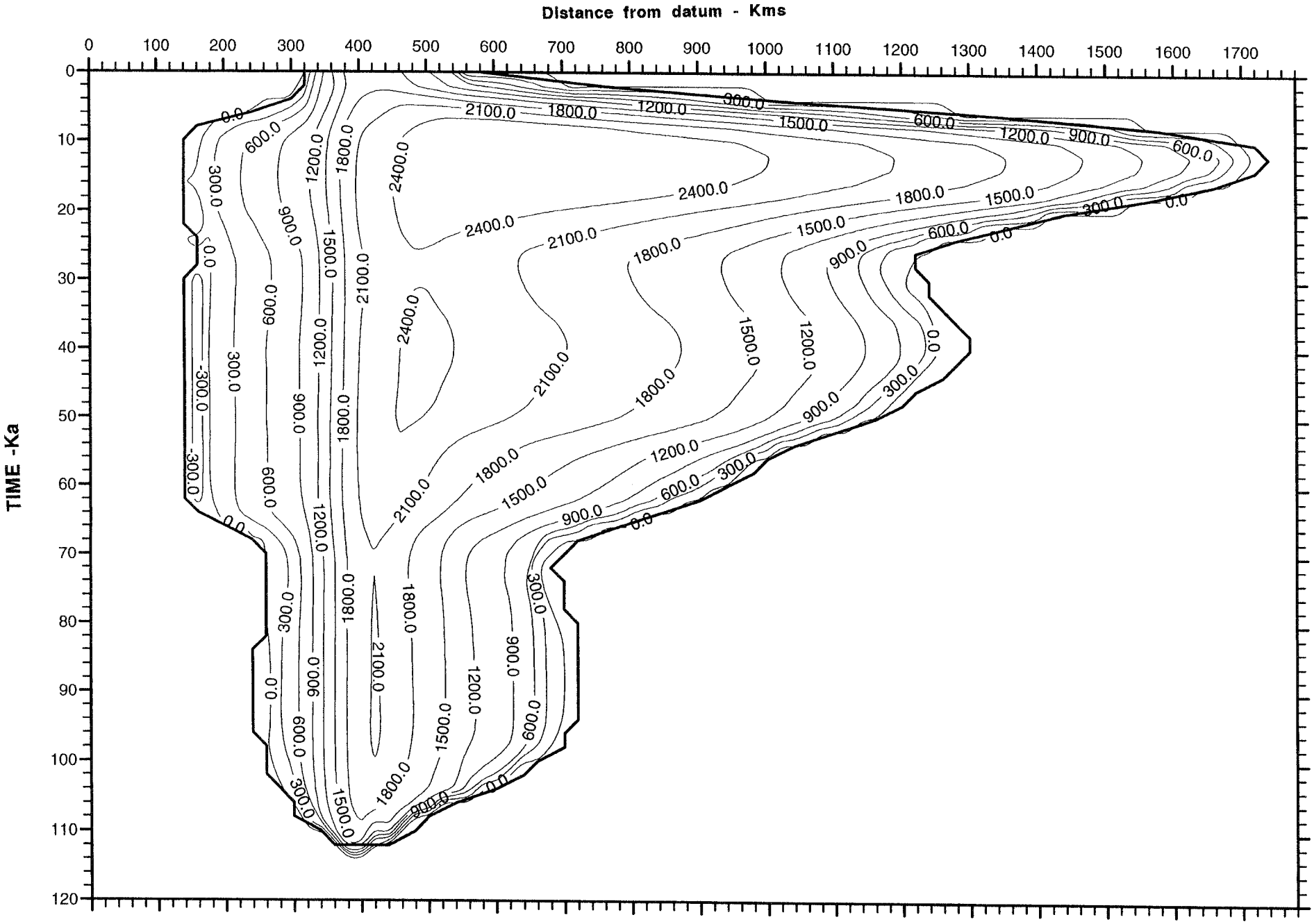

Figure 5.4 **Predicted variation of surface elevation (m) during the Weichsellan using the -10°C air temperature time series and without bedrock temperature calculations.**

Figures 5.3 and 5.4 can be used to investigate the history of ice divide migration through the Weichselian. The divide stays close to the seeding area in the Jotunheimen mountains during most of the first 90 kyears of the model run. The middle Weichselian maximum causes the divide to migrate some 60 km to the East. It is not until the late Weichselian maximum that significant migration occurs, when the divide moves rapidly East by over 260 km in 8 kyears. In both runs a maximum surface elevation in excess of 2500 m is predicted.

Figure 5.5 and 5.6 show the basal temperature evolution predicted by the model. The temperatures shown are not corrected for the pressure melting point variation caused by varying thicknesses of ice overburden.

The general spatial pattern is of a broad band of warm ice, which stretches from the margin towards the divide, behind which is a band of cooler ice. The rate of temperature variation with distance from the margin is initially very slow but becomes far more rapid as the divide is approached. This pattern accords with that found by other workers (for instance Sugden 1977, Huybrechts and Oerlemans 1988 and Hindmarsh and others 1989). It is caused by:

- the large amount of strain heating near the margin (in the rapid ice flow zone), which decreases towards the divide; and

- the increased rate of cold ice advection near the divide.

The mechanics of these processes are detailed in section (2.2.3).

This general pattern is maintained despite the expansion and contraction of the ice sheet. Two further features are, however, introduced when one considers temporal variation. The first is that the margin of the ice sheet appears to be able to move faster than the various temperature zones. The expansion of the ice sheet therefore leads to a disproportionate increase in the fraction of the span which has warm basal ice. Although the zone of cool ice expands, it does so at a far slower pace. This is evidence that the predicted thermal regime of the ice sheet is not in equilibrium with the form of the ice sheet. The rapidly changing ice sheet extent does not allow sufficient time for the internal temperature structure of the ice sheet to come into equilibrium.

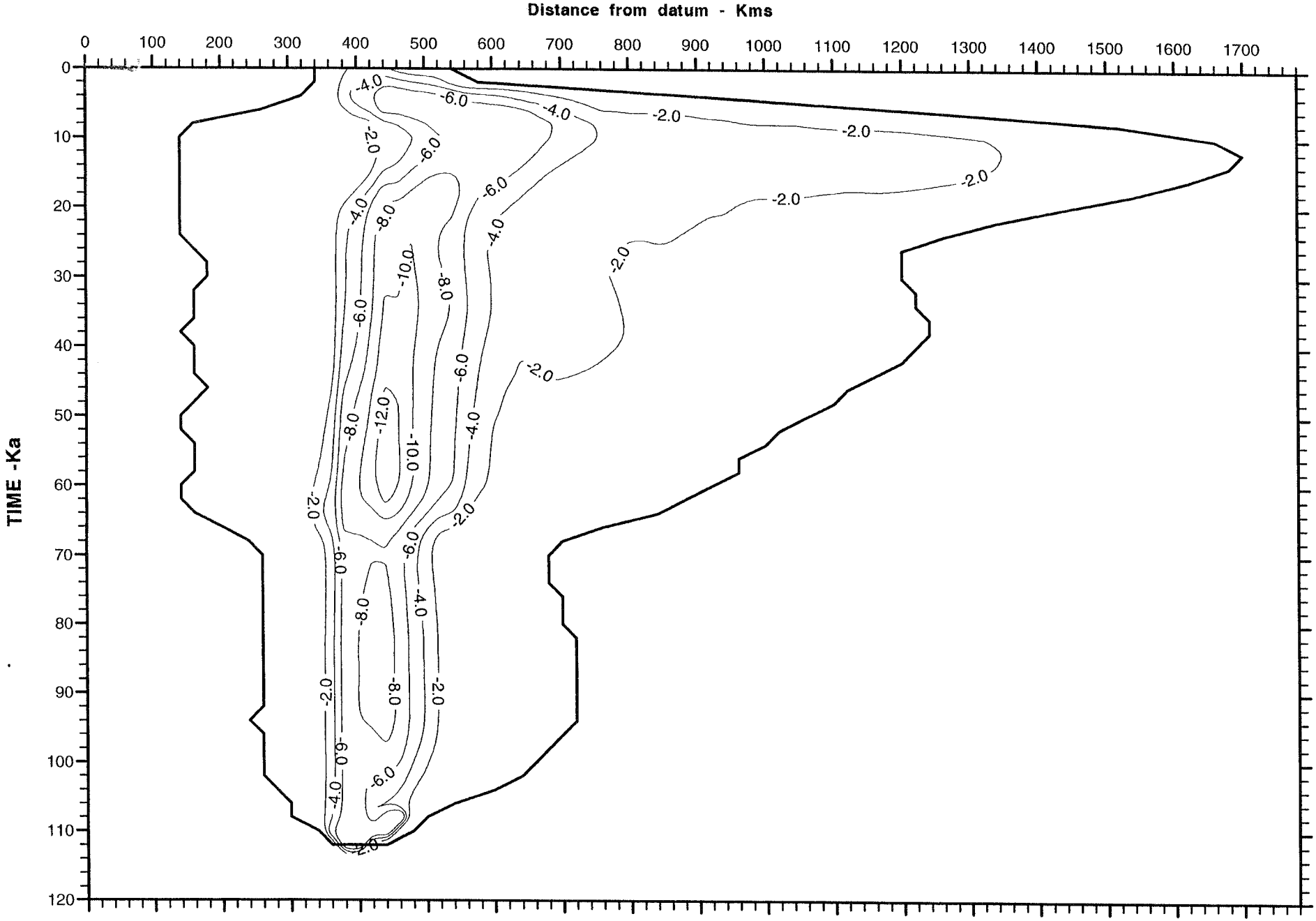

Figure 5.5 Predicted variation of basal ice temperature (^{o}C)during the Weichselian using the -5^{o}C air temperature time series and without bedrock temperature calculations.

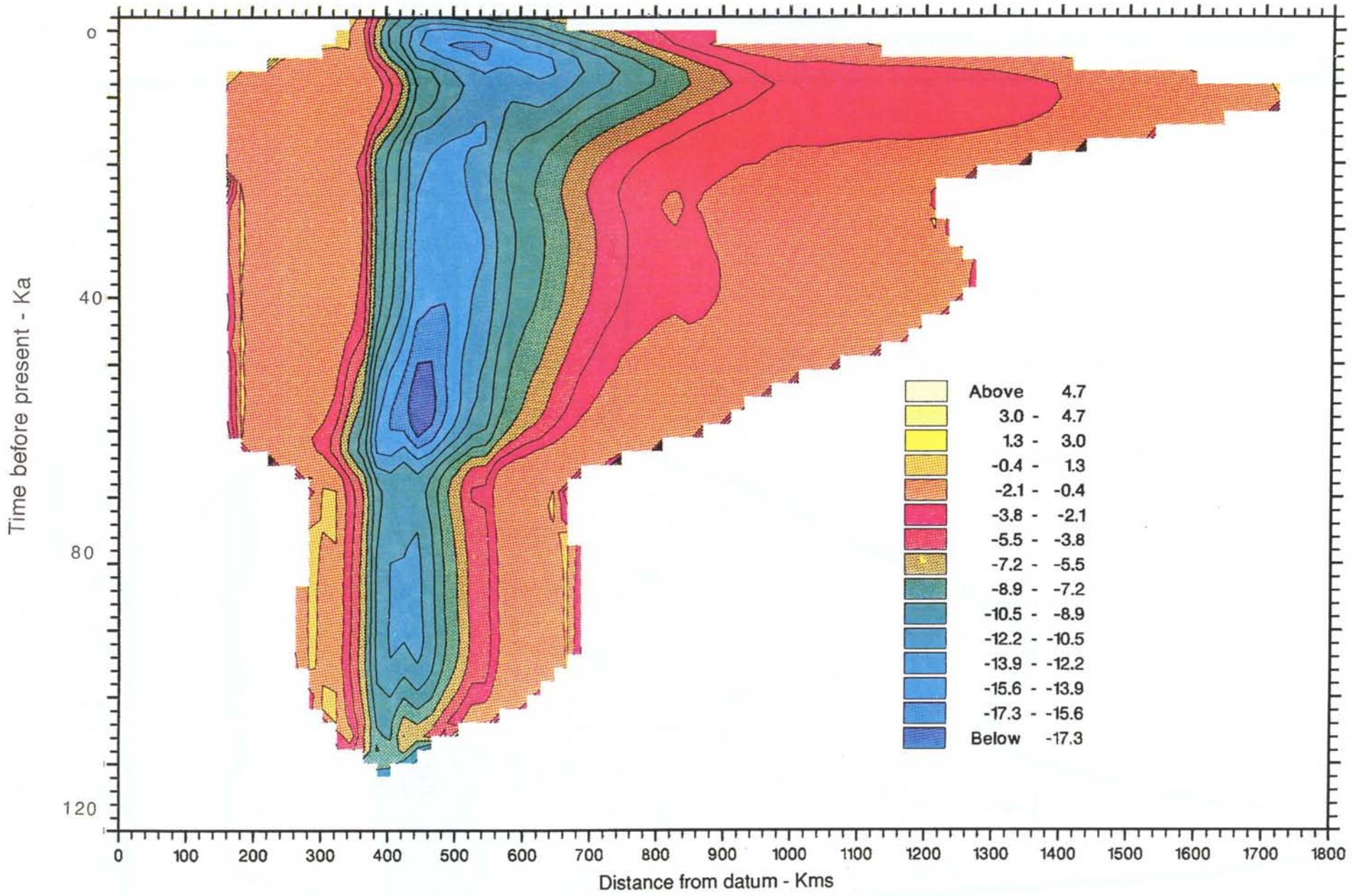

Figure 5.5a W-E TRANSECT EUROPEAN ICE SHEET-BASALTEMPERATURE

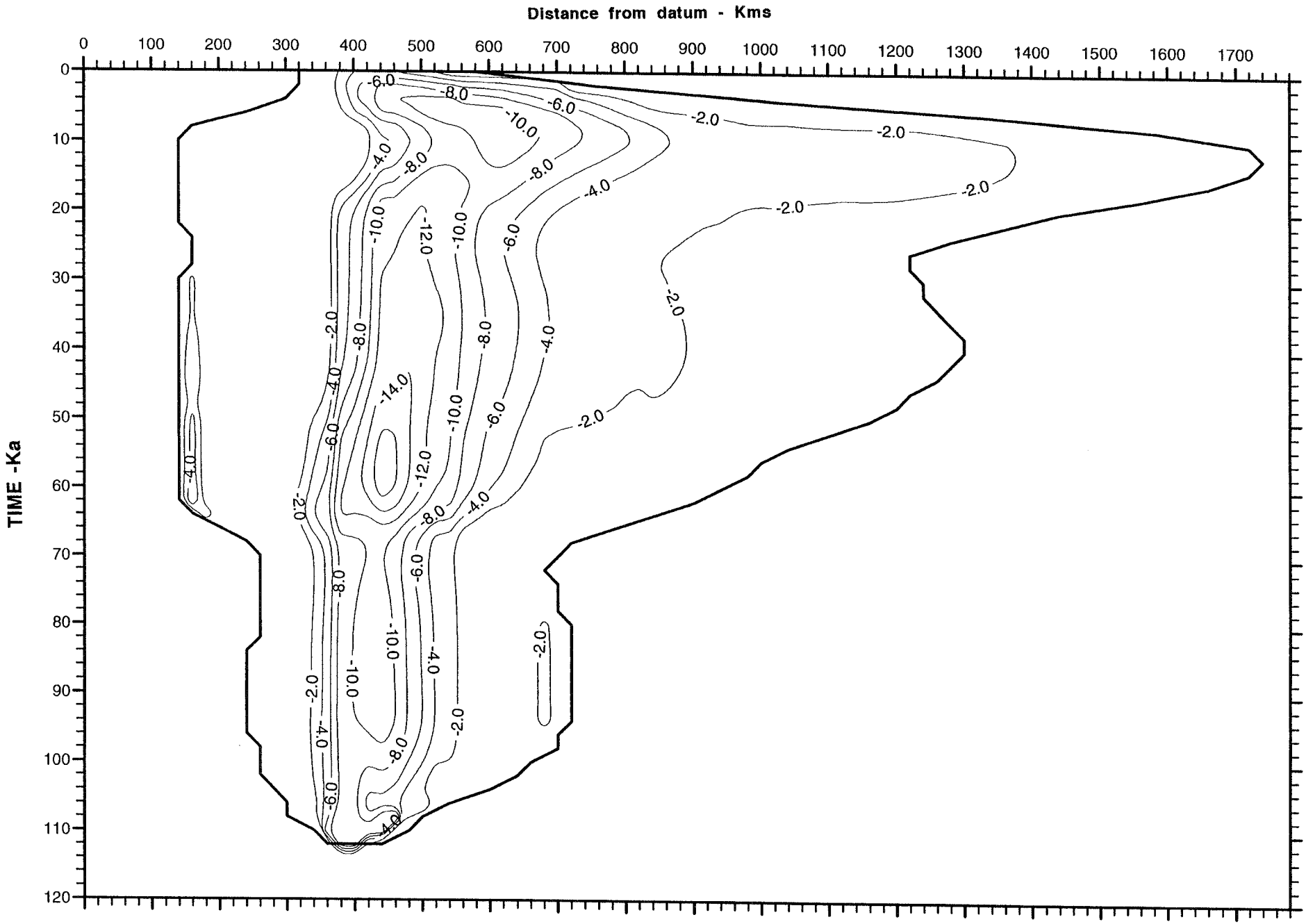

Figure 5.6 **Predicted variation of basal ice temperature (^{o}C)during the Weichselian using the -10^{o}C air temperature time series and without bedrock temperature calculations.**

The second temporal feature is that the lowest basal temperatures are felt some time after the corresponding minimum in the air temperature time series. For instance, the air temperature minimum at 75 kyears BP leads to a basal ice temperature minimum under the divide some 20 kyears later. This is caused by the slow rates of vertical ice advection at the divide; a long time is needed for the wave of cooler ice to migrate from the ice sheet surface to the bed. This feature is not observed during the 18 kyears BP air temperature minimum because the ice sheet has disappeared before the wave of cool ice can reach the ice sheet bed.

The differences between the two air temperature time series runs are not great. In fact the response in the zone behind the margin appears to be identical. This is because basal ice temperatures in this zone are principally controlled by strain heating and by local pressure melting. These factors buffer the basal temperature against variation in air temperature. In the cold ice zone towards the divide it is clear that basal ice temperature does respond to air temperature variation. Minimum basal ice temperatures of -12 and -15 ^{o}C are respectively obtained in the -5 and -10 ^{o}C air temperature runs. These minima occur between 60 and 50 kyears BP.

The patterns of basal melt associated with these temperature distributions are shown in Figures 5.7 and 5.8. They are remarkably similar, given the different air temperature time series used in the model runs. This is because of the temperature buffering mentioned above. The two model runs have slightly different predicted spans throughout the Weichselian, once this is taken into account the actual width of the basal melt zone in the two runs is virtually identical. The maximum value of 4.2 mm year^{-1} reflects the situation where all of the available geothermal heat input to the basal ice layer is used in basal melt.

Figures 5.9 and 5.10 show cross-sections through the temperature structure of the predicted Weichselian maximum ice sheet (12 kyears BP). The vertical structure within the ice sheet owes much to the air temperature boundary condition at the ice sheet surface and so differences between the two runs are greater than they were for the basal temperatures. The overall pattern is similar to that found in previous studies (for instance Sugden 1977, Huybrechts and Oerlemans 1988 and Hindmarsh and others 1989).

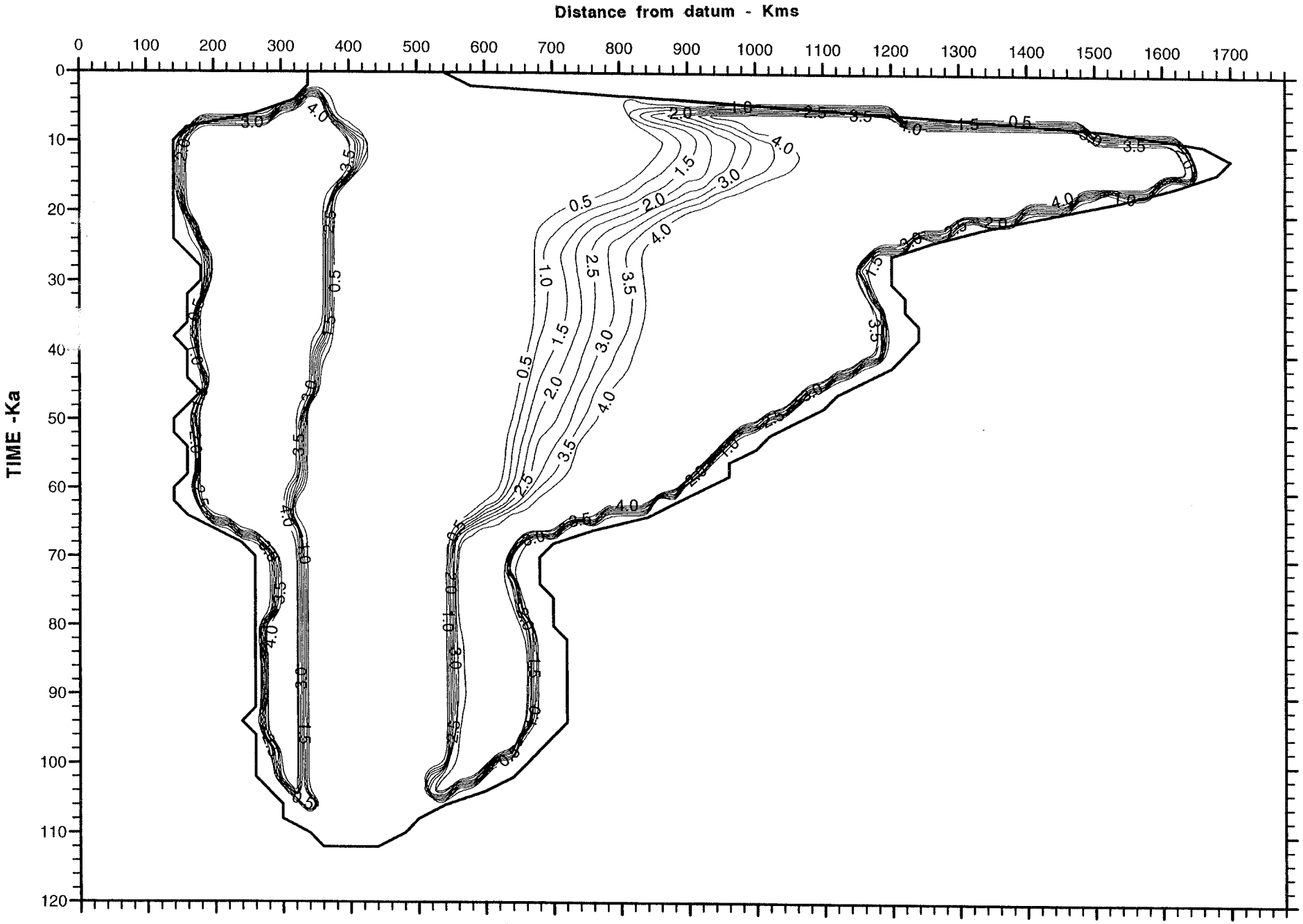

Figure 5.7 Predicted variation of basal melt rate (mm year^{-1}) during the Weichselian using the -5°C air temperature time series and without bedrock temperature calculations.

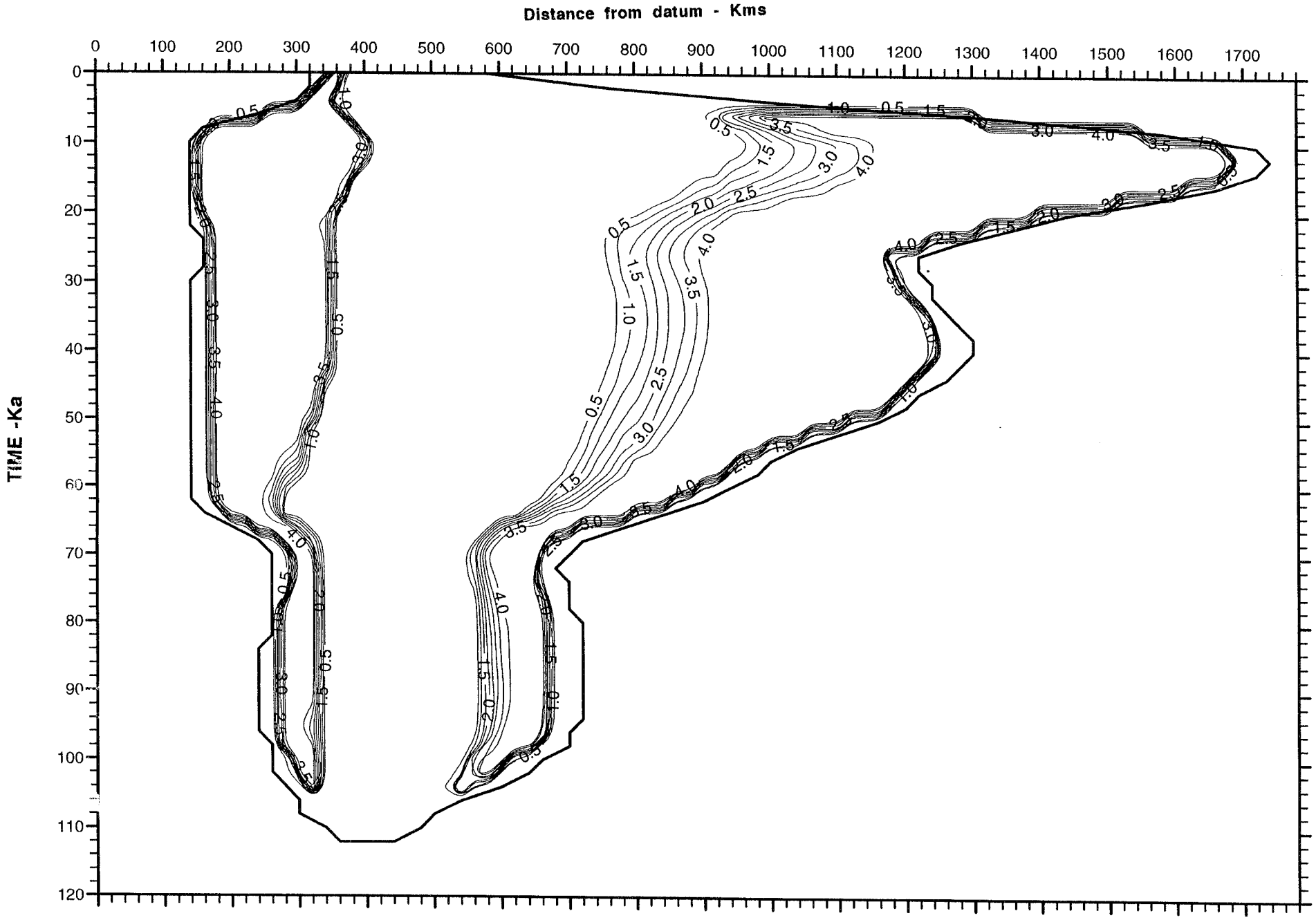

Figure 5.8 Predicted variation of basal melt rate (mm year^{-1}) during the Weichselian using the -10^{o}C air temperature time series and without bedrock temperature calculations.

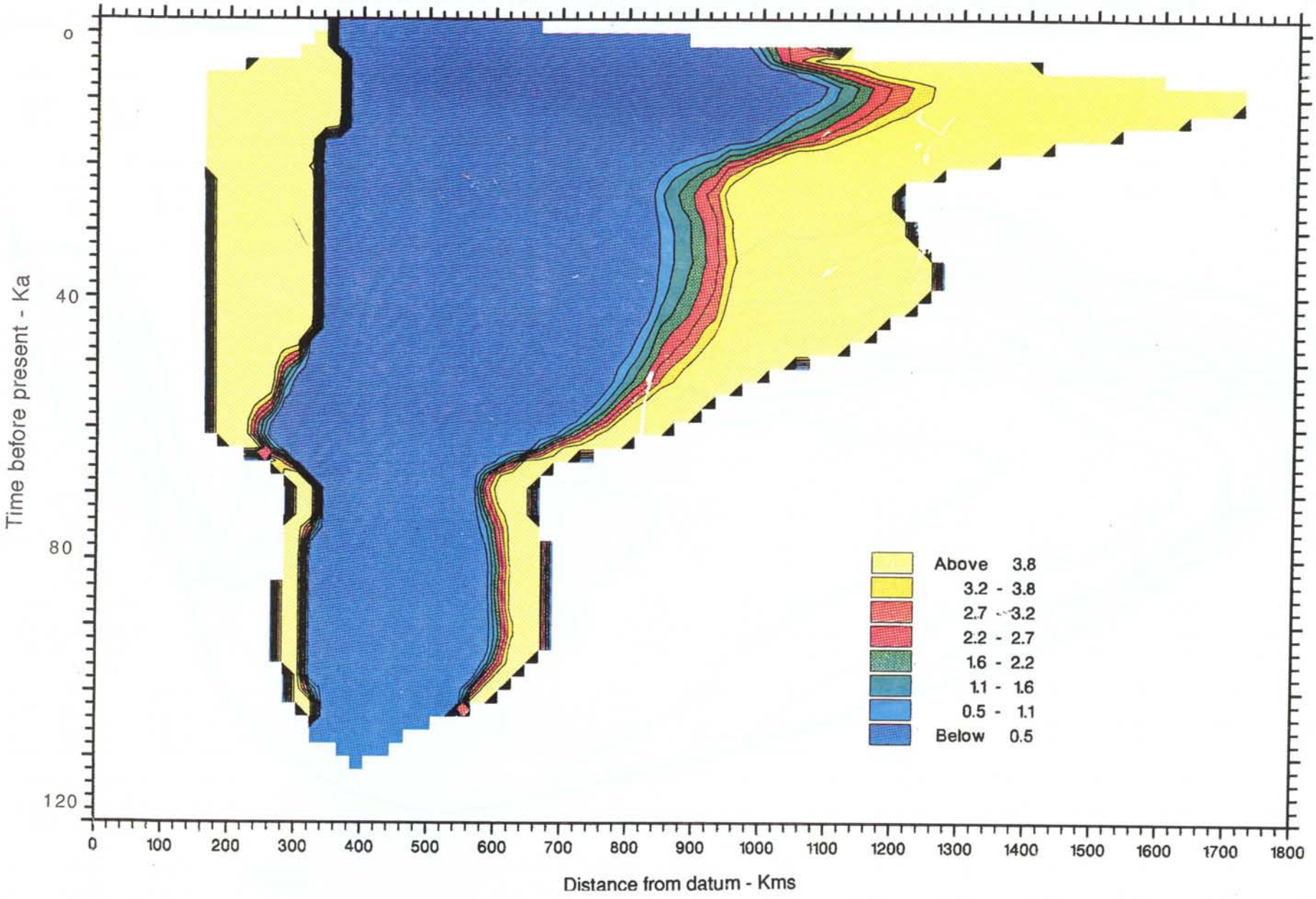

Figure 5.8a W-E TRANSECT EUROPEAN ICE SHEET -BASAL MELTING RATE - cm per year

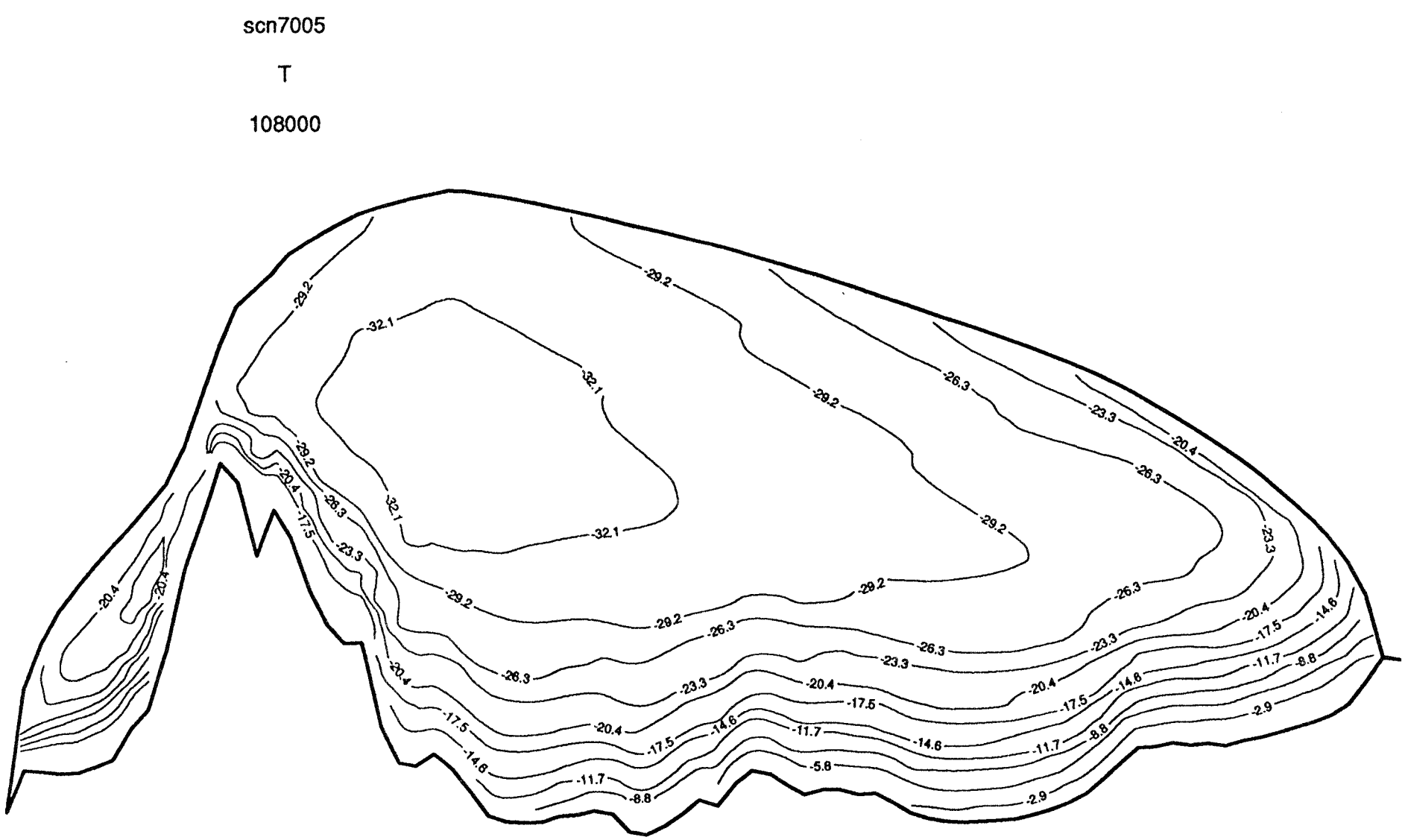

Figure 5.9 The predicted ice sheet temperature field (^{o}C) at the Last Glacial Maximum along the standard transect from thewestern Norwegian continental shelf to Poland using the -5^{o}C air temperature time series and without bedrock temperature calculations.

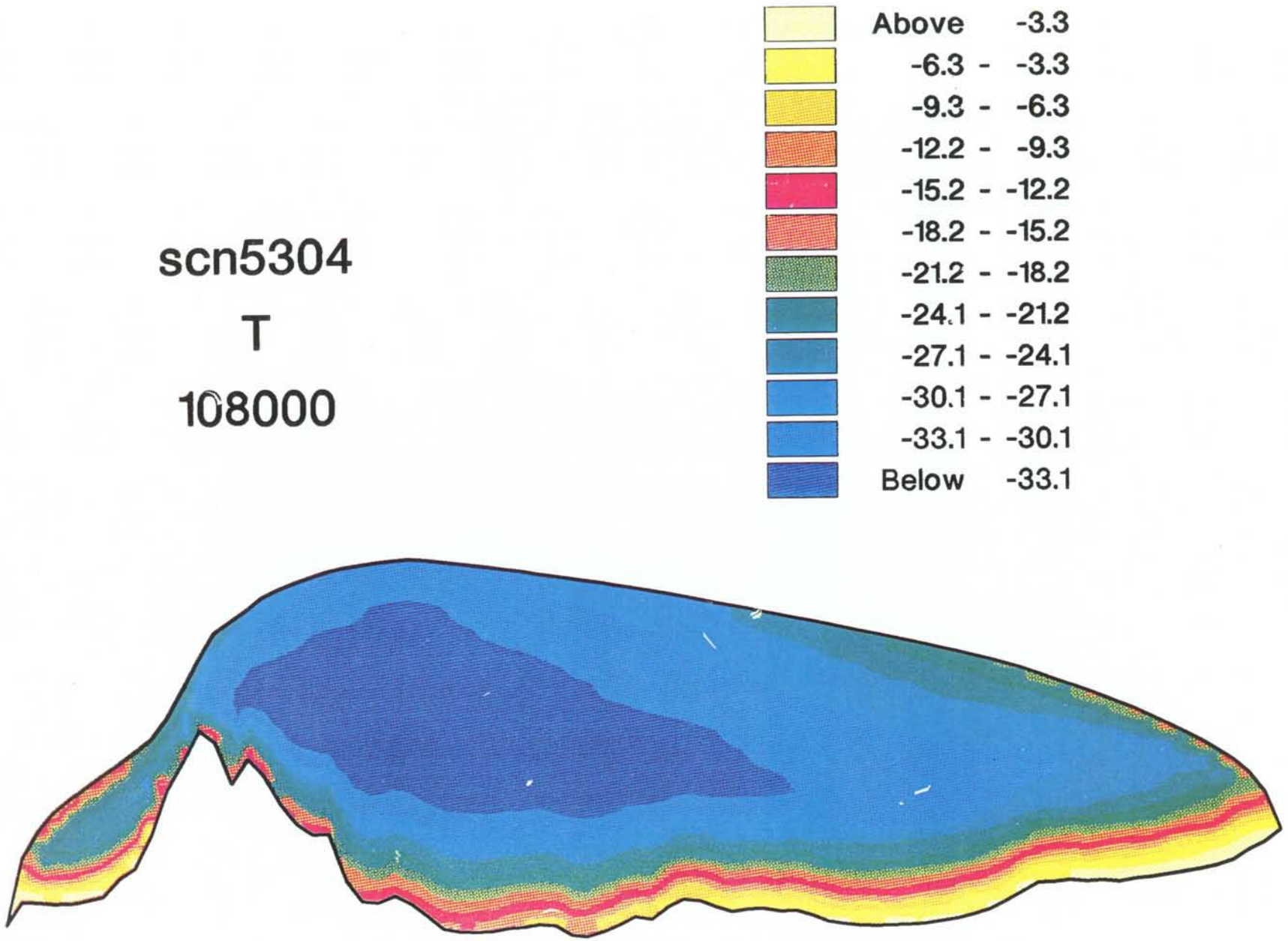

Figure 5.9a W-W-E TRANSECT EUROPEAN ICE SHEET INTERNAL TEMPERATURE

scn7006

T

108000

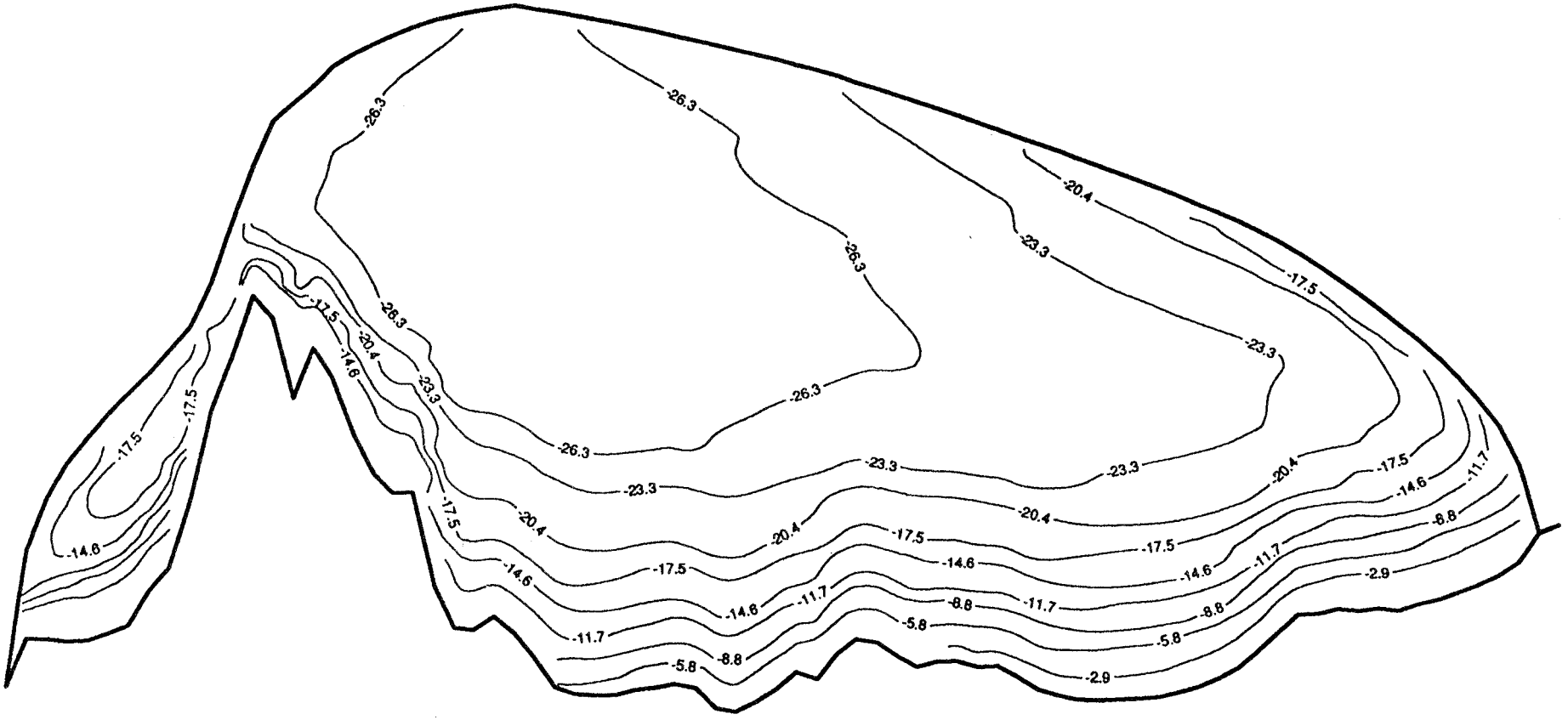

Figure 5.10 The predicted ice sheet temperature field (^{o}C) at the last glacial maximum using the -10^{o}C air temperature time series and without bedrock temperature calculations.

The predicted patterns of vertically averaged horizontal velocity are shown in Figures 5.11 and 5.12. The flow can be divided into three broad zones. Under the divide flow is very slow but gradually increases away from the divide. The flow reaches a maximum approximately 200 km upstream of the margin. This reflects the point where the equilibrium line altitude and the ice sheet surface intersect, it is therefore the point at which the greatest horizontal flux of ice occurs. In both model runs the maximum flow was in excess of 120 m $year^{-1}$. Finally, the flow slows slightly as the margin is approached. This pattern is characteristic of virtually all ice masses (Paterson 1981). The patterns shift through time in response to both margin and divide motion; they do not show the time lags of the basal temperature evolution. In addition, the patterns predicted by the two air temperature runs are very similar.

Figures 5.13 and 5.14 show cross-sections through the velocity field of the predicted Weichelian maximum ice sheet (12 kyears BP). These plots emphasise the extreme slowness of flow near the divide, and show the expected downward flow in the accumulation area and upward flow in the ablation area They indicate that, at a given point along the flowline, velocity does not vary greatly throughout most of the ice thickness. Velocity increases rapidly from the bed to a point at roughly 20% of the ice thickness, and thereafter remains fairly constant. This pattern is caused by the concentration of shear stress at the base of the ice sheet, and by the higher temperatures near the bed.

5.4 RESULTS FROM THE MODEL WITH BEDROCK TEMPERATURE CALCULATIONS.

The results in this section were obtained using the ice sheet model described in chapter 2 complete with the calculation of temperature within the underlying bedrock (see section 2.2.4). The results from two model runs will be described. These runs use different air temperature forcing (as outlined in section 4.4), which reach minimum sea level air temperatures of -5 ^{o}C and -10 ^{o}C respectively. Figures showing various aspects of the model's predictions are listed in Table 5.2.

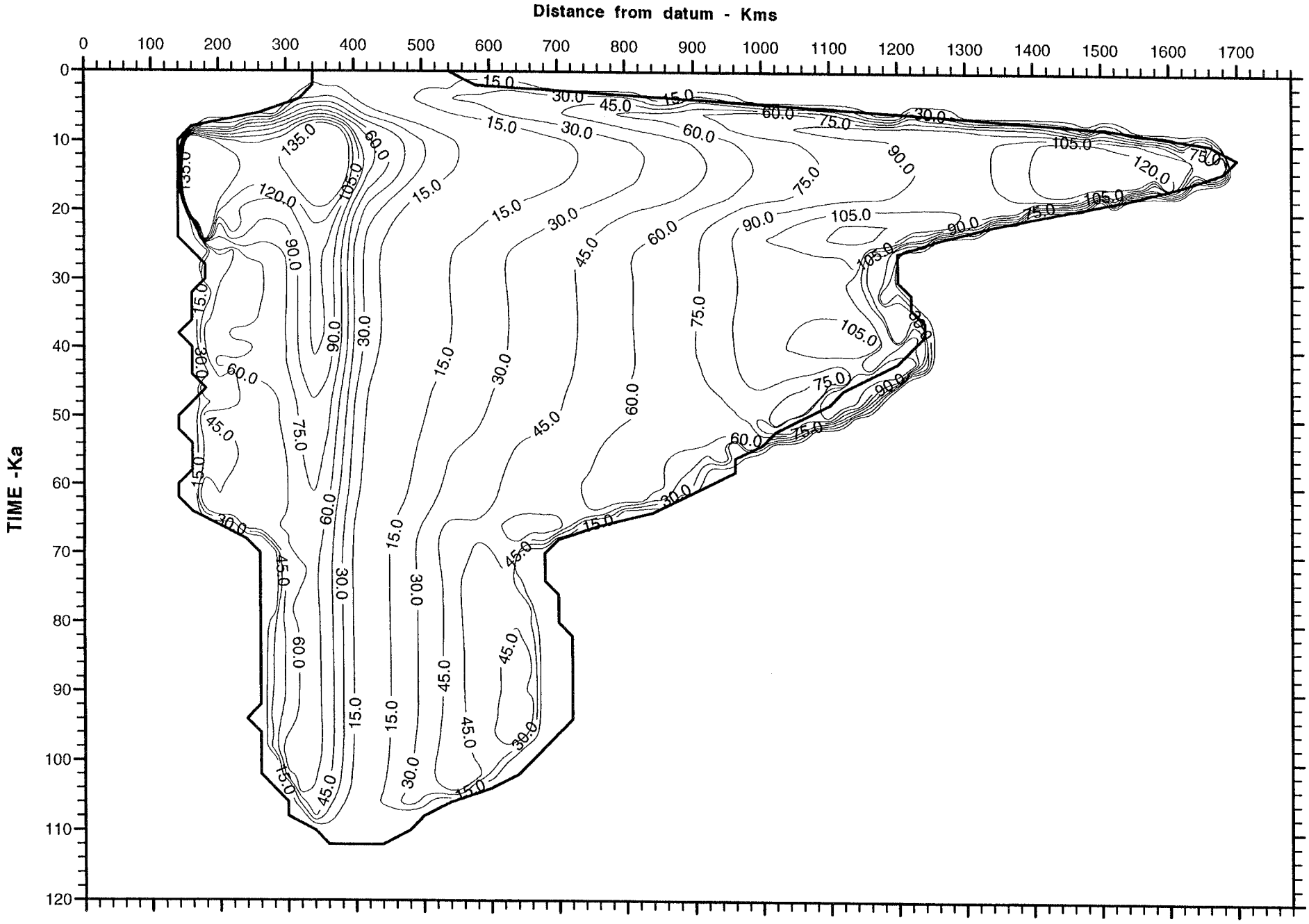

Figure 5.11 **Predicted variation of vertically averaged horizontal ice velocity (m year^{-1}) during the Weichselian using the -5^{o}C air temperature time series and without bedrock temperature calculations.**

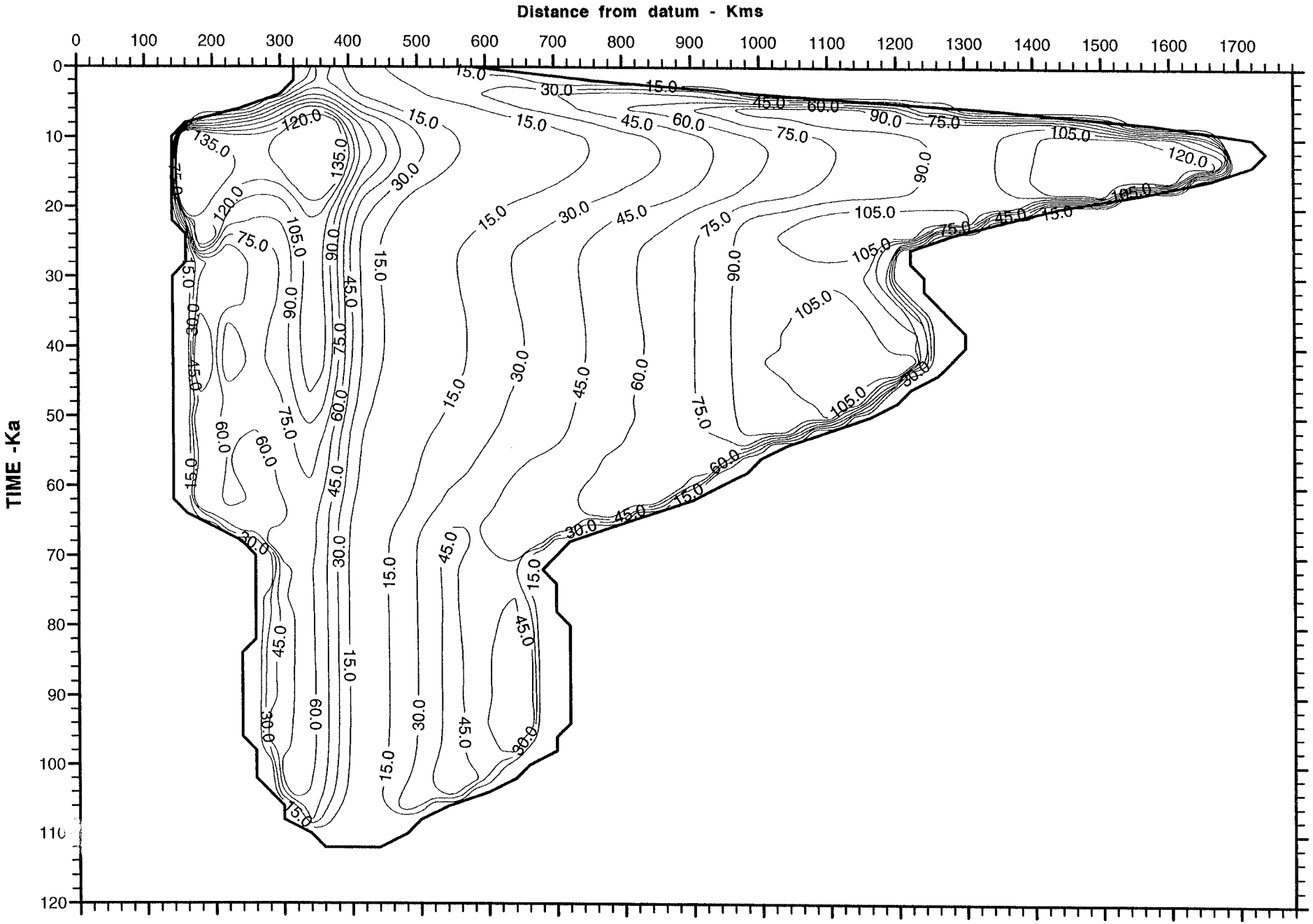

Figure 5.12 Predicted variation of vertically averaged horizontal ice velocity (m year^{-1}) during the Weichselian using the -10°C air temperature time series and without bedrock temperature calculations.

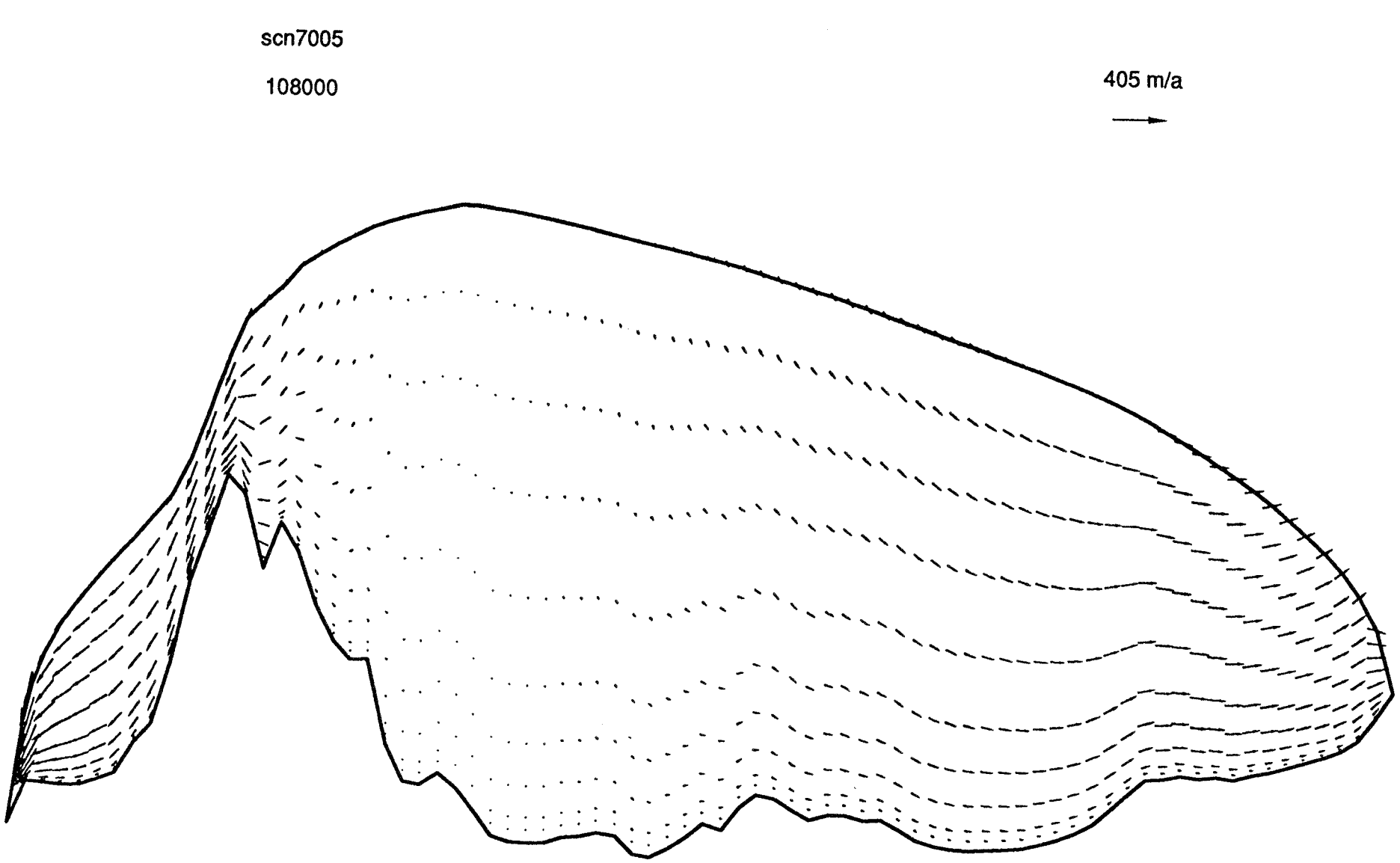

Figure 5.13 The predicted ice sheet velocity field (m year^{-1}) at the Last Glacial Maximum using the -5°C air temperature time series and without bedrock temperature calculations.

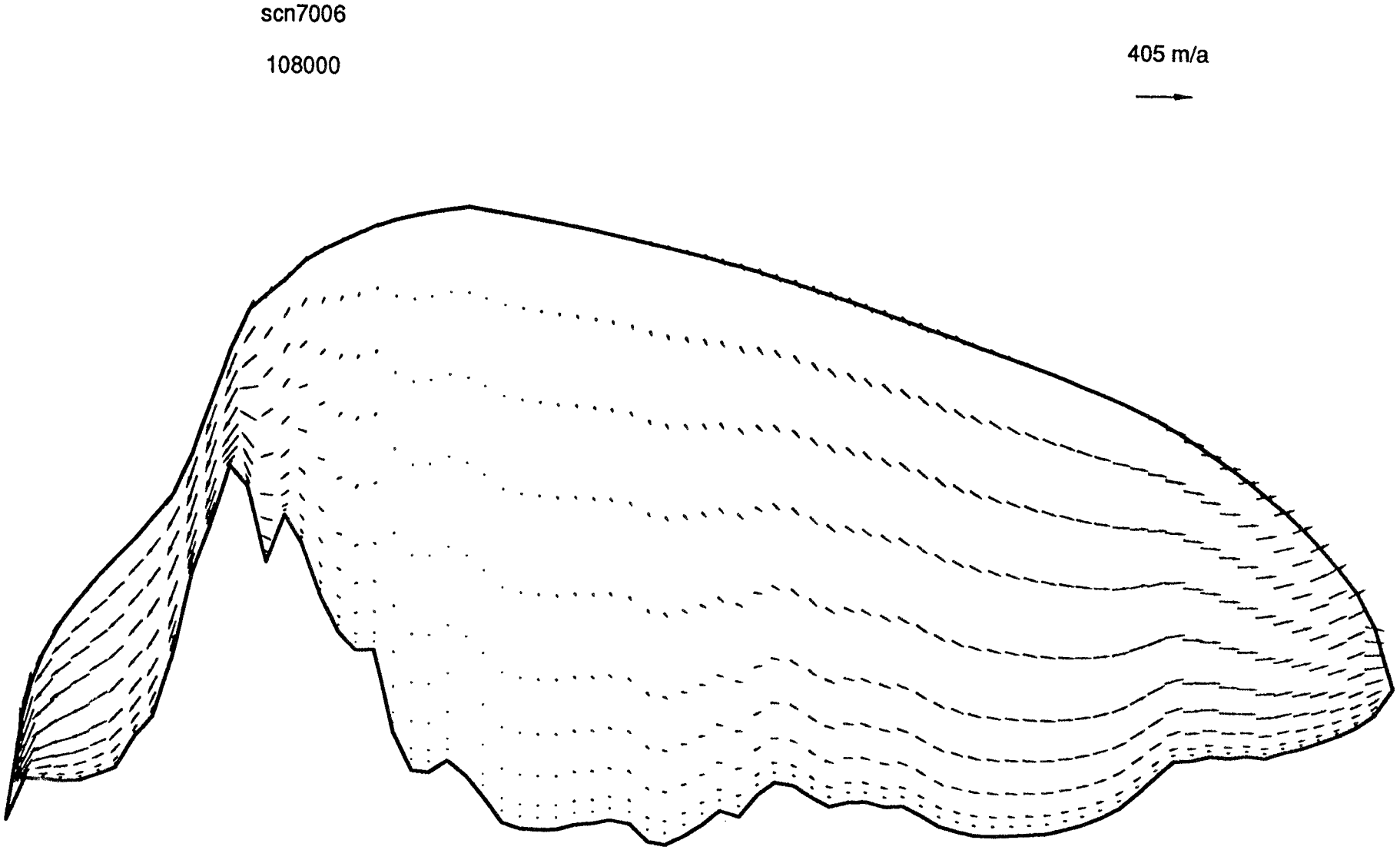

Figure 5.14 The predicted ice sheet velocity field (m year^{-1}) at the Last Glacial Maximum using the -10°C air temperature time series and without bedrock temperature calculations.

Table 5.2 Figures relating to the results of the model without temperature calculation in the underlying bedrock.

Figure	Type of plot	Variable plotted (units)	Forcing
5.15	time-space	thickness (m)	-5 °C
5.16	time-space	thickness (m)	-10 °C
5.17	time-space	ice sheet surface elevation (m)	-5 °C
5.18	time-space	ice sheet surface elevation (m)	-10 °C
5.19	time-space	basal ice temperature (°C)	-5 °C
5.20	time-space	basal ice temperature (°C)	-10 °C
5.21	time-space	basal melt rate (mm $year^{-1}$)	-5 °C
5.22	time-space	basal melt rate (mm $year^{-1}$)	-10 °C
5.23	time-space	geothermal heat flux (mW m^{-2})	-5 °C
5.24	time-space	geothermal heat flux (mW m^{-2})	-10 °C
5.25	time-space	depth of permafrost (m)	-5 °C
5.26	time-space	depth of permafrost (m)	-10 °C
5.27	time-space	vertically averaged horizontal ice velocity (m $year^{-1}$)	-5 °C
5.28	time-space	vertically averaged horizontal ice velocity (m $year^{-1}$)	-10 °C

The coupling between ice temperature and ice flow mentioned in the previous section and in section (2.2.3) implies that, if the ice temperatures are consistently different between two otherwise identical runs then the evolution of the overall ice sheet form may differ between the runs. This is the case when the output of the runs with and without bedrock temperature calculation are compared. If the same equilibrium line depression and sea level air temperature time series are used then the runs including bedrock temperature calculation are consistently warmer and do not reach the desired Weichselian maximum extent. The reasons for this are:

- the inclusion of bedrock temperature calculation buffers the basal ice against cooling, it is therefore consistently warmer;

- this warmer ice flows faster and therefore the thickness of ice which can build up is smaller;

- the thinner ice sheet has a less positive overall mass balance because of the coupling between surface elevation and mass balance; and

- the overall size is therefore reduced.

This situation is unsatisfactory for two reasons. First, he rationale used in driving the model was to attain a specified, known Weichselian maximum (section 4.2). Second, the comparison of the runs with and without bedrock temperature calculation can only be made if the two have similar Weichselian maximum spans.

The equilibrium line depression used to drive the model was therefore altered from that described in section (4.3). The value of f_1 (in equation 4.1) was set equal to 90.0 m $^oC^{-1}$ rather than the 88.4 m $^oC^{-1}$ previously used. The effect of this increase is to make the amplitude of the equilibrium line depression time series slightly greater. This opposes the tendency of the bedrock temperature calculation runs to produce smaller ice sheets, with the result that a similar Weichselian maximum is achieved. The input to these runs is otherwise identical to that used in the runs of the previous section.

The evolutions of thickness (Figures 5.15 and 5.16), surface elevation (Figures 5.17 and 5.18) and vertically averaged horizontal velocity (Figures 5.27 and 5.28) show only minor differences compared to their equivalents in the previous section. They will not therefore be discussed further.

Figures 5.19 and 5.20 show the evolution of basal temperature in the two runs. Two features are worthy of note. First, the temperature distribution in the broad warm ice zone behind the margin is very similar to that shown in previous the runs. It appears that the strain heating/basal melt buffering mentioned above is strong enough to oppose changes in the geothermal heat flux. The second feature is that temperature beneath the divide does not fall as low as in the previous set of runs. This is because the basal cooling caused by cold ice advection is countered by an increased geothermal heat flux, which is in turn caused by the increased contrast between basal ice and rock temperatures.

Similar basal melt rate distributions are also found (Figures 5.21 and 5.22). However, the runs with bedrock temperature calculations have a more complex

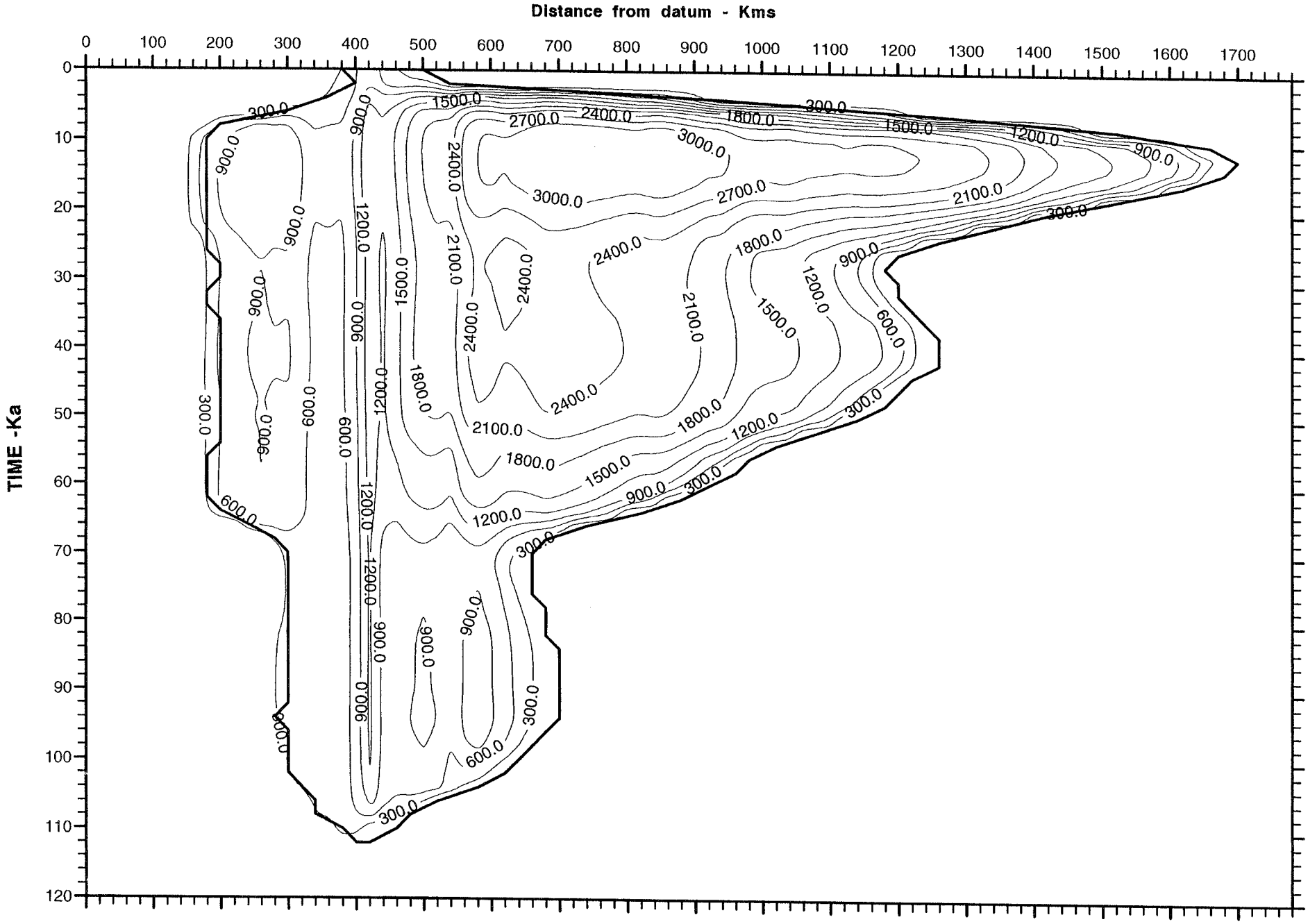

Figure 5.15 **Predicted variation of thickness (m) along a transect from Norway to Poland (figure 2.4) during the Weichselian using the -5°C air temperature time series and with bedrock temperature calculations.**

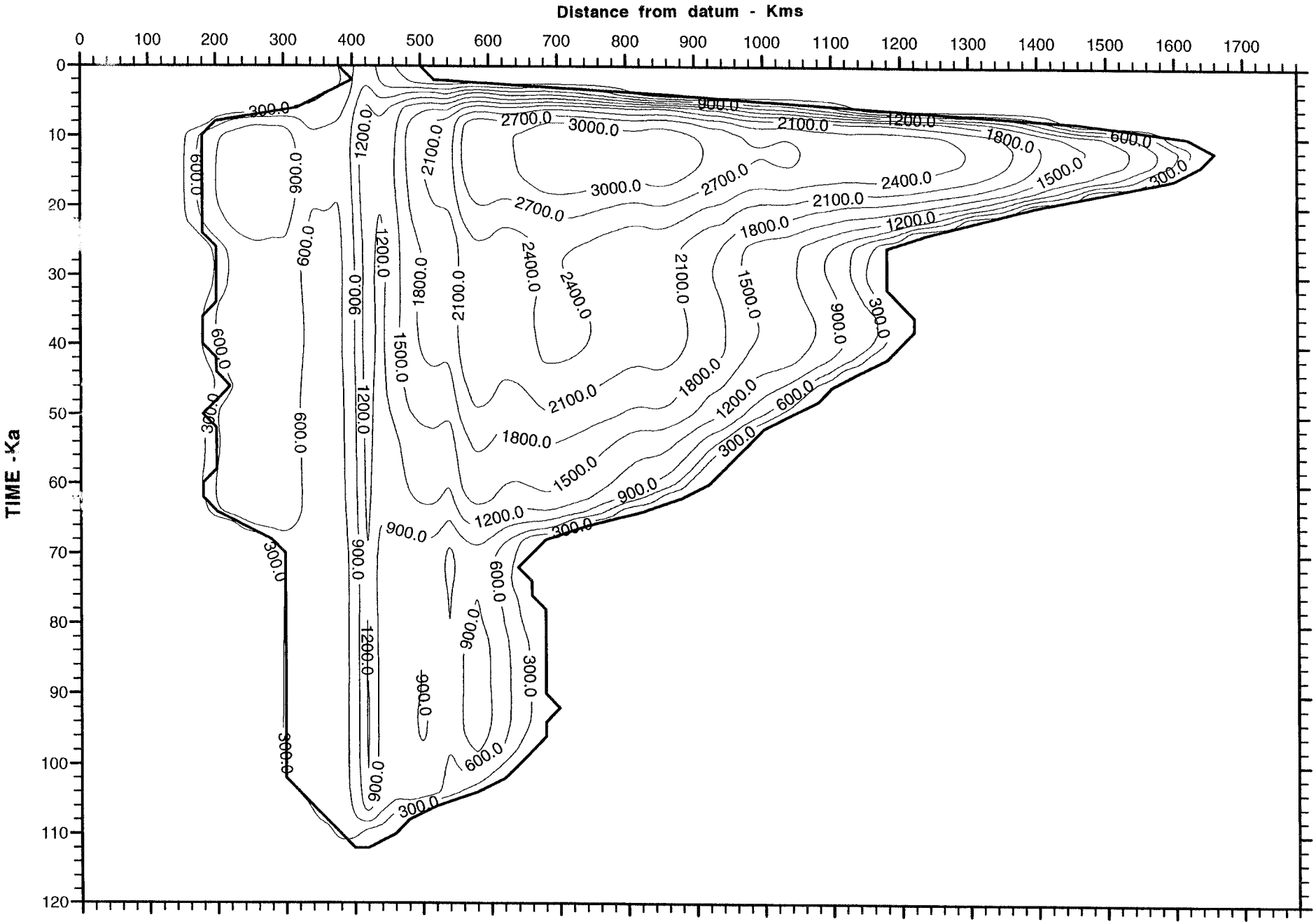

Figure 5.16 **Predicted variation of thickness (m) during the Weichselian using the -10°C air temperature time series and with bedrock temperature calculations.**

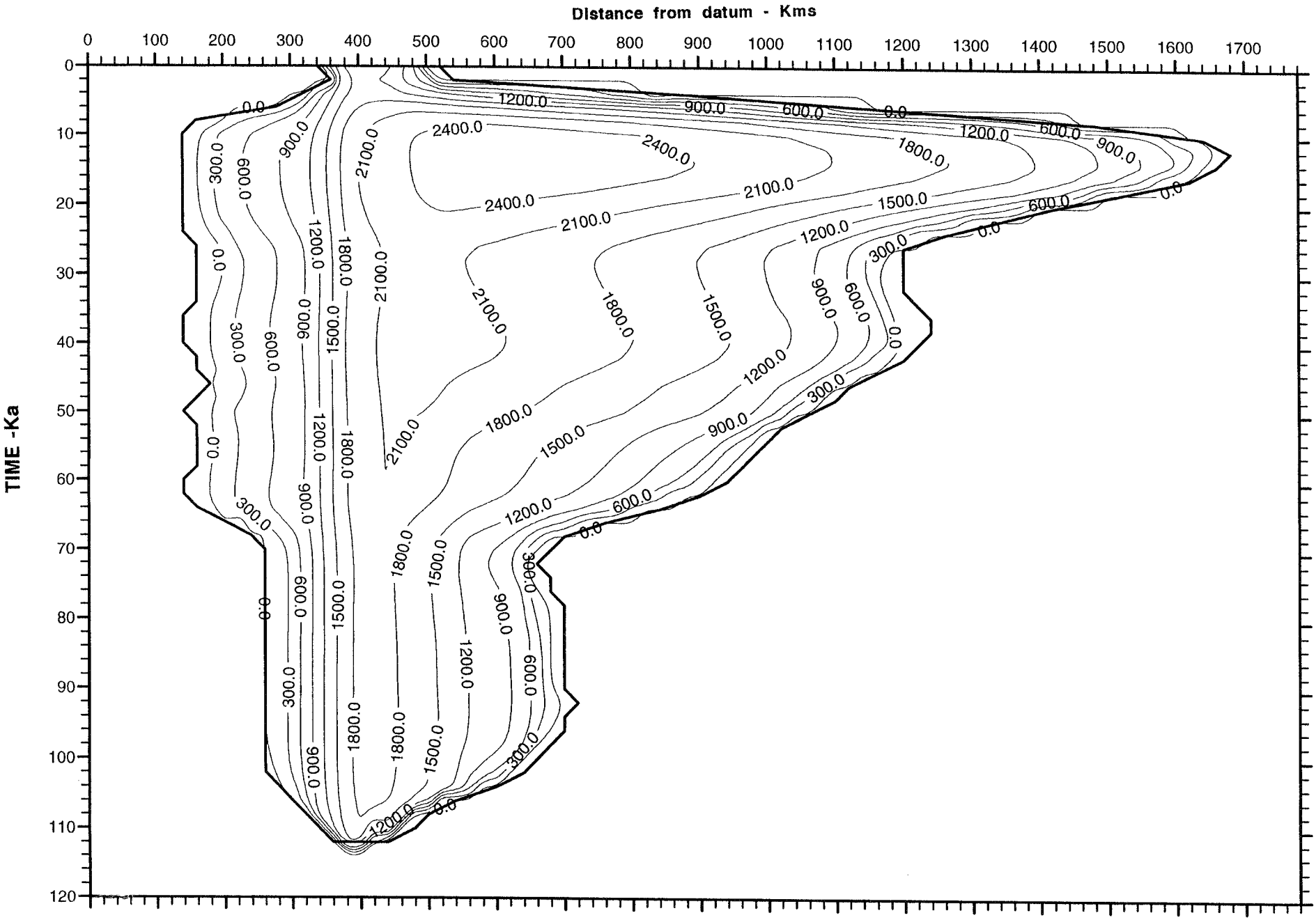

Figure 5.17 Predicted variation of surface elevation (m) during the Weichselian using the -5°C air temperature time series and with bedrock temperature calculations.

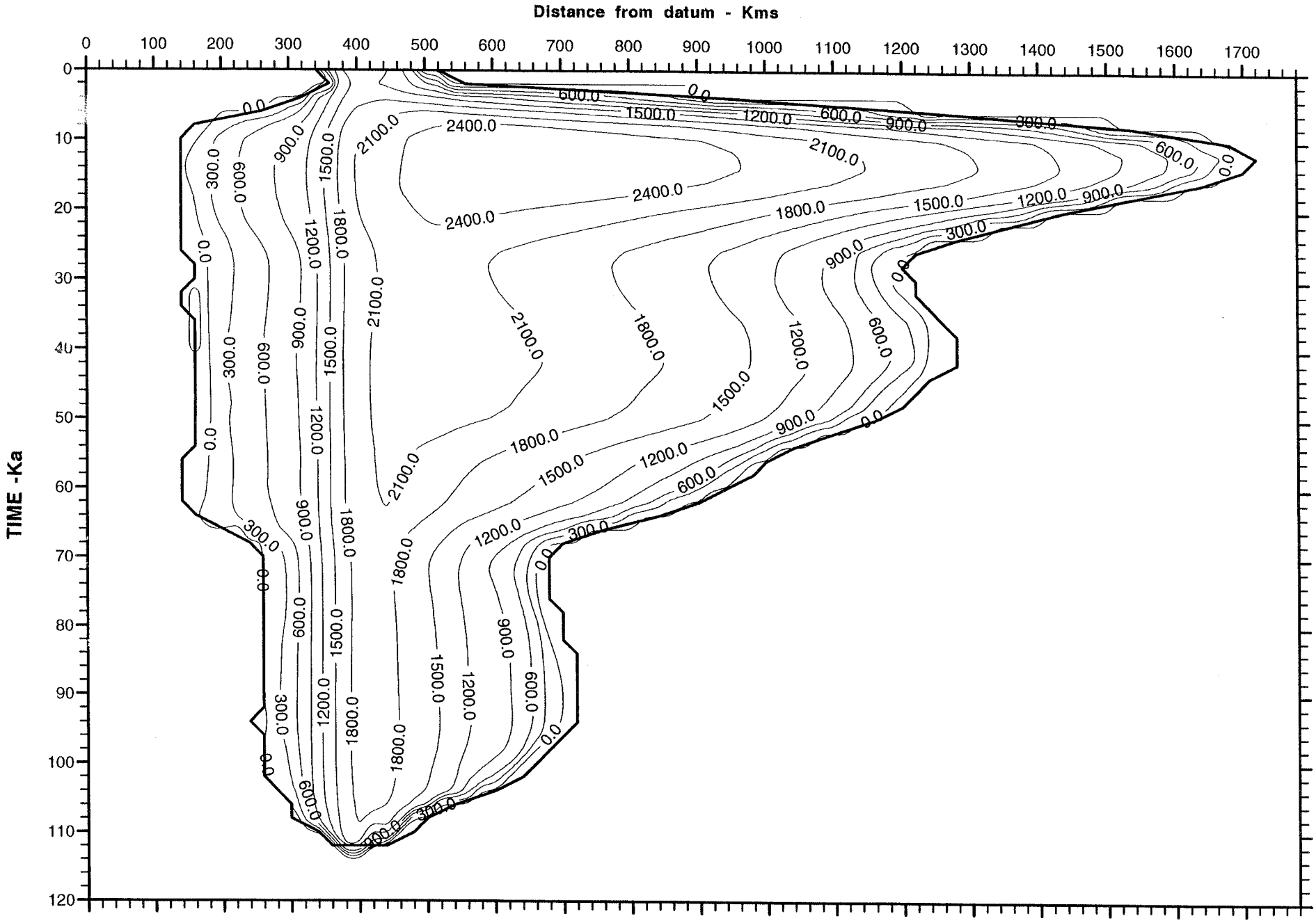

Figure 5.18 **Predicted variation of surface elevation (m) during the Weichselian using the -10°C air temperature time series and with bedrock temperature calculations.**

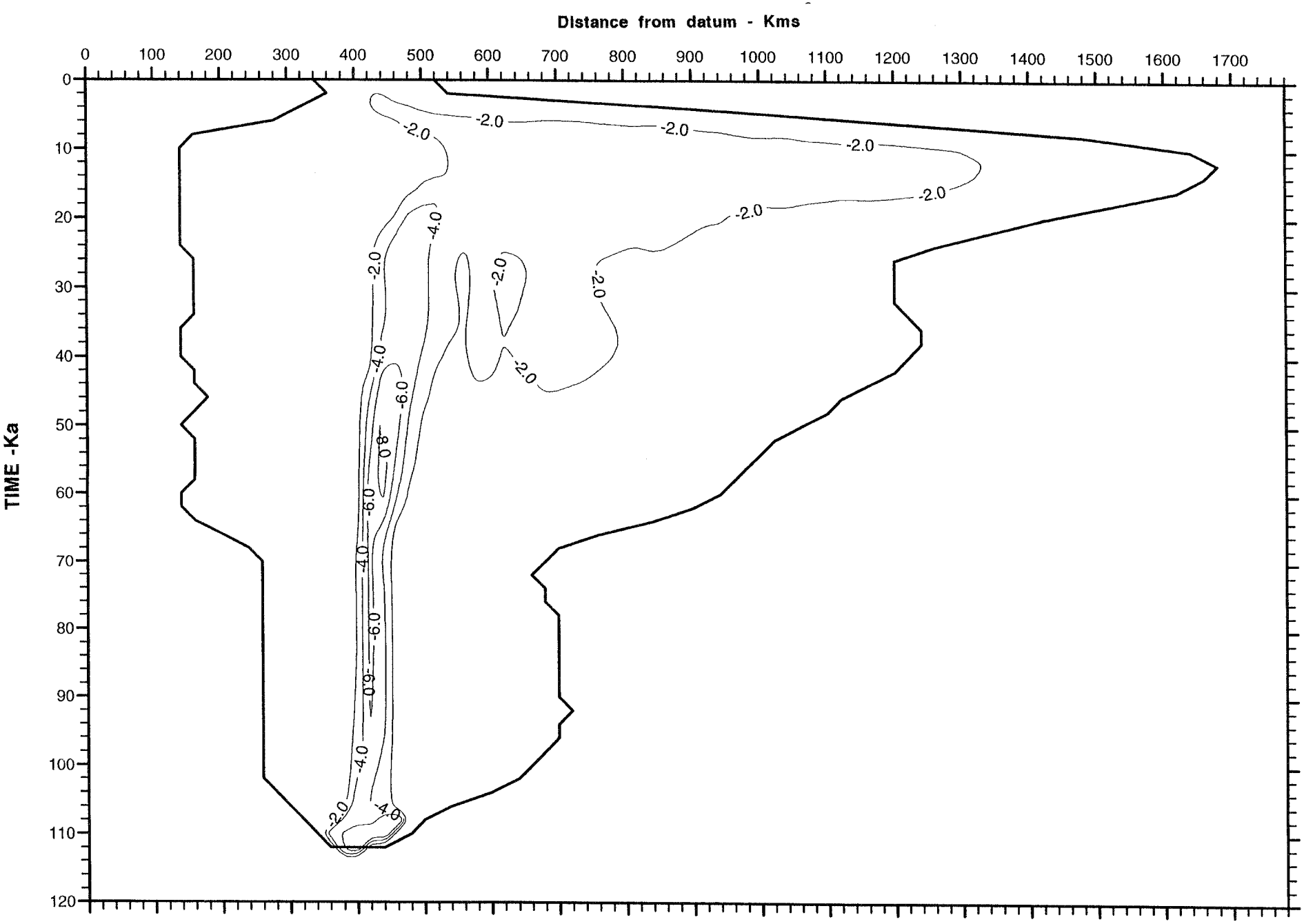

Figure 5.19 Predicted variation of basal ice temperature (^{o}C) during the Weichselian using the -5^{o}C air temperature time series and with bedrock temperature calculations.

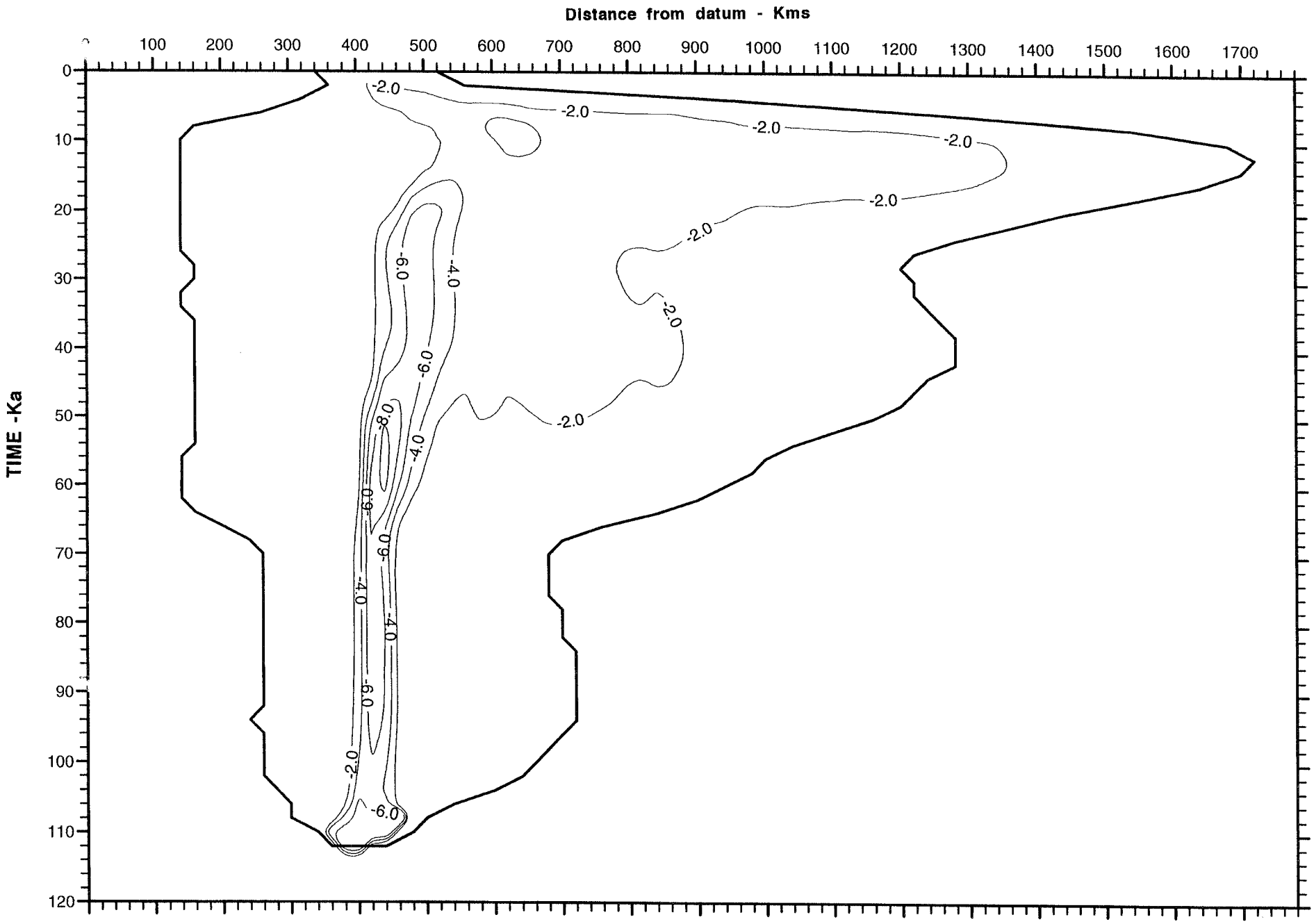

Figure 5.20 **Predicted variation of basal ice temperature (^{o}C) during the Weichselian using the -10^{o}C air temperature time series and with bedrock temperature calculations.**

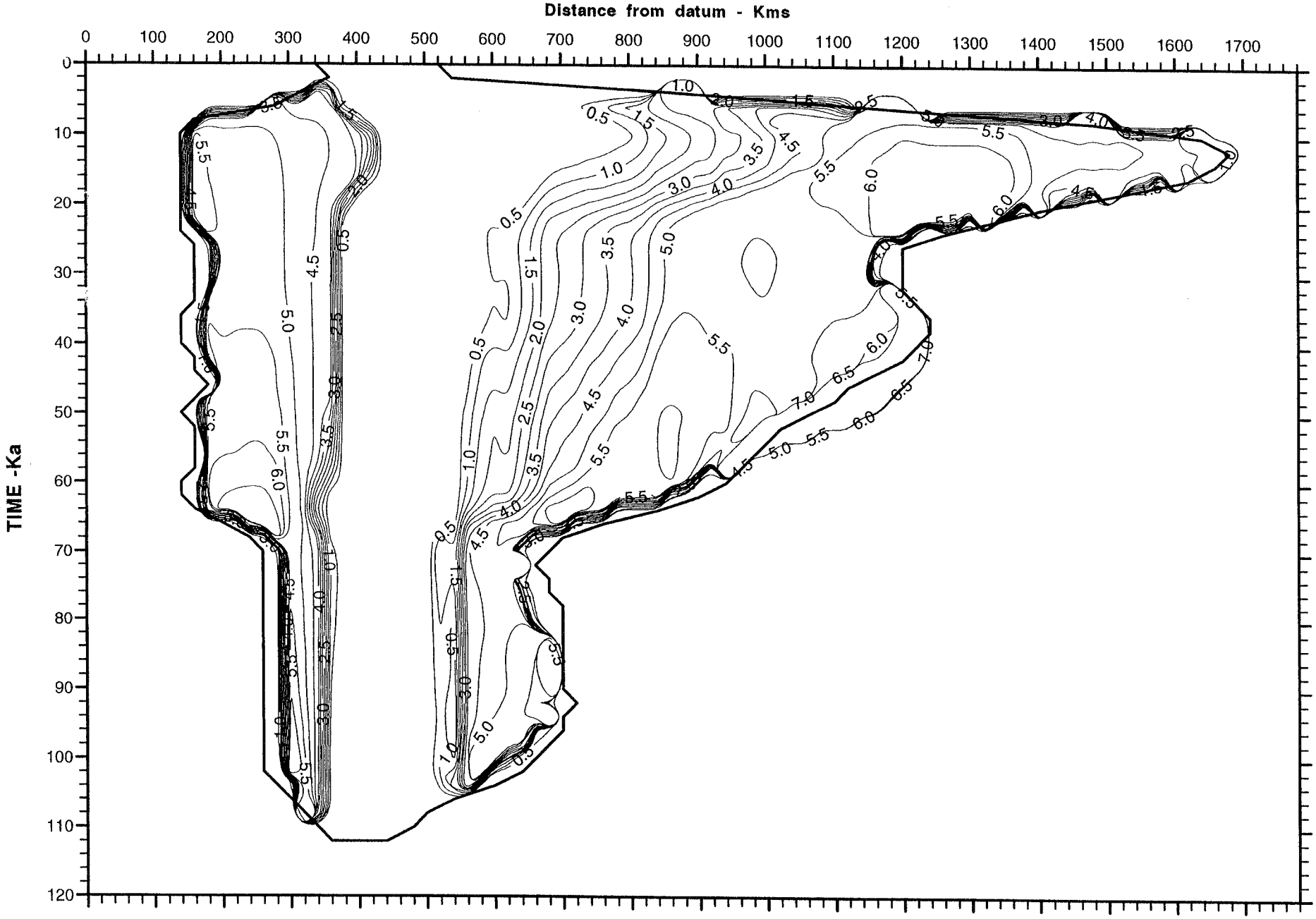

Figure 5.21 Predicted variation of basal melt rate (mm year^{-1}) during the Weichselian using the -5°C air temperature time series and with bedrock temperature calculations.

Figure 5.22 Predicted variation of basal melt rate (mm year^{-1}) during the Weichselian using the -10°C air temperature time series and with bedrock temperature calculations.

detailed distribution. In particular, the -10 ^{o}C run has a zone immediately behind the margin where basal melt rates increase with distance upstream up to approximately 500 km from the margin, where the gradual upstream decline of the previous runs is found. This pattern arises because the warm ice behind the advancing margin preferentially warms the underlying bedrock, leaving a reduced amount of energy available for basal melt. As the bedrock warms more energy is available for basal melt, which therefore increases. Eventually cold ice advection reduces the amount of basal melt. The speed of this reduction is reduced by the release of heat stored within the underlying bedrock, producing an enhanced geothermal heat flux. This is why the zone of basal melt is slightly wider in this set of runs than in the previous set.

Figures 5.23 and 5.24 show the variation of the geothermal heat flux throughout the runs. They should be compared to a value of 42 mW m^{-2}, which is the constant value used in the previous set of runs. The area outside of the ice sheet domain suffers variation in geothermal heat flux because of the rapid sea level air temperature fluctuations (see Figure 4.2). The heat flux increases when air temperatures fall, and decreases when they rise. The period of rapid warming at 10 kyears BP leads to a negative heat flux for this reason.

Inside the ice sheet domain, the fluctuation of geothermal heat flux is not so severe. The area behind the margin is associated with reduced a heat flux. The basal ice here is warmer than the ground level air temperature (especially in the -10 ^{o}C run), which reduces the near-surface bedrock temperature gradient and hence the geothermal heat flux. Further away from the margin, the heat flux increases as bedrock temperature gradients steepen in response to the advection of cold ice.

The depth of permafrost is shown in Figures 5.25 and 5.26. These depths were calculated by finding the point at which bedrock temperature equals 0 ^{o}C; this depth was then corrected for the pressure melting point variation caused by the overlying mass of ice (if present) and bedrock, using equation (2.8).

The permafrost results can be divided into three regions. First, outside the ice sheet domain, permafrost depth reflects the variation of sea level air temperature. Maximum depths occur shortly after the air temperature lows at 75 and 18 kyears BP. In the -10 ^{o}C run a maximum depth in excess of 300 m is attained, while in

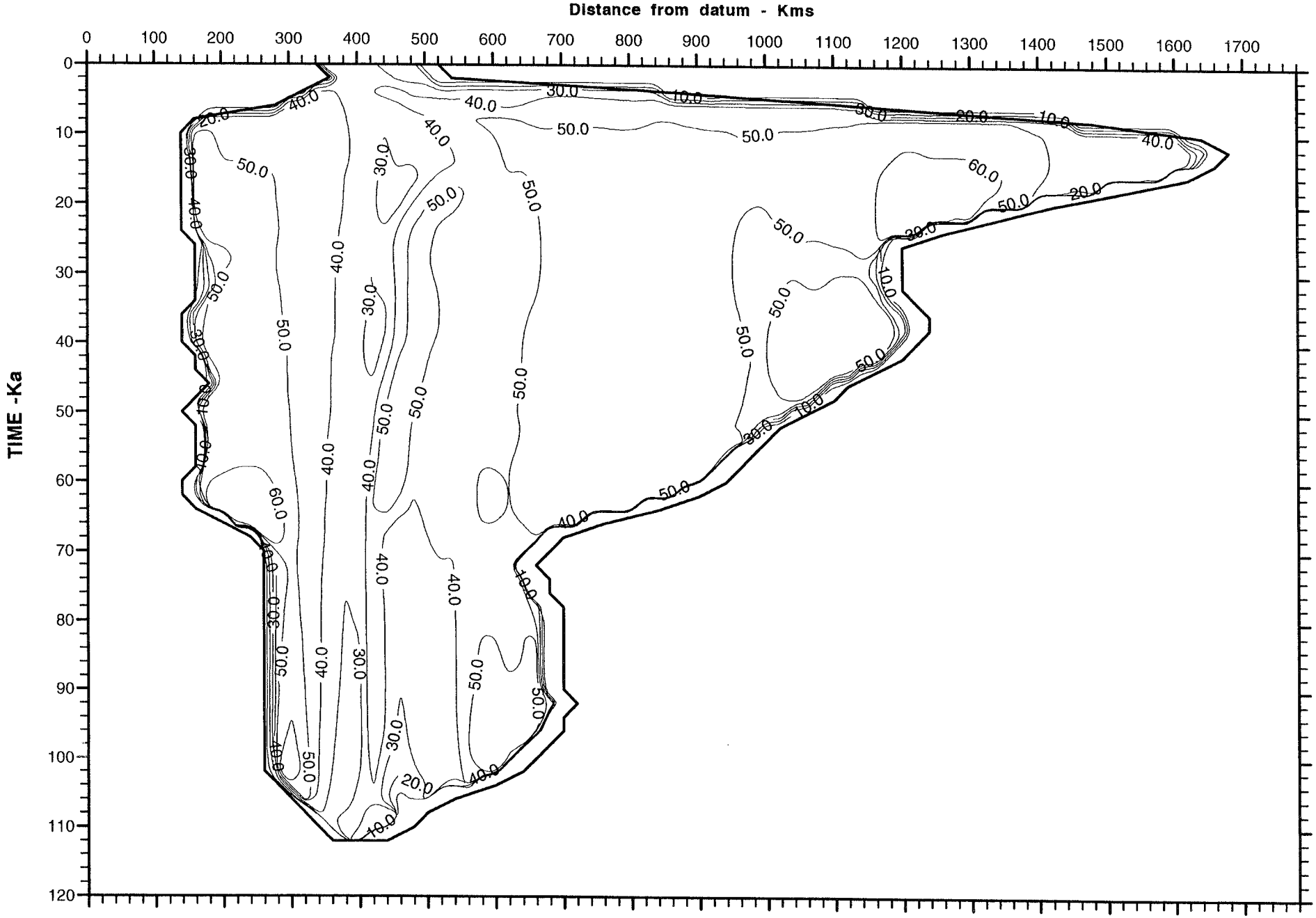

Figure 5.23 Predicted variation of geothermal heat flux (mW m^{-2}) during the Weichselian using the -5°C air temperature time series and with bedrock temperature calculations.

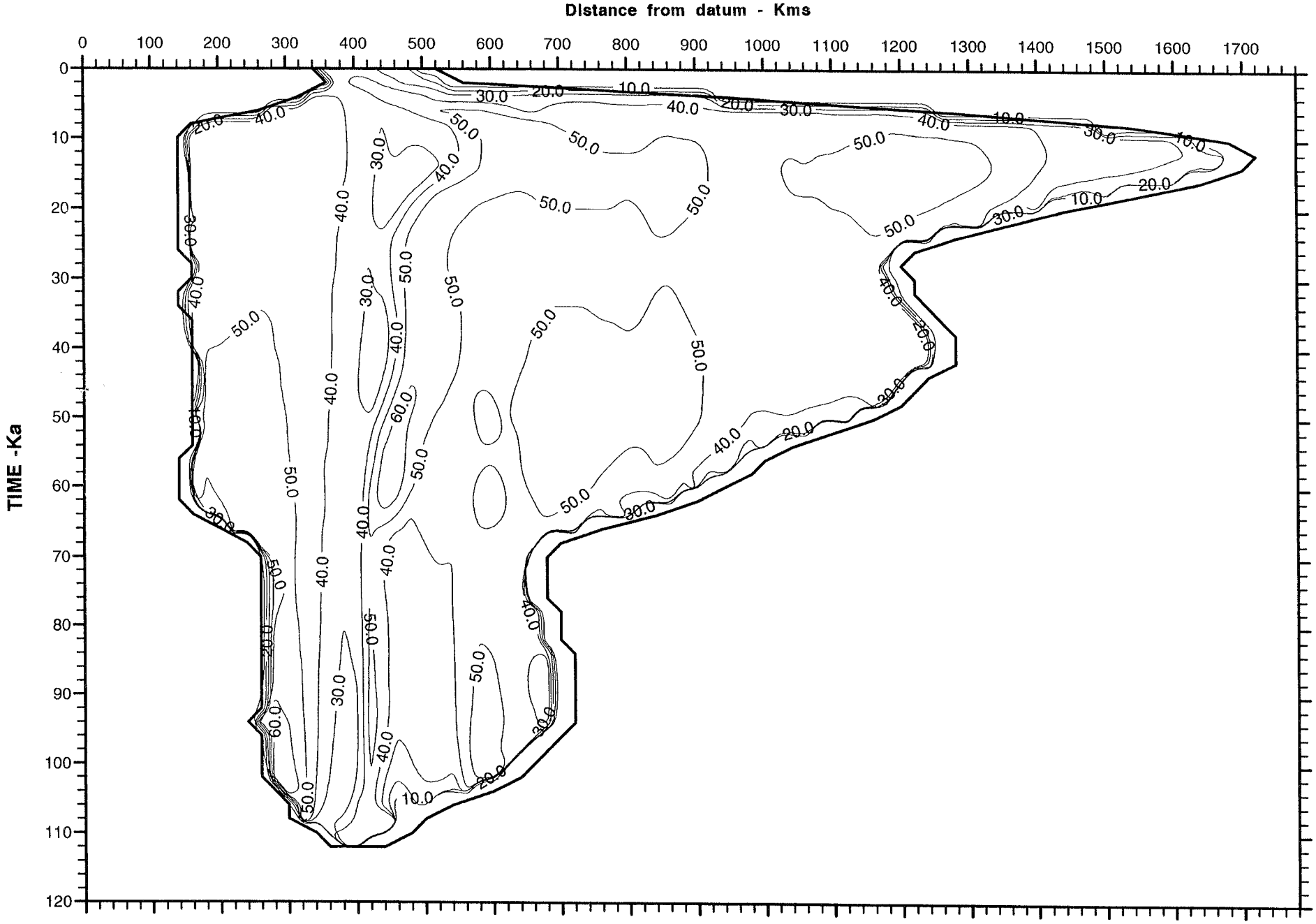

Figure 5.24 **Predicted variation of geothermal heat flux (mW m^{-2}) during the Weichselian using the -10°C air temperature time series and with bedrock temperature calculations.**

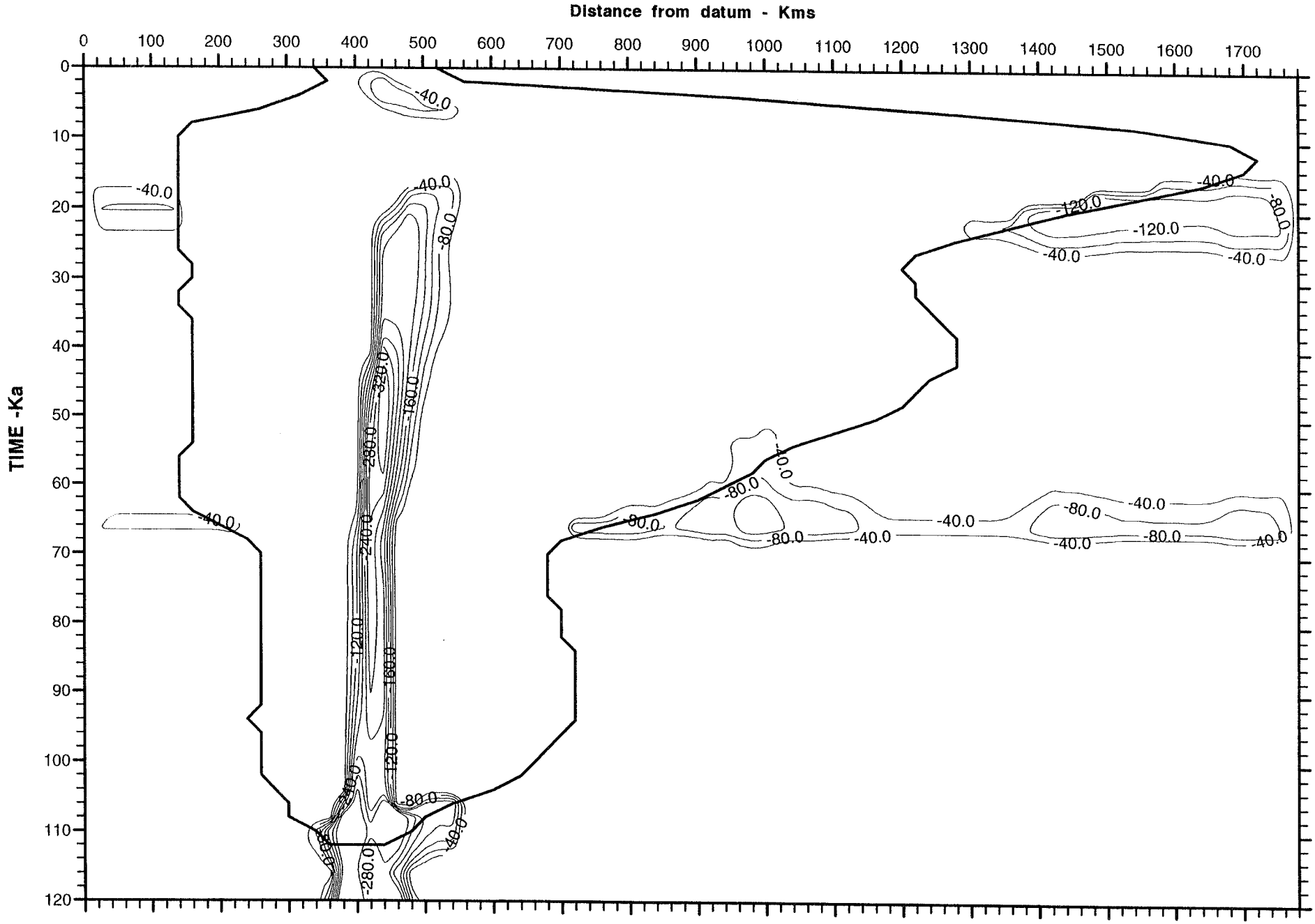

Figure 5.25 **Predicted variation of depth of permafrost (m) during the Weichselian using the -5°C air temperature time series and with bedrock temperature calculations.**

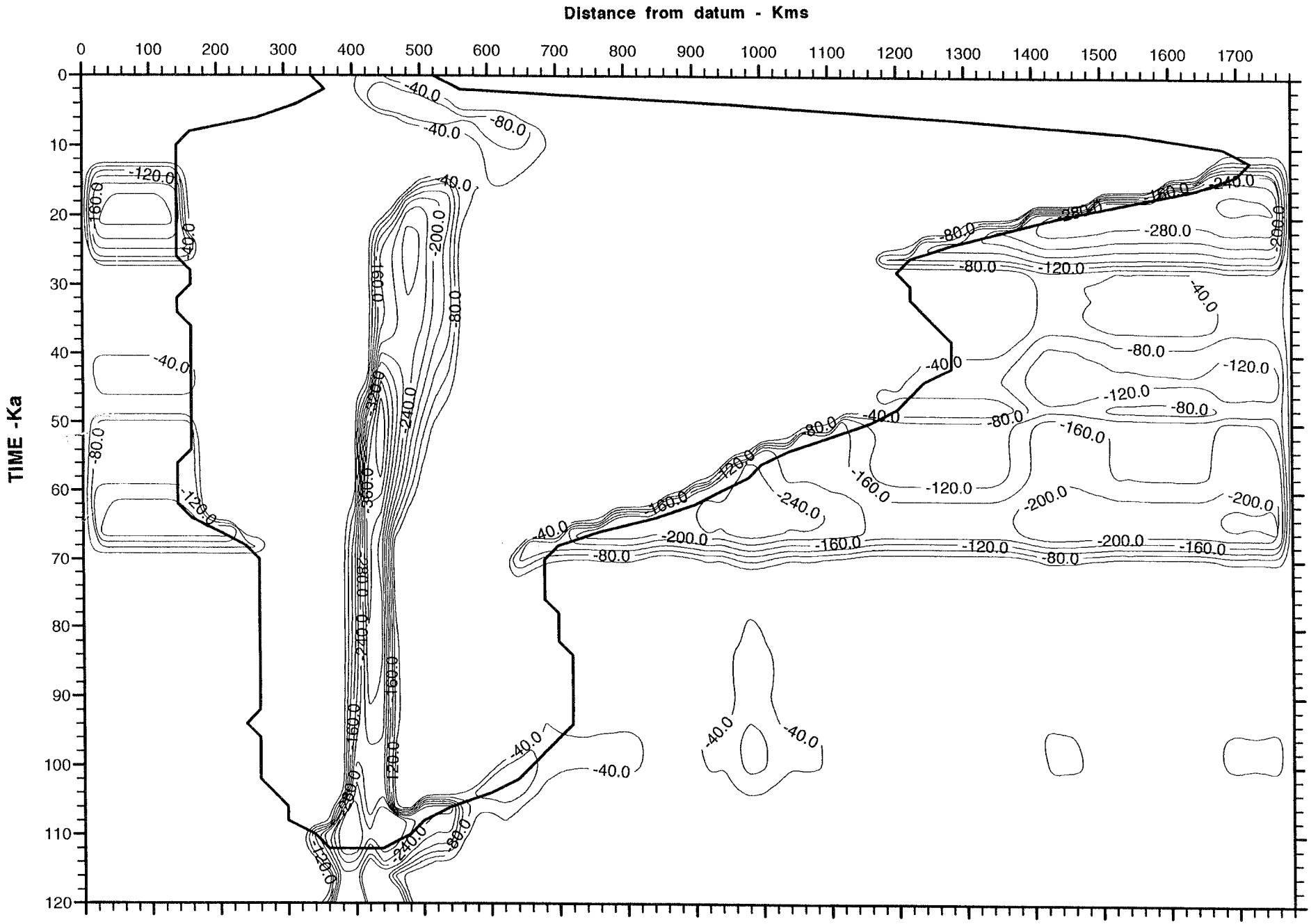

Figure 5.26 Predicted variation of depth of permafrost (m) during the Weichselian using the -10°C air temperature time series and with bedrock temperature calculations.

the -5 ^{o}C run this depth is 113 m. The variation of permafrost depth with distance is caused by the different surface elevations along the flowline, which lead to different ground surface temperatures.

The second region is within the ice sheet under the divide. Here cold ice advection leads to an unbroken sequence of permafrost development. The maximum permafrost depth occurs at 55 kyears BP and lags the initial sea level air temperature drop by 20 kyears. This maximum depth is in excess of 413 m (in the -10 ^{o}C run) and 375 m (in the -5 ^{o}C run). The third region is the remaining parts of the ice sheet not under the divide. Here the effects of the relatively warm basal ice and the pressure melting point reduction (caused by the overburden of ice) combine to remove all permafrost.

The permafrost depth results are derived by assuming dry bedrock throughout. It is expected that the predicted rate of permafrost progression downwards will be considerably slowed by the introduction of latent heat flux considerations. The predicted permafrost depths should therefore only be taken as maximum possible values.

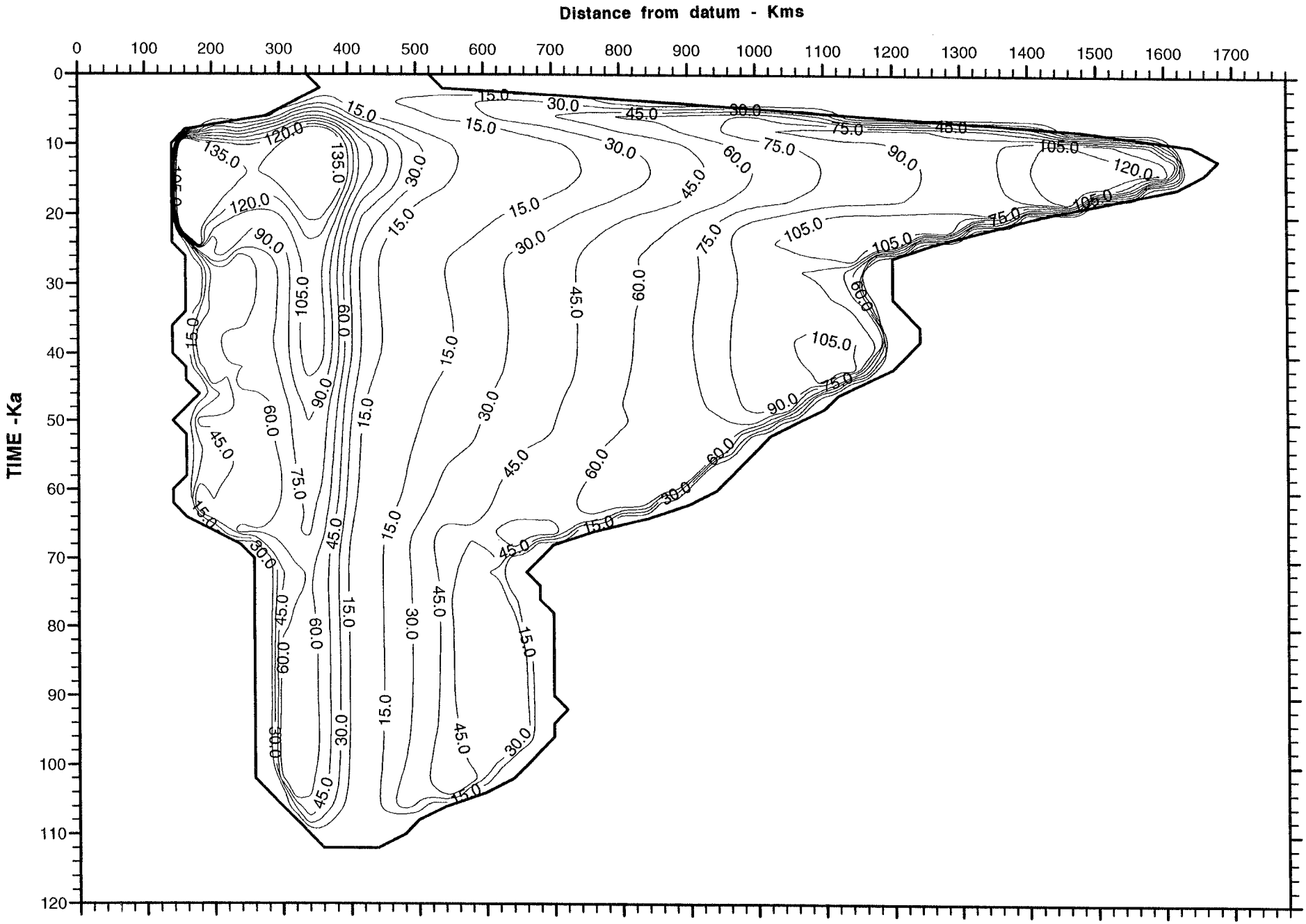

Figure 5.27 **Predicted variation of vertically averaged horizontal ice velocity (m year $^{-1}$) during the Weichselian using the -5°C air temperature time series and with bedrock temperature calculations.**

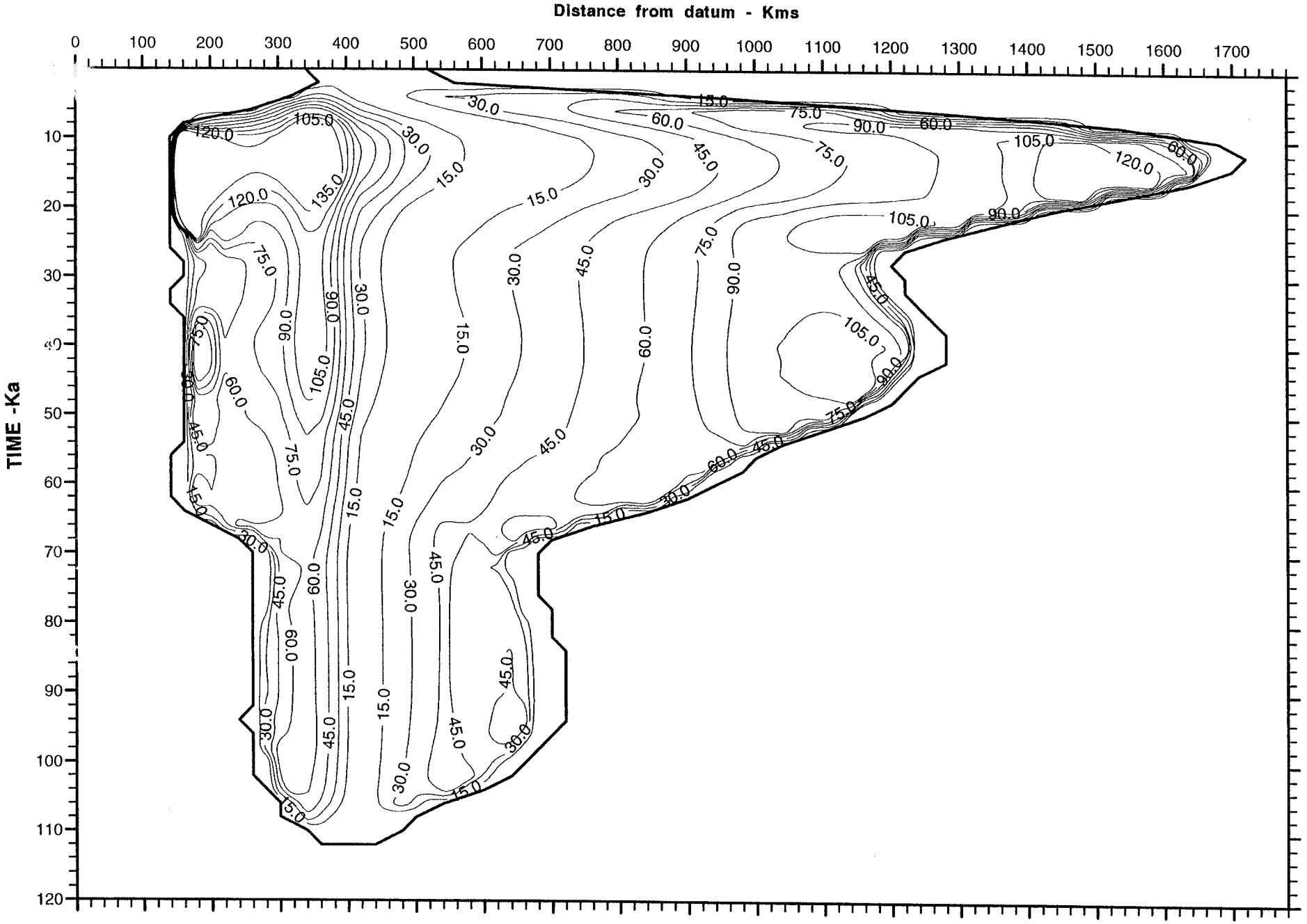

Figure 5.28 Predicted variation of vertically averaged horizontal ice velocity (m year $^{-1}$) during the Weichselian using the -10°C air temperature time series and with bedrock temperature calculations.

6 TESTING THE MODEL.

The ice sheet model has been "tuned" so that it reproduces the pattern of fluctuation of the ice sheet during the last glacial cycle in Europe. It was tested against the precise areal pattern of expansion and decay of the ice sheet; the pattern of erosion and deposition generated by the ice sheet in the southern Baltic and adjacent areas of Poland/Germany; the pattern of lithosphere flexure, and therefore of post-glacial relative sea-level change.

..... ***** .....

6.1 GENERAL APPROACH.

The model has been constrained by the presumed time/distance fluctuation of the European Weichselian ice sheet along the chosen transect. A parameterisation of a ELA fluctuation which varies in simple proportion to the sea surface temperatures in the N.E. Atlantic has been chosen so that the modelled glacier fluctuation along the transect fits the geological evidence. Figure 1.6 shows the range of theoretical output from the model which could be tested against geological data. However, some of this data has not yet been compiled (e.g. erratic transport information) and some of the sub-routines of the model are not yet adequately developed. As a consequence, testing has been undertaken by three routes:

- If the climate drive for the two-dimensional flowline model is applied to the three-dimensional model, does the modelled ice sheet show a pattern of expansion which agrees with the geological evidence?

- Does the pattern of relative sea level change predicted by the model conform with the geological evidence?

- Does the pattern of till distribution predicted by the model conform with the geological evidence?

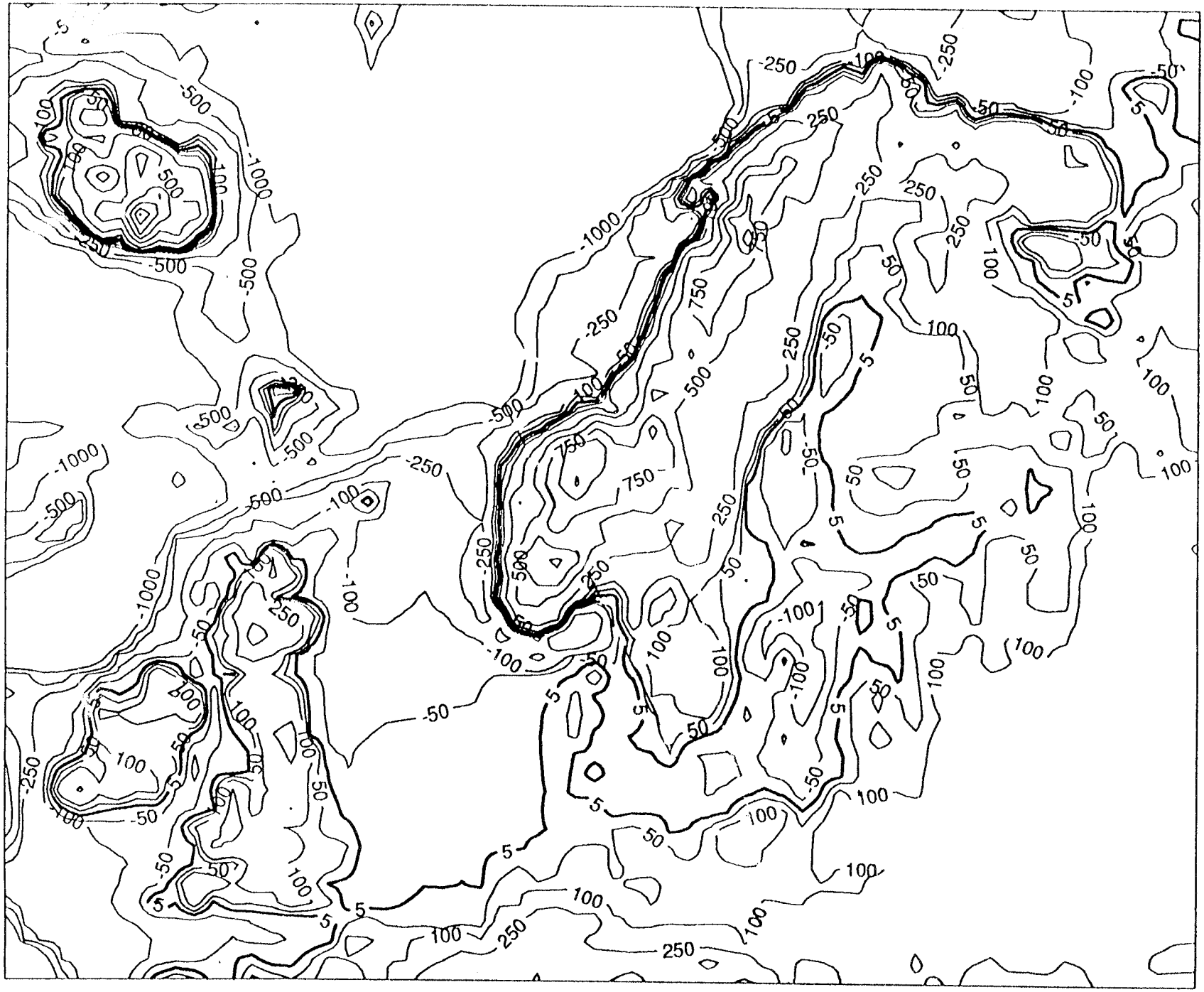

Figure 6.1 Topographic basis for the modelling exercises.

6.2 THE AREAL PATTERN OF ICE SHEET EXPANSION.

The model has been driven over the topography shown in Figure 6.1 by an areally uniform ELA forcing of the form shown in Figure 4.1. Figures 6.2, 6.3 and 6.4 show the form of the ice sheet at different periods after initiation. The ice sheet first forms along the mountainous spine of Scandinavia, showing particularly strong early growth in the south-west, in the area of Hardangervidda, and in the north-east, in the area of Nordland/W. Norrbotten. From there, the ice sheet grows rapidly with roughly parallel margins to the north-west and south-east. The north-western margin is controlled by iceberg calving into deep water off the Norwegian coast. The basal temperatures after 10,000 years of growth is shown in Figure 6.5.

Subsequent growth is concentrated in the south-eastern sector, where it is relatively uninhibited by calving. It is most rapid in the central south-east sector where there is the least marine influence. The Norwegian Channel, the deep water trough which fringes the coast of south-west Norway as far as the mouth of the Kattegat, inhibits ice expansion in the Skagerak-Kattegat re-entrant , thereby creating a major re-entrant in the ice sheet margin as it expands into northern Germany and Denmark.

The general form of the modelled ice sheet margin conforms extremely well with geological evidence of the pattern of development of the Late Weichselian ice sheet shown in Figure 6.6. In particular, the Skagerak-Kattegat re-entrant is well simulated. Moreover, the model also reproduces changes in flow direction through time which conform to geological data. For instance it suggests that there will be an anti-clockwise rotation of flow direction through time in the north-eastern sector of the ice sheet and a clockwise rotation in the southern Baltic area, resulting from the relatively rapid expansion of the central south-eastern sector of the ice sheet during advanced stages of growth. This is precisely what has been documented in the southern Baltic (Böse, 1990), and in northern Scandinavia (Punkari, 1985).

We conclude that the model output is compatible with the geological evidence of the pattern of expansion of the ice sheet.

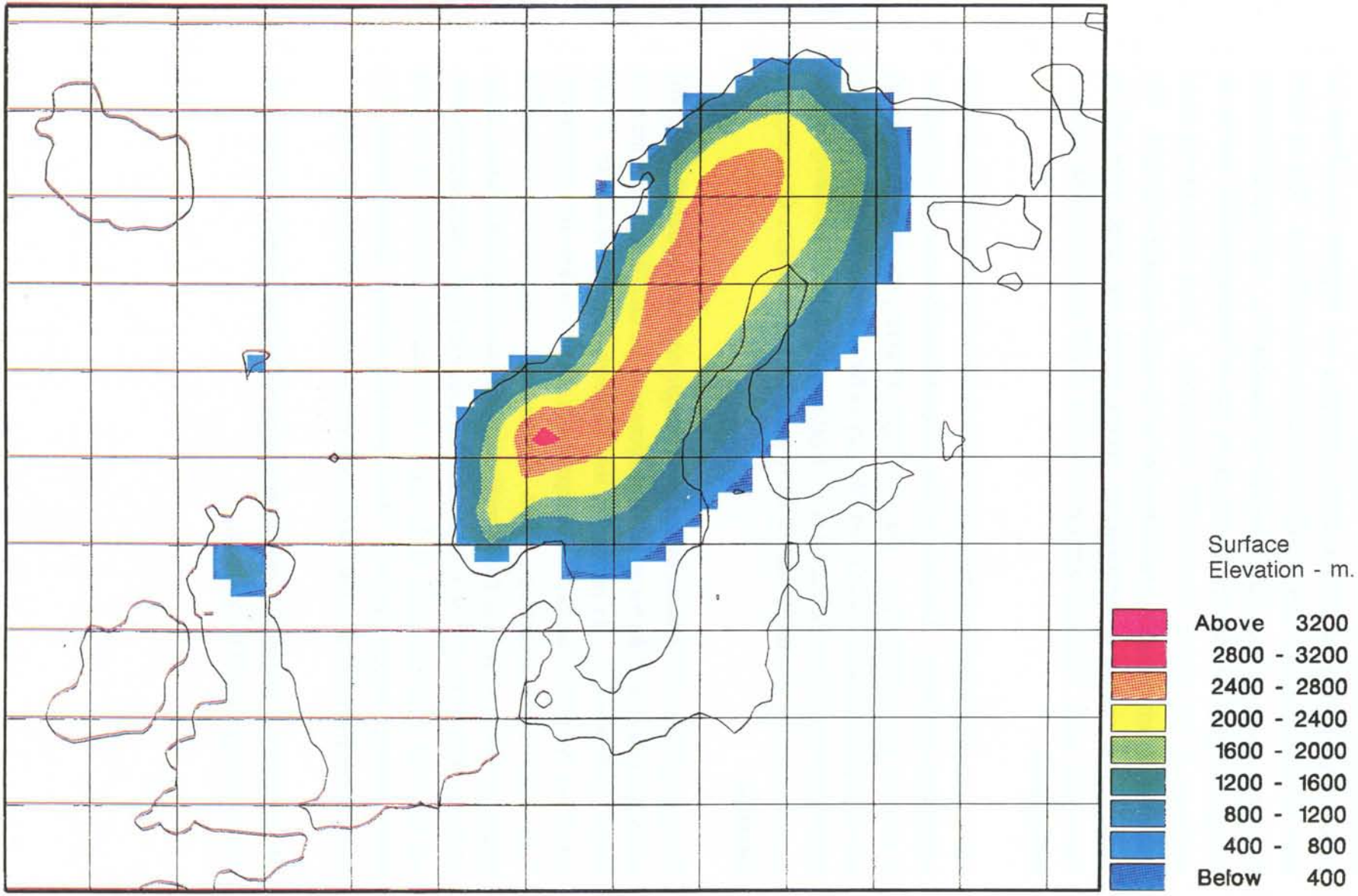

Figure 6.2 Development of a European ice sheet on the topographic base shown in Figure 6.1, 10 Ka after initiation. It is assumed that the pattern of growth will be similar, irrespective of whether it is interrupted by retreat phases or not, or whether the growth rate is faster, driven by a larger positive mass balance.

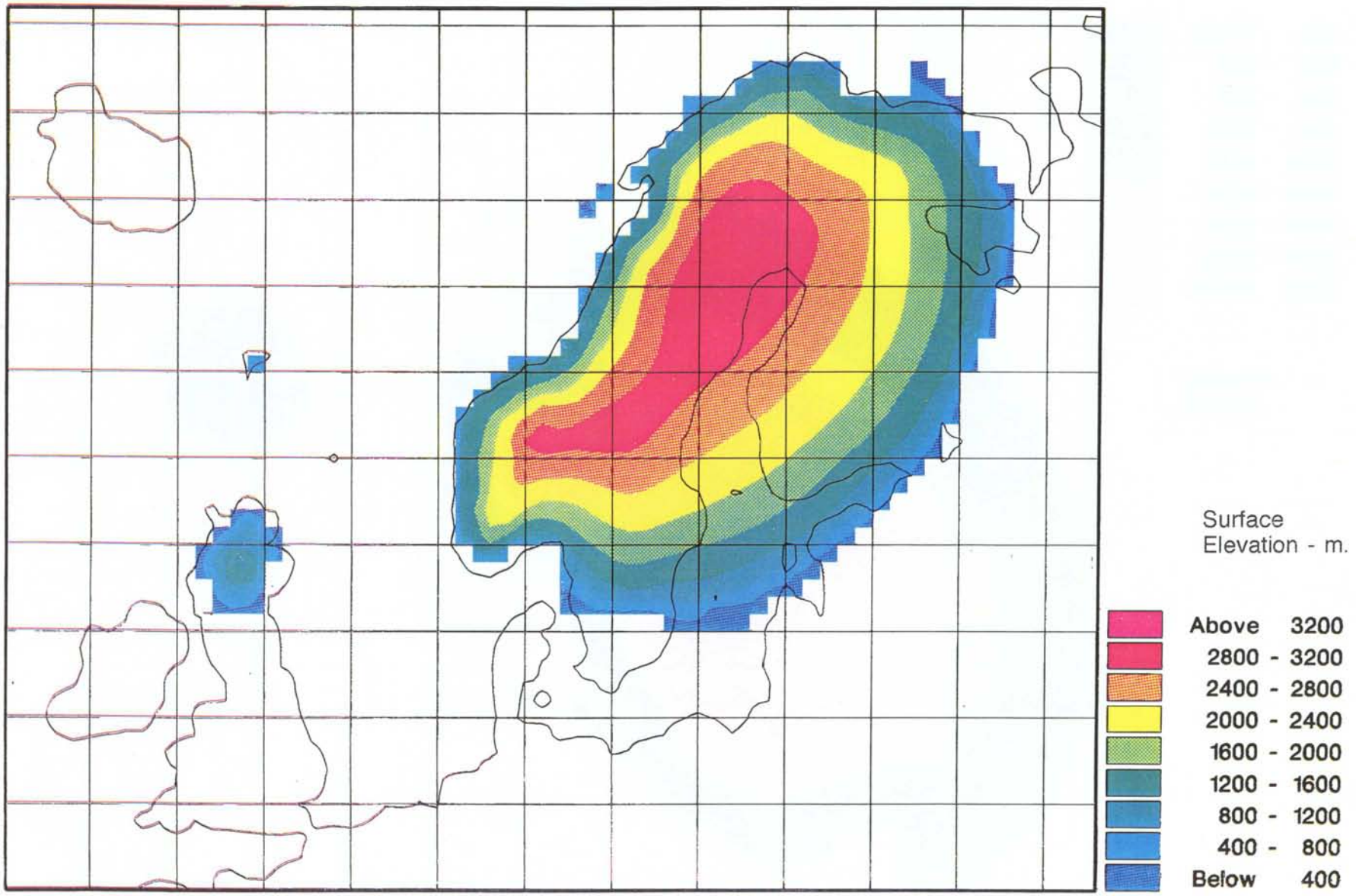

Figure 6.3 Development of the ice sheet after 15Ka of growth.

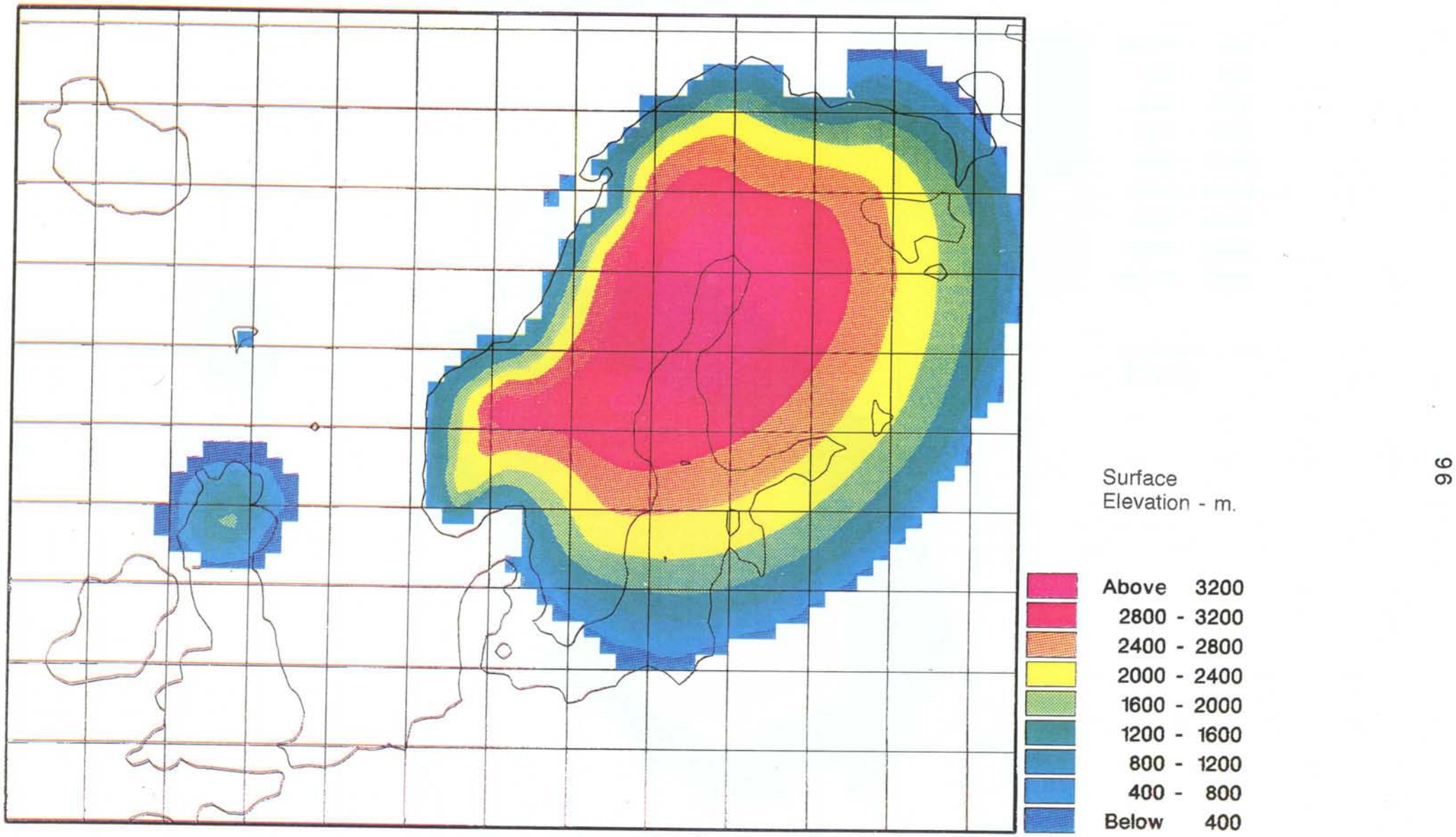

Figure 6.4 Development of the ice sheet after 20Ka of growth. Note the very large re-entrant in the ice sheet margin caused by iceberg calving in the Oslo Fjord region. This agrees well with the geological evidence of ice sheet form during both the Saalian and Weichselian (Figure 6.6) stages.

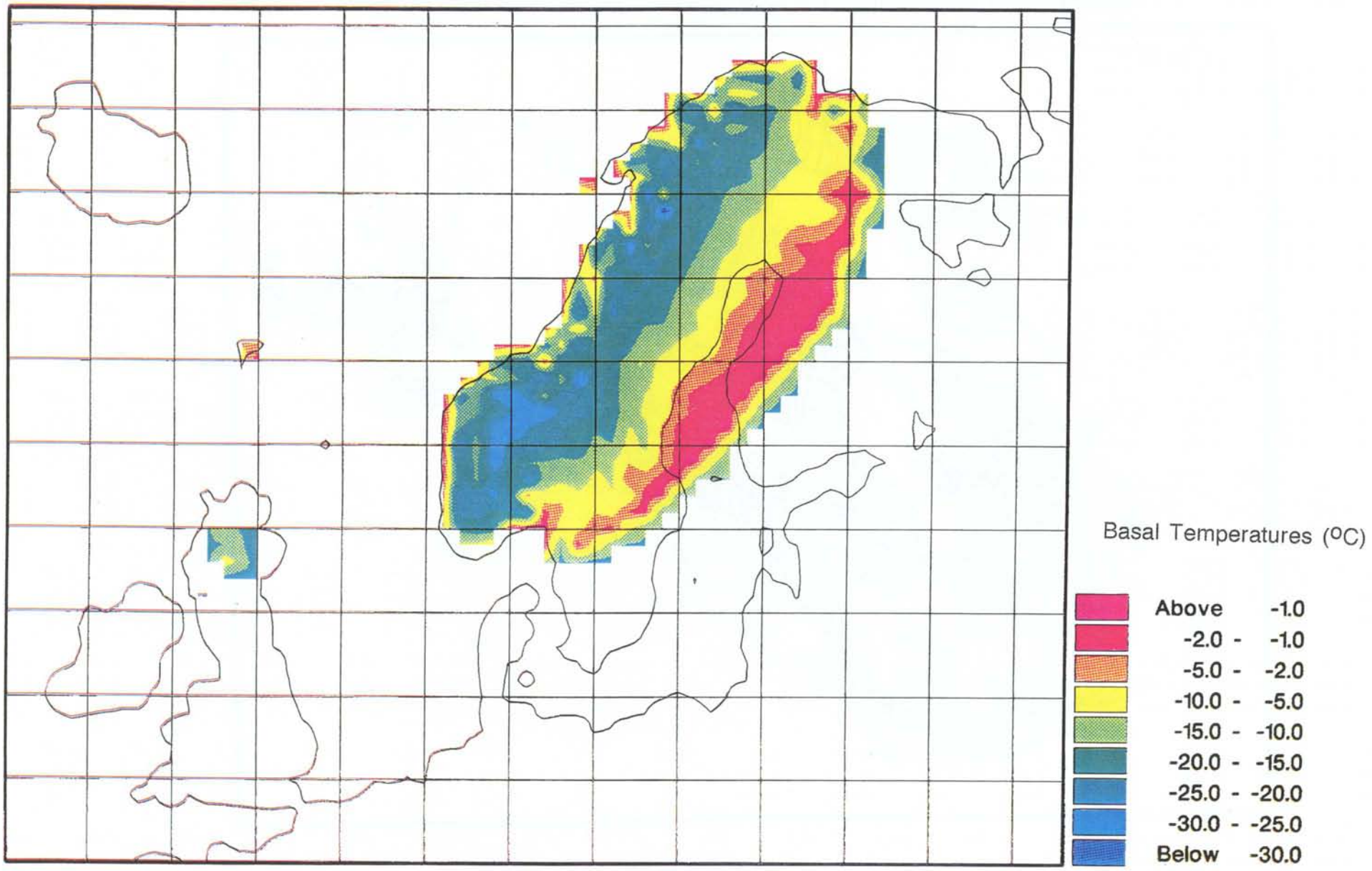

Figure 6.5 Basal temperatures after 10Ka of growth. The broad red zone is roughly coincident with the zone of melting at the pressure melting point

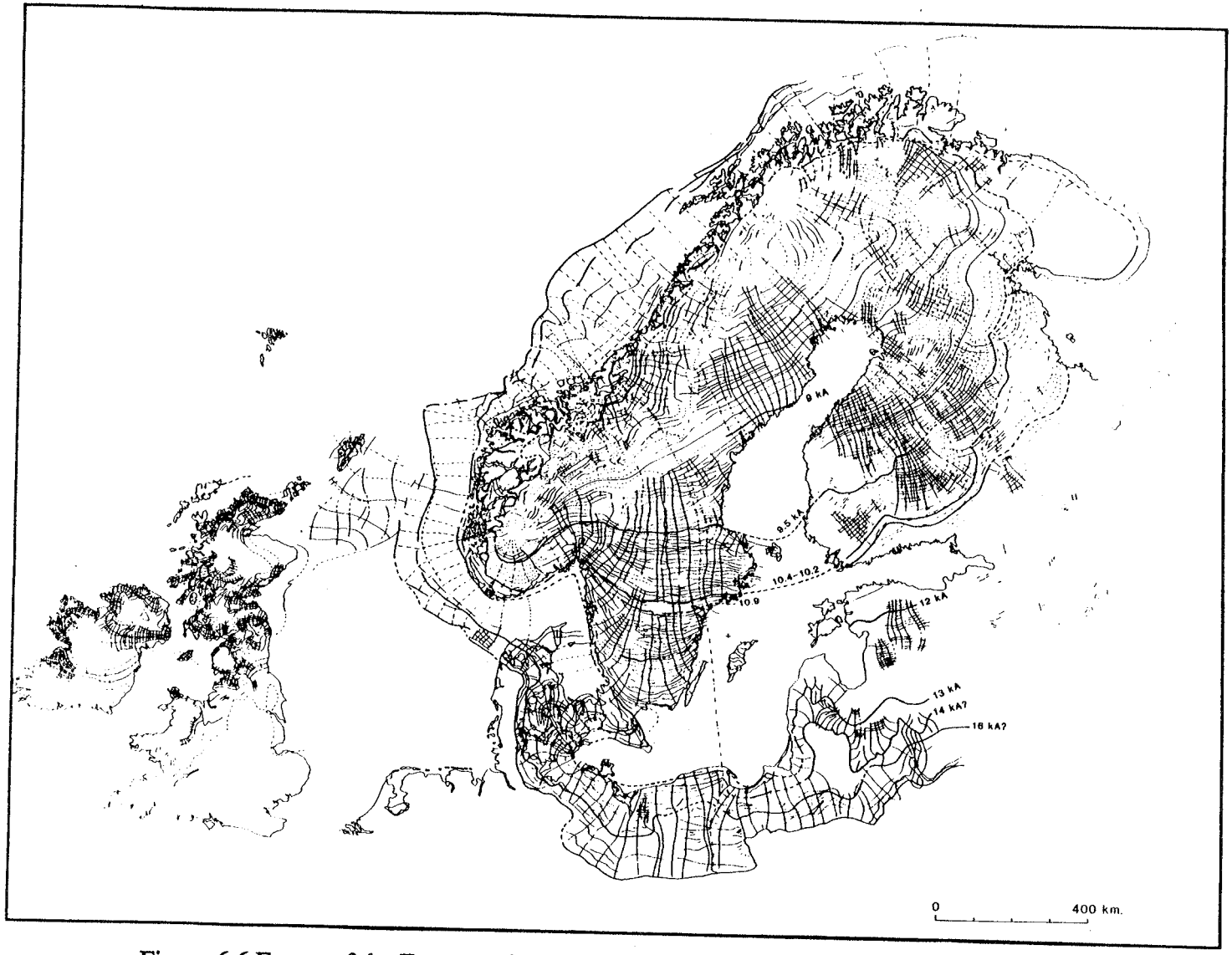

Figure 6.6 Extent of the European ice sheet at the last glacial maximum and it's pattern of retreat (Boulton, 1985).

6.3 THE EVIDENCE OF RELATIVE SEA LEVEL.

The pattern of relative sea level in north west Europe has been very well established for the Holocene and, in many places, for the later part of the Late-Glacial. Figure 6.7 shows the locations of sites in the area for which relative sea level curves have been established for at least part of the Holocene. Figure 6.8 shows isobases plotted from this data for a number of Holocene time periods. They clearly reflect the dominant pattern of crustal uplift resulting from loading and unloading by ice during the Late Weichselian phase of ice sheet expansion and decay.

In order to test the compatibility of the ice sheet model with the relative sea level data, a series of loads, representing the modelled European ice sheet ,have been superimposed in sequence on the area. In addition, ice masses which have been assumed to have been roughly contemporaneous on the Barents Sea area and on Britain have been included as far-field loads. Although we do expect a Laurentide Ice Sheet effect on European sea levels, this is assumed to have been small compared with the effect of the nearer ice sheet loads.

The loading history of the European ice sheet is extrapolated from the history of loading along the standard transect. The distribution of mass within these areas is plotted in a series of squares covering the whole area of the ice sheet, and is derived from the 3-D models shown in Figures 6.10-6.12. The loading / unloading time steps are shown in Figure 6.9. The British and Barents Sea ice sheets in the far field are assumed to show a similar pattern of fluctuation, although sensitivity tests show that the precise pattern of fluctuation is relatively unimportant. The length of the time steps for these ice sheets was chosen to be 2 kyrs, although this is also assumed to be relatively unimportant.

The pattern of loading is then used as input into a model derived relatively faithfully from that developed by Lambeck et al. (1990) to test patterns of ice sheet loading.

In the absence of tectonic movement, sea level change can be expressed as

$$\Delta\xi(\phi,\lambda:t) = \xi(\phi,\lambda:t) - \xi(\phi,\lambda:t_o) \qquad (6.1)$$

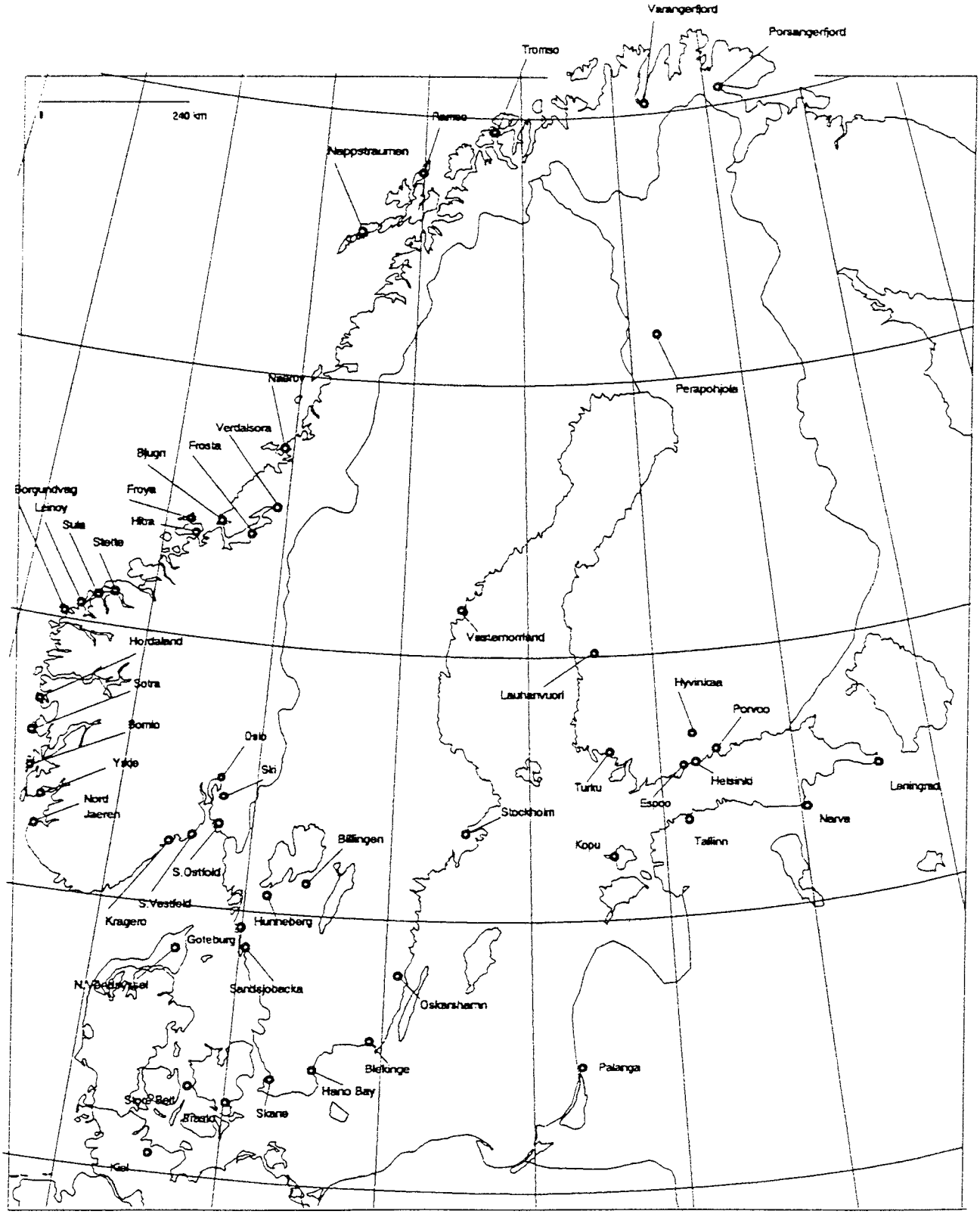

Figure 6.7 Sites at which geological records of late glacial and post glacial relative sea level exist.

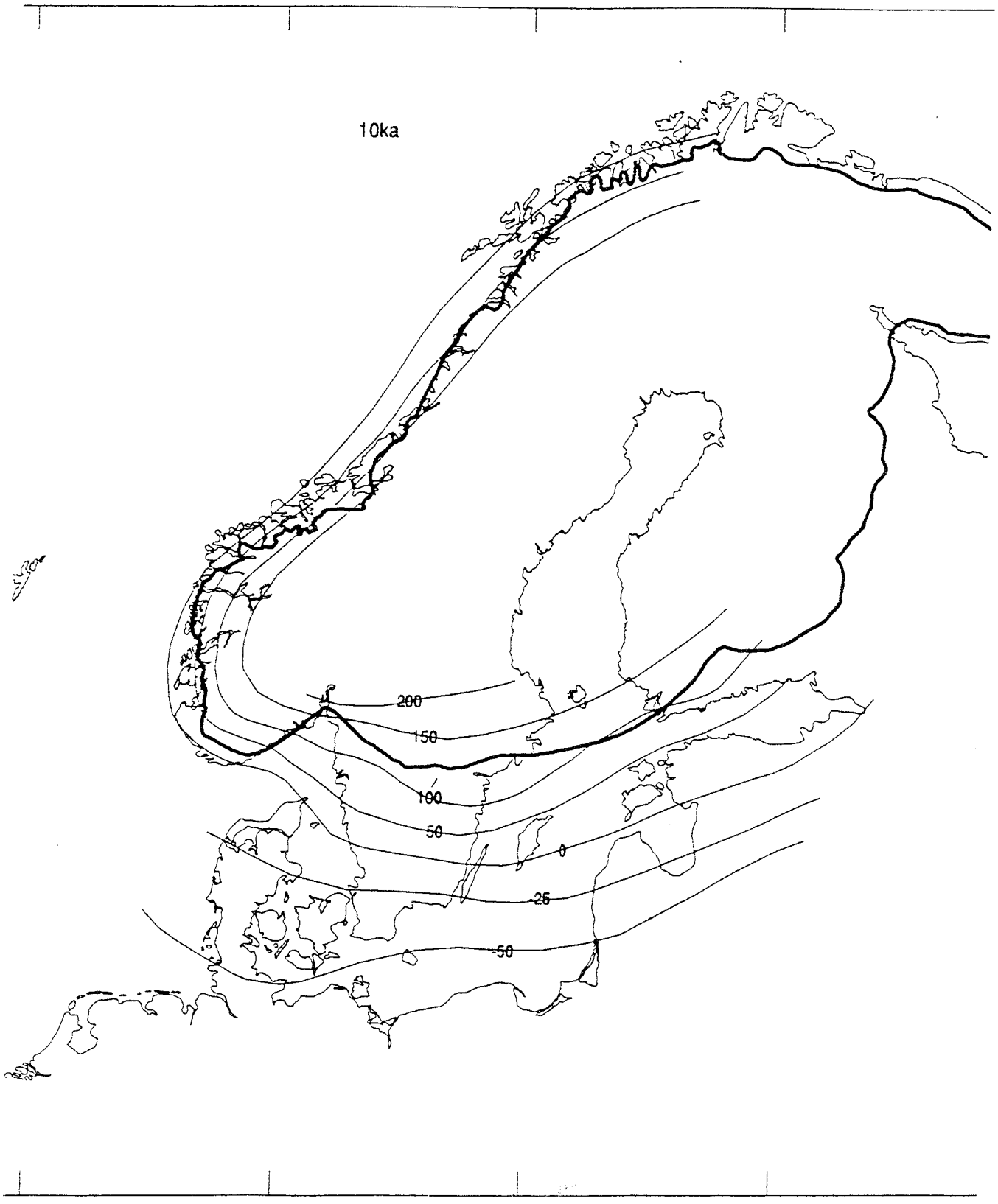

Figure 6.8 a-c

a) Isobases for the European ice sheet for 10ka, showing the contemporary extent of the ice sheet.

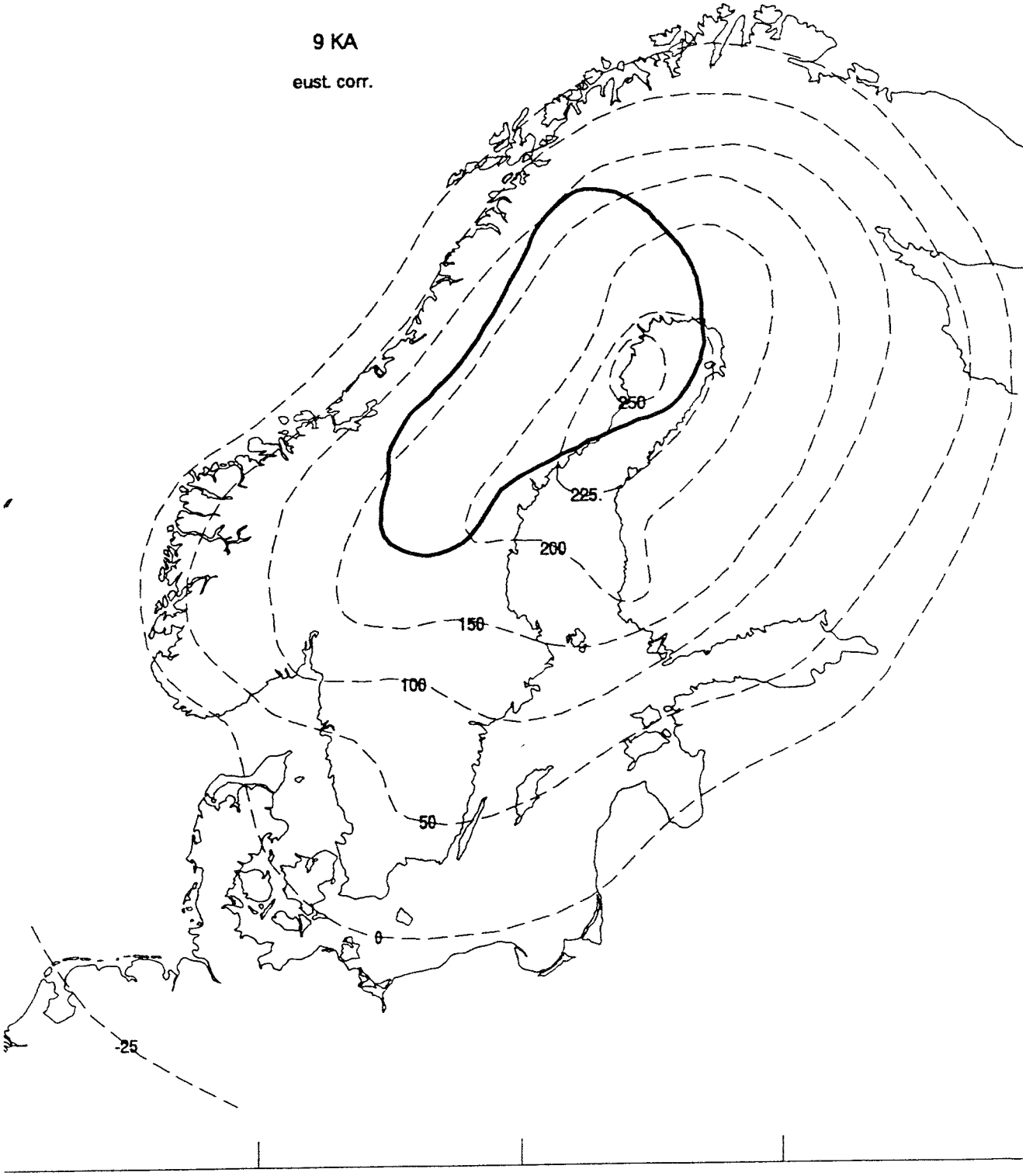

Figure 6.8 a-c

b) Isobases for 9ka.

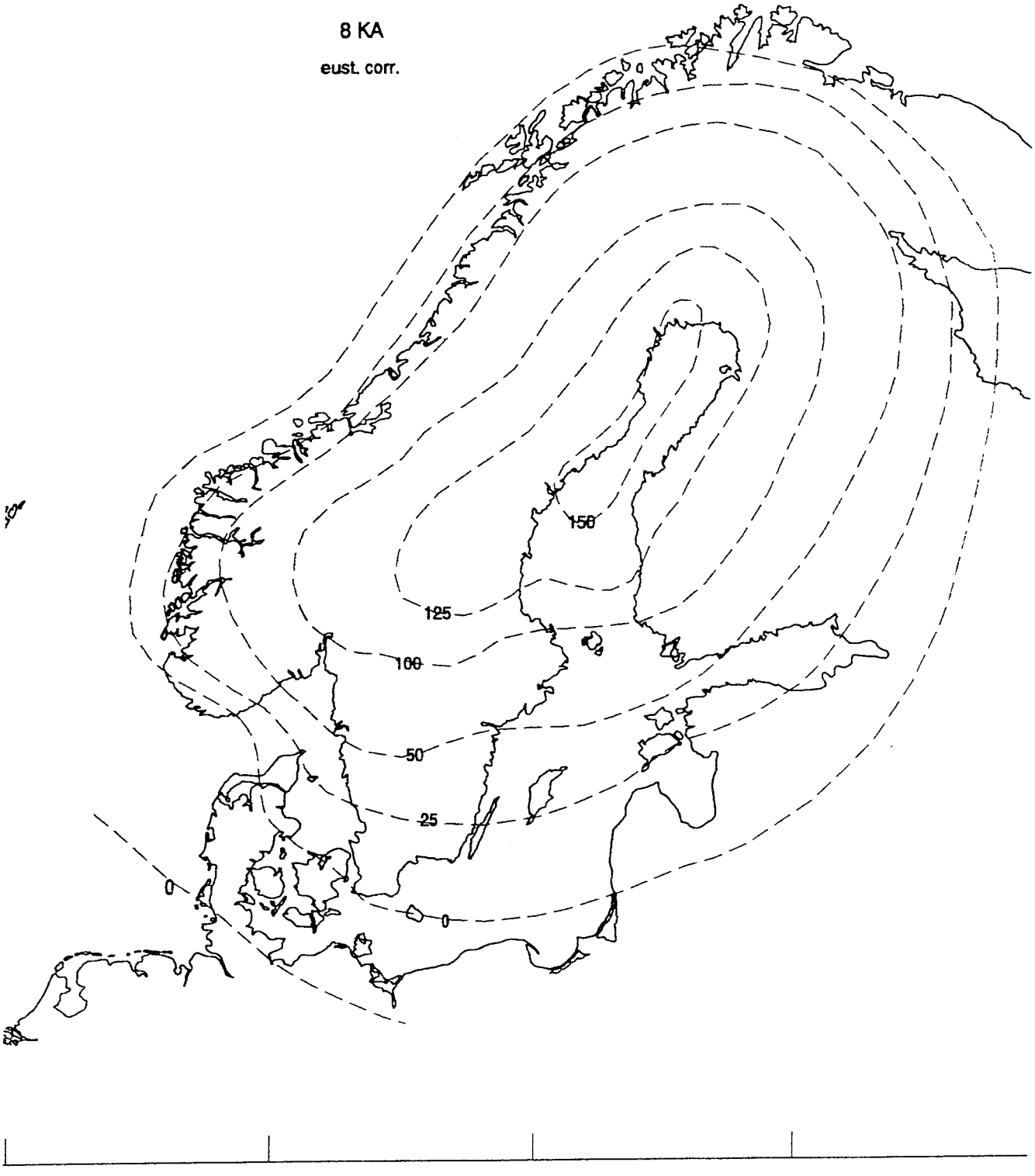

Figure 6.8 a-c
c) Isobases for 8Ka

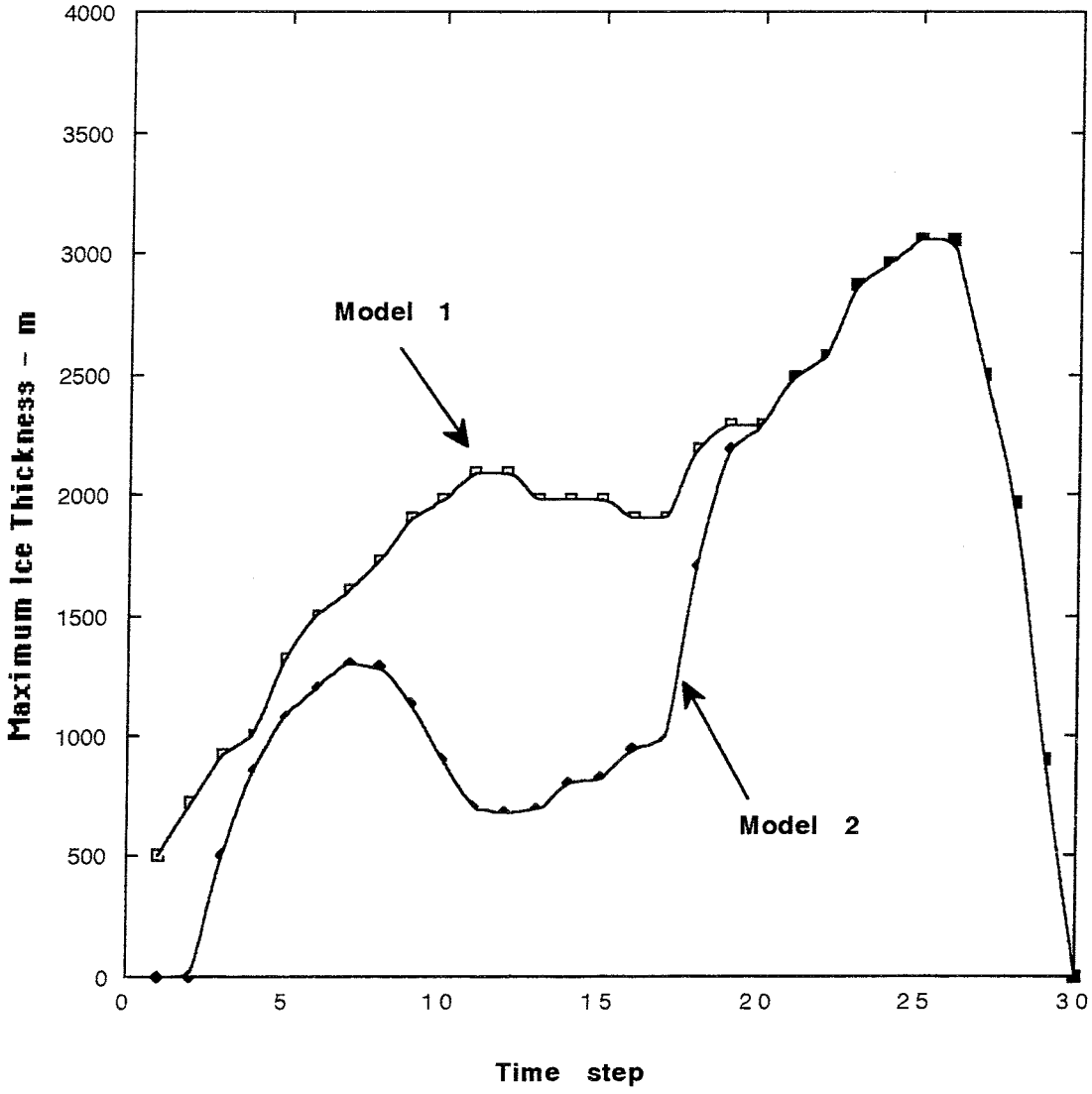

Figure 6.9 Model 1 shows the loading history at 900km in the time/distance model shown in figure 5.1. Model 2 shows an alternative loading history which gives a better fit to the geological evidence of relative sea level change. Time steps are of 2ka, time step one being 60-58ka and time step 30 being 8-6ka.

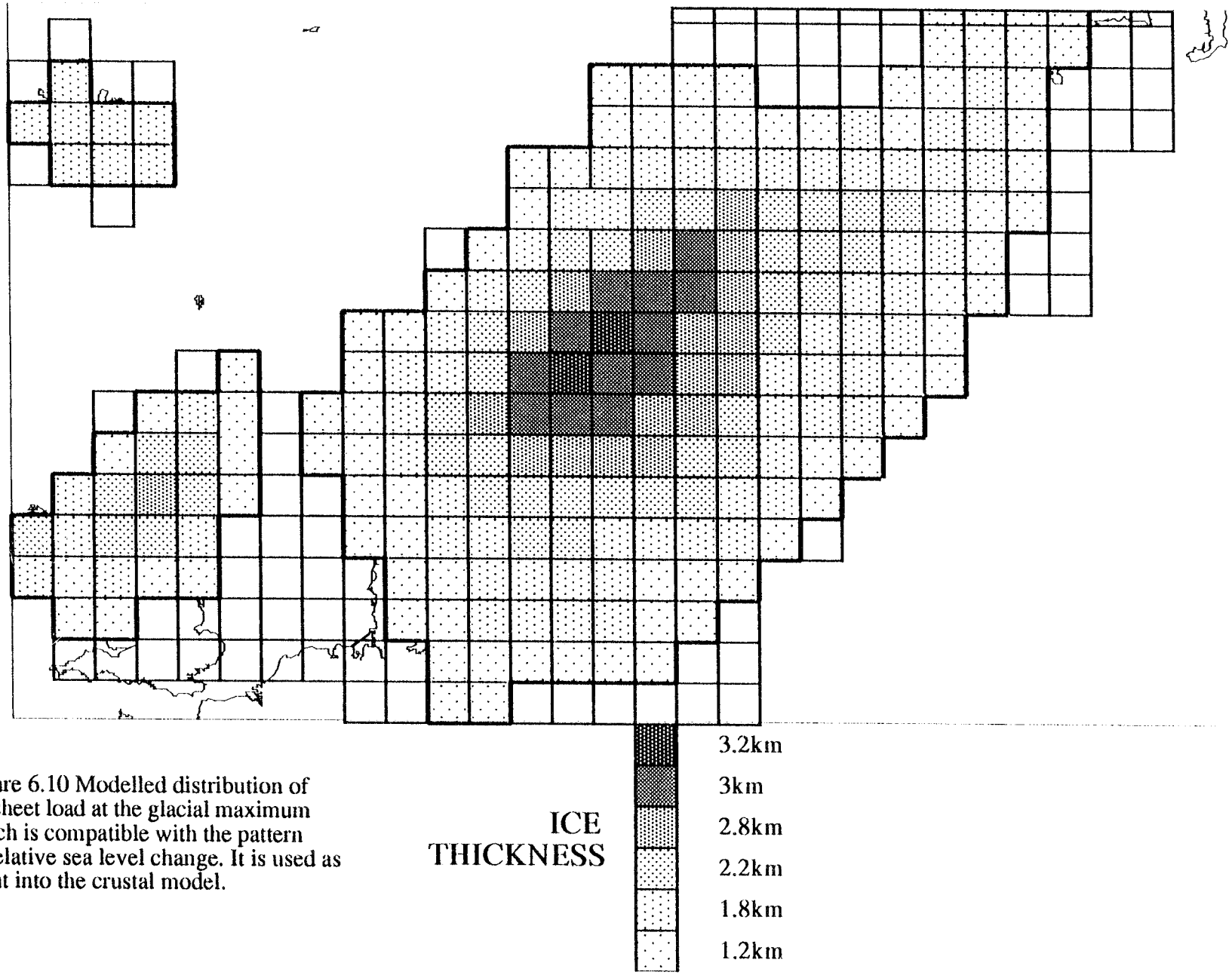

Figure 6.10 Modelled distribution of ice sheet load at the glacial maximum which is compatible with the pattern of relative sea level change. It is used as input into the crustal model.

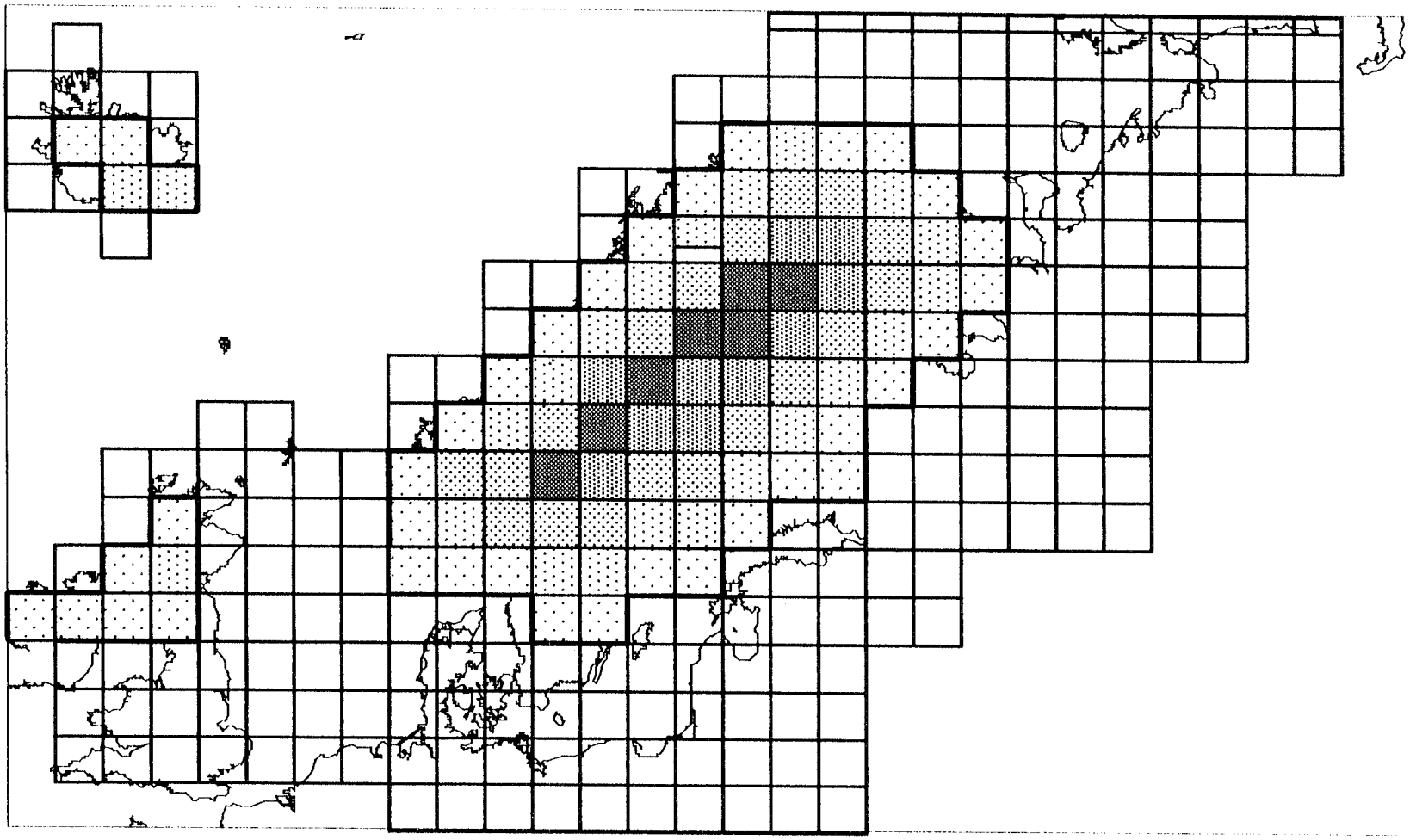

Figure 6.11 Modelled distribution of ice sheet load during a build-up or decay phase of the ice sheet.

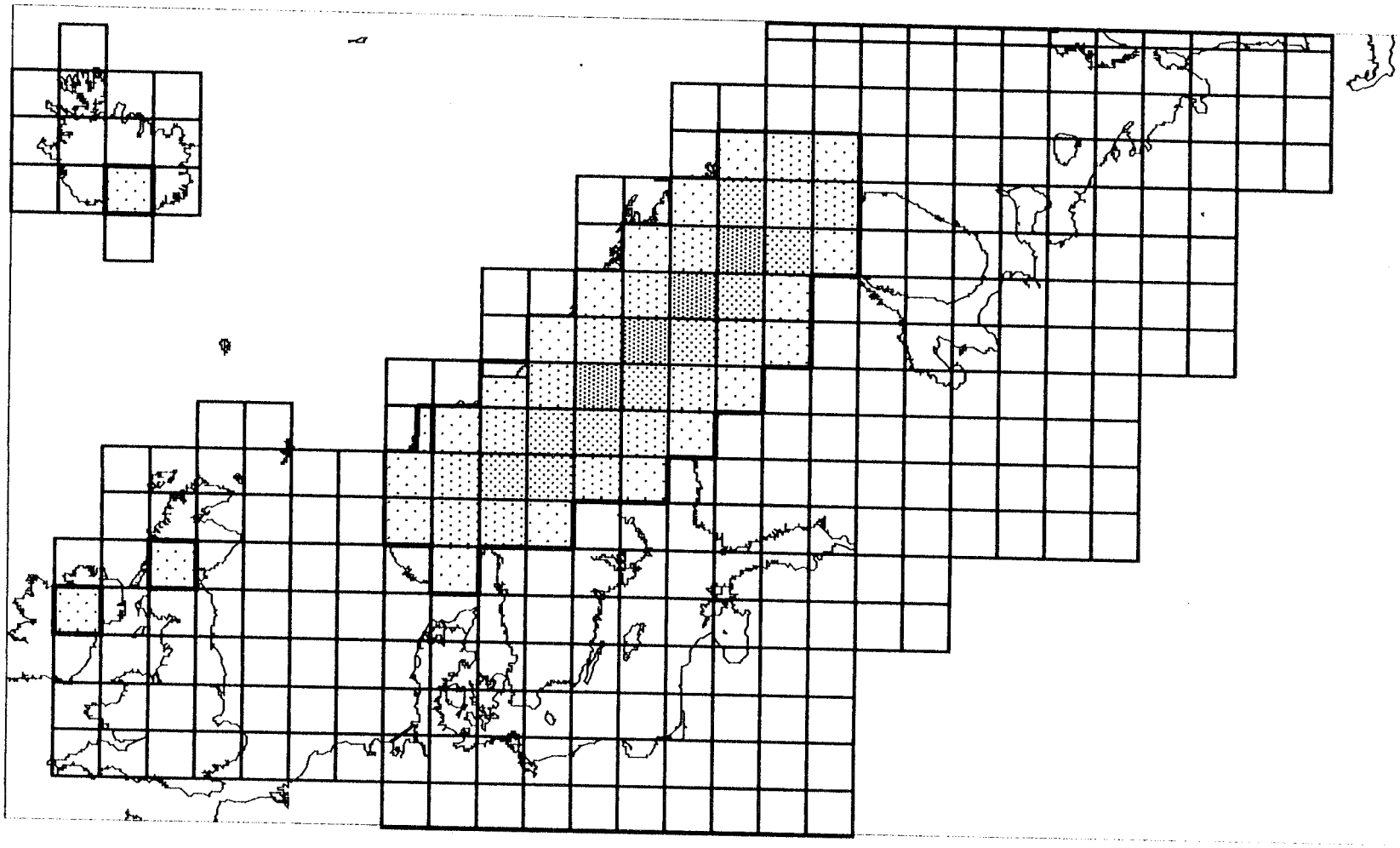

Figure 6.12 Modelled distribution of
ice sheet load during a build-up or decay phase.

where $\Delta\xi(\phi,\lambda:t)$ is the position of mean sea level at latitude Ø, longitude λ and time t, relative to the present (time t_o) position at the same location.

$$\xi(\phi,\lambda:t) = \xi_\tau(\phi,\lambda:t) - \xi_i(\phi,\lambda:t) + \xi_w(\phi,\lambda:t) \qquad (6.2)$$

where ξ_τ is the change in sea level resulting from cie melting on a rigid earth (eustatic). ξ_i is the earth response to glacier loading/unloading. It is a function earth rheology (ξ and ice load (I_t). ξ_w is the deformation produced by meltwater loading. It is a function of ξ, of ocean geometry $O_{(t)}$ and sea level change (ξ (t)).

6.2 is solved iteratively for ξ (t) subject to mass conservation, and the assumption that the oceanic surface remains an equipotential at all times. The solution is obtained from a spherical harmonic explosion:

$$\Delta\xi = n = o\sum_{n=o}^{N}\Delta\xi(n) = \sum_{n=o}^{N}\left[\Delta\xi^{(n)} + \Delta\xi_i^{(n)} + \Delta\xi_w^{(n)}\right] \qquad 6.3$$

The limit N is taken as 18° (Lambeck et al (1990). A value of $\xi = 5 \times 10^{20}$Pa was taken.

The output from the model is a pattern of relative sea level change which is computed for specific points for which geological evidence of relative sea level change exists. A good fit is assumed between predicted and observed relative sea change when they lie within 15% . Results for a number of sites are shown in Figure 6.13. In general, there is a good fit between predicted and observed data when a relatively low slope model is used.

The largest discrepancies occur for the Late Glacial in the southern Baltic, where the model predicts too great a magnitude of crustal depression, particularly for the high slope model. A series of sensitivity tests were undertaken to explore possible reasons for this. We assume that the pattern and tempo of decay are too well established too be markedly erroneous, and therefore examined effects of varying the rate of build-up. Understandably, the model proved very insensitive to changes in the build-up pattern prior to 40ka, but did show sensitivity to the build-up prior to 25-30ka. It was found that a smaller ice sheet mass between 25 and 40ka in the

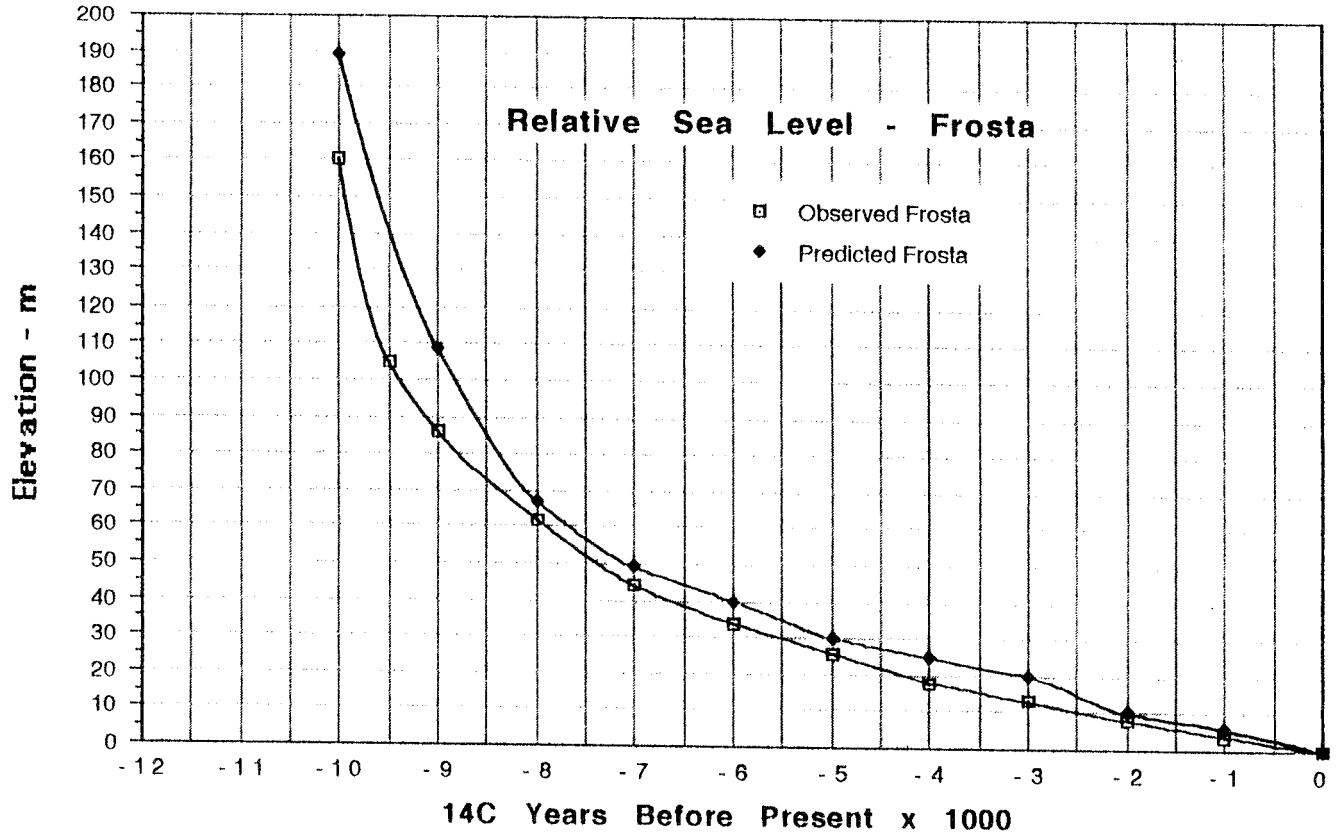

Figure 6.13a Predicted and observed relative sea level curves for Frosta (fig. 6.7).

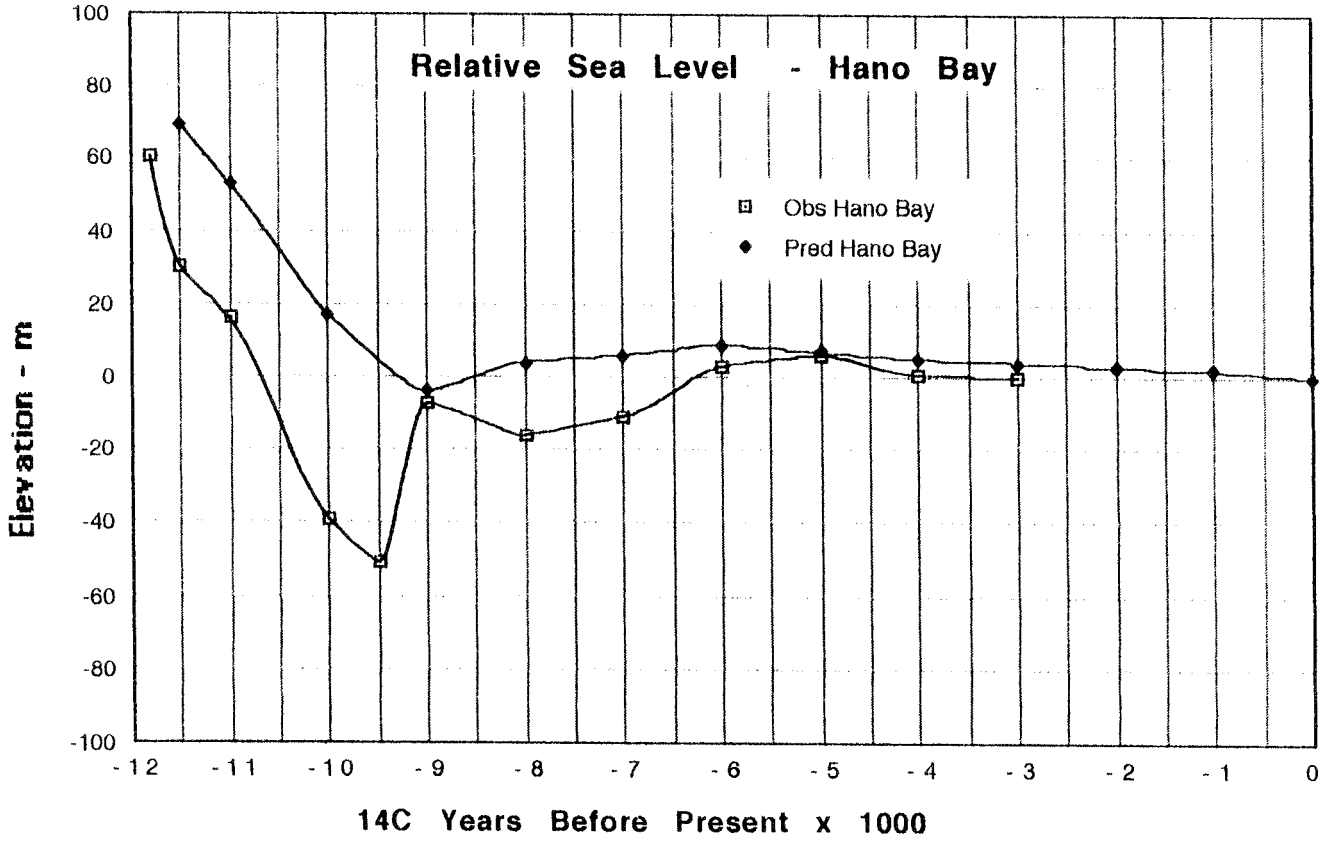

Figure 6.13b Predicted and observed relative sea level curves for Hāno Bay (fig. 6.7).

area of southern Scandinavia was able to reduce the discrepancy in the southern Baltic region to acceptable limits (Figure 6.9).

A similar result was also achieved by reducing the surface slope, and therefore the thickness, of the ice mass in the southern Baltic area. Boulton et al.(1985) suggested that a soft deformable ice sheet bed in this area would tend to draw down the surface because of a low basal shear resistance.

We suggest that in broad outline that the model is compatible with the geological evidence of Late Glacial and Holocene relative sea level change.

6.4 THE EVIDENCE OF TILL THICKNESS DISTRIBUTION.

Recent research suggests that a large proportion of the tills produced by ice sheets which invade sediment-covered lowland terrain is produced by re-working of pre-existing sediment (Boulton and Jones, 1979; Alley et al., 1987; Boulton, 1987). It is possible, for such till, to apply a theory of sediment transport which relates large scale patterns of erosion and deposition to the integrated time/space behaviour of the ice sheet (Boulton, in press). In this theory, deformation of subglacial sediments plays the primary role in determining the rate of movement at the glacier sole in response to the driving stress. Where the glacier sole is at the melting point, and provided that subglacial beds are not so permeable as to permit subglacial water pressures to dissipate to low values because of efficient subglacial drainage, subglacial sediment will deform to a depth (T_a) given by:

$$T_A = \frac{\tau_b}{\left[(1-n)(\rho_s-\rho_w)g - \frac{\xi\rho_w g}{k}\right]\left[c' + \tan\phi\right]} \quad (6.4)$$ (Boulton and Hindmarsh, 1987)

Where n is sediment void ratio ρ_s & ρ_w are densities of sediment ground and water and K is for hydraulic conductivity.

The deformation velocity (U_b) at the top of this horizon will be:

$$U_b = 2\int_o^{Tn} \Sigma_{xz}[p'(z)\tau_b]dz \qquad (6.5)$$

where p' is effective pressure

The discharge of sediment (Q_A)will be:

$$Q_A = \int_o^{T_A} U \; dz \qquad (6.6)\text{ (Boulton, in press)}$$

Equation 6.2 now defines the basal boundary condition for glacier flow. The glacier flux will be sustained by a combination of flow in the sediment bed and flow in the ice. In a steady state this flux balances the net accumulation flux so that:

$$U_b + \int_o^H U_i dz = \int_o^x A dx \qquad (6.7)$$

where A is the mass balance.

If the flux in the sediment bed increases down glacier, net erosion of the bed will occur, whilst if the flux decreases down glacier, deposition will occur. The rate of erosion (E) will be:

$$E = \frac{\partial Q_A}{\partial x} \qquad (6.8)$$

and the rate of deposition (D) will be:

$$D = \frac{\partial Q_A}{\partial x} \qquad (6.9)$$

Writing this in terms of mean velocity (equation 6.2) and thickness of the deforming horizon (from 6.1) gives:

$$E = \frac{dU}{dx}T + \frac{dT}{dx}U + \frac{dU}{dx}\frac{dT}{dx} \qquad (6.10)$$

Above the equilibrium line the longitudinal strain rate and $\frac{dT_A}{dx}$ will be positive, negative below the equilibrium line, leading to erosion above the equilibrium line and deposition below it. Although this leads to a relatively simple instantaneous pattern of erosion and deposition, time-dependent patterns of ice sheet fluctuation can be complex. For an ice sheet varying in time and space, the erosional/depositional resultant will be achieved by integrating 6.7 through time at each locality along the profile.

For an ice sheet whose pattern of variation in time and space can be prescribed, it should be possible to predict the resultant pattern of erosion and deposition if we assume that sediment is always available to be eroded. We have used a till rheology derived from a till in Iceland (Boulton & Hindmarsh, 1987) which permits the magnitude of erosion and deposition to be calculated. Although sandy Icelandic tills and sandy Swedish tills may well have a similar rheology, we are still able to calculate the normalised distribution of till along a flow line provided that the general form of the rheological relationship is correct and till rheology remains constant along the flowline.

Figure 6.14 shows the variation through time of the longitudinal vertical strain rate in the ice along the line of the transect. It is assumed that strain in the till mirrors this. This, together with computed values of deforming layer thickness, permit us to calculate (from 6.7) the resultant till thickness . This is shown in Figure 6.15 normalised to the maximum till thickness. However, if we assume that neither erosion nor deposition will occur in a zone where the glacier sole is below the melting point, we can use the patterns of basal melting and freezing shown in Figures 5.5-5.6 to determine where there will be no basal activity.

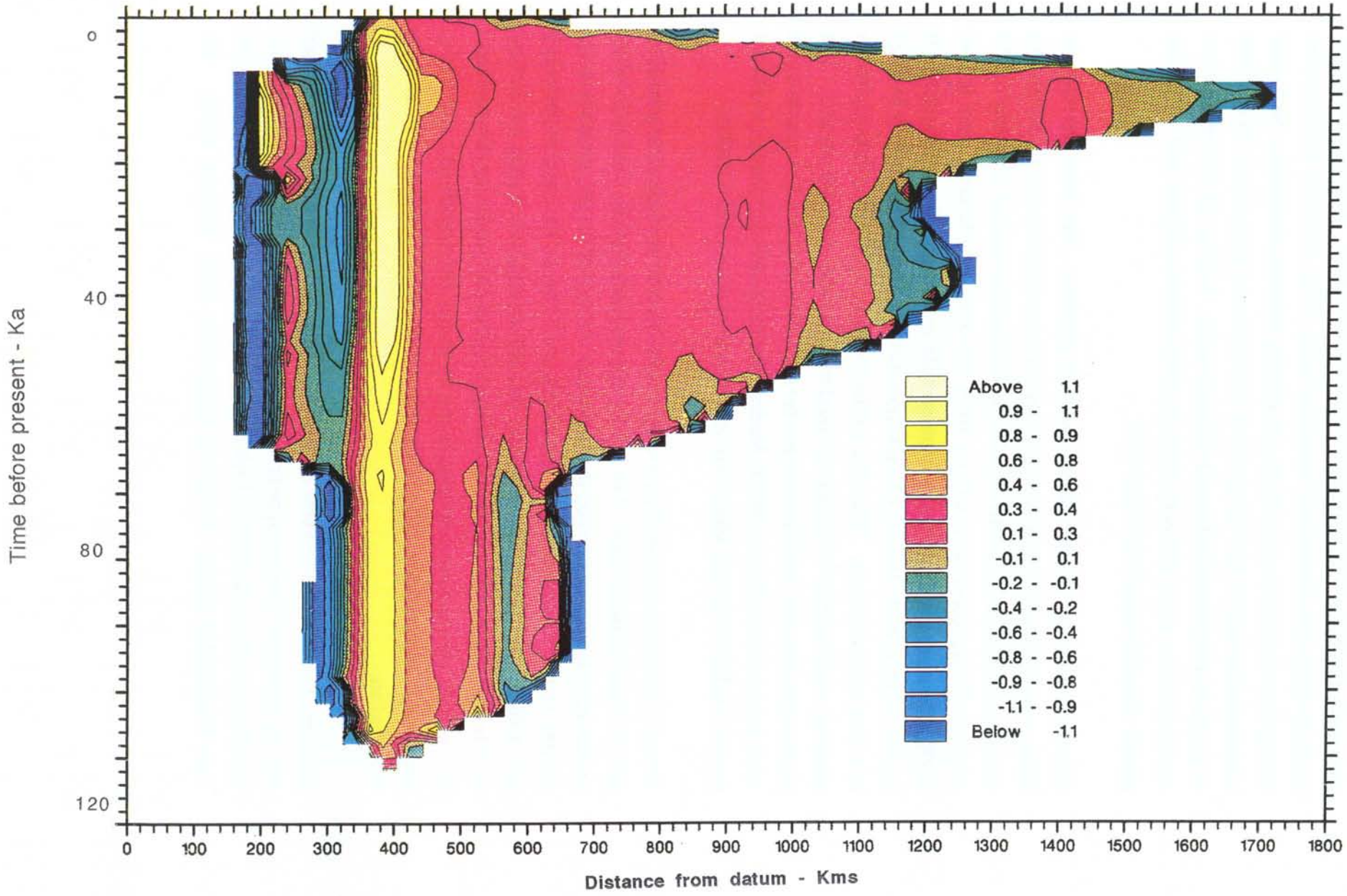

Figure 6.14 Distribution of ice sheet longitudinal strain rate in time along the transect.

In order to test this prediction, careful interrogation of borehole and other records held by the Swedish Geological Survey was undertaken along the line of the transect by Professor J. Lundqvist of Stockholm University. However, in view of the likely local, three-dimensional variability in the pattern of erosion and deposition arising from topographic irregularity, pre-existing sediment availability, rheological inhomogeneity and the low frequency of exposures and boreholes, it was decided to sample in a broad swath of terrain 90 km in width. Average till thicknesses were established for a series of blocks along the swath shown in Figure 6.16. They are plotted along the transect in Figure 6.15.

This data was only collected for the Swedish mainland. Data from the southern Baltic was obtained from marine geophysical traverses (Uscinowisc, Kramarska and Przezdziecki, 1988), whilst data for the Weichselian terminal zone south of the southern Baltic coast was derived from the work of Eissmann and Müller (1979).The complete till thickness transect made up from these three components is shown in Figure 6.15. It is important to note that this distribution can only be taken as a first approximation. The data on the Swedish mainland is derived from a relatively small number of sites and would repay a more complete analysis. The marine data from the Baltic is averaged between three profiles taken normal to the coast just east of the German/Polish border. The German/Polish land data is based on two borehole transects, which may conceal a great deal of 3-D variation.

However, there is a surprisingly good agreement between the theoretical prediction and the observed distribution. The best agreement is achieved by a model in which sedimentary activity is assumed to cease where the sole of the glacier is below the melting point. This simulates the thickening of till seen on the traverse between 0 and 400km. According to the model, this till accumulates during the earliest Weichselian phase of glacier expansion when molten bed conditions occurred here, but is protected from erosion susequently by frozen bed conditions. Lundqvist (personal communication, 1991) also believes that these tills date from the early Weichselian.

In general this model would also explain why areas just to the east of the mountain belt in northern Sweden appear to have a topography which reflects early Weichselian glacier activity and which has survived relatively intact through the Late Weichselian glacial maximum (Lagerbäck, 1988; Kleman, 1990). We

suggest that during the Early Weichselian, when the ice sheet had extended only a little way beyond the mountain belt, melting point temperatures and high velocities were typical of this zone, where the glacier was able to erode and deposit relatively strongly. Whereas during the later part of the glacial cycle, when the ice sheet was very much larger, this was an area of low ice velocity and temperature, producing little geomorphological activity.

We therefore conclude that the model is compatible with the evidence of till distribution in the southern Baltic region.

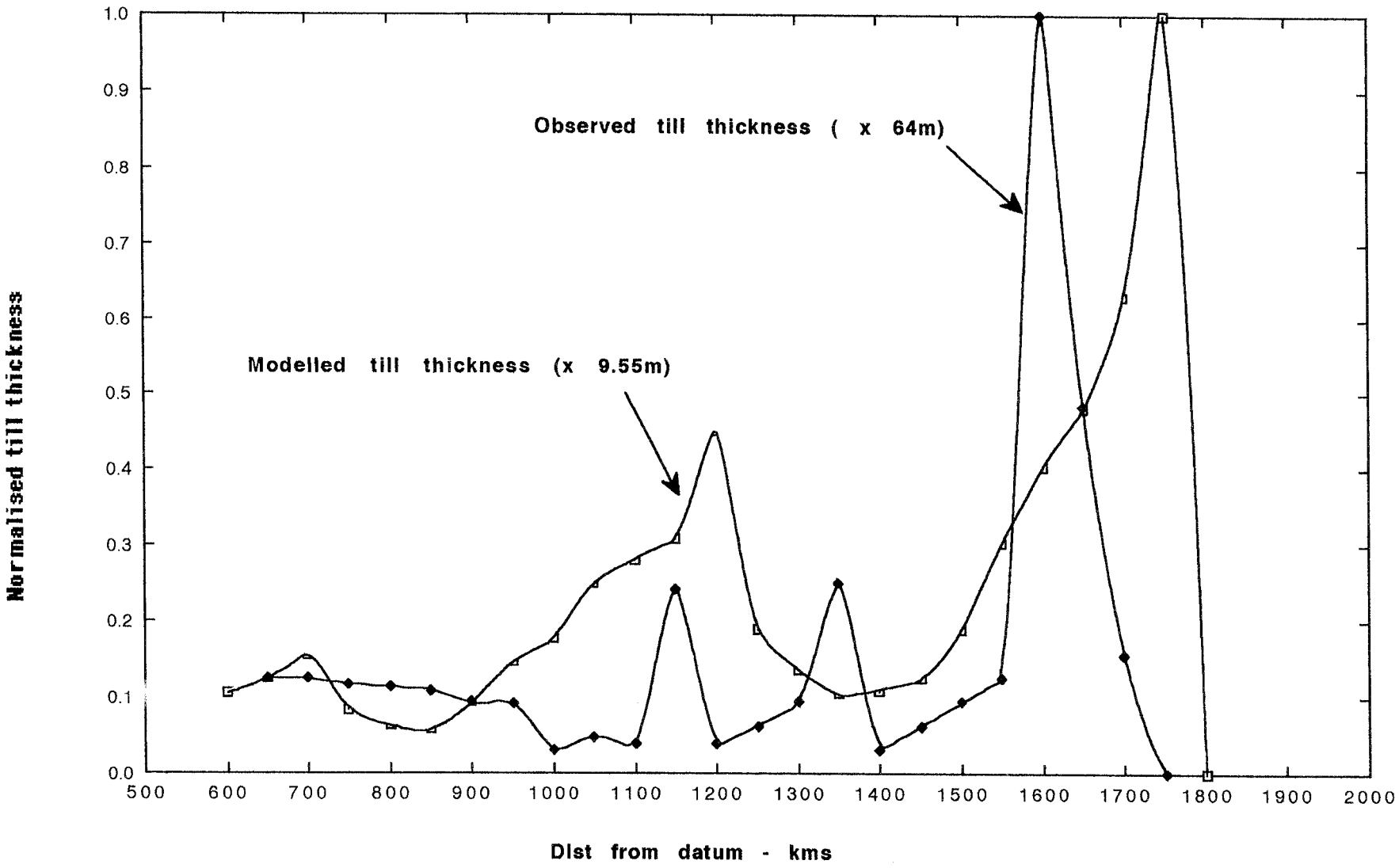

Figure 6.15 Normalised predicted and observed till thicknesses along the transect shown in figure 6.16.

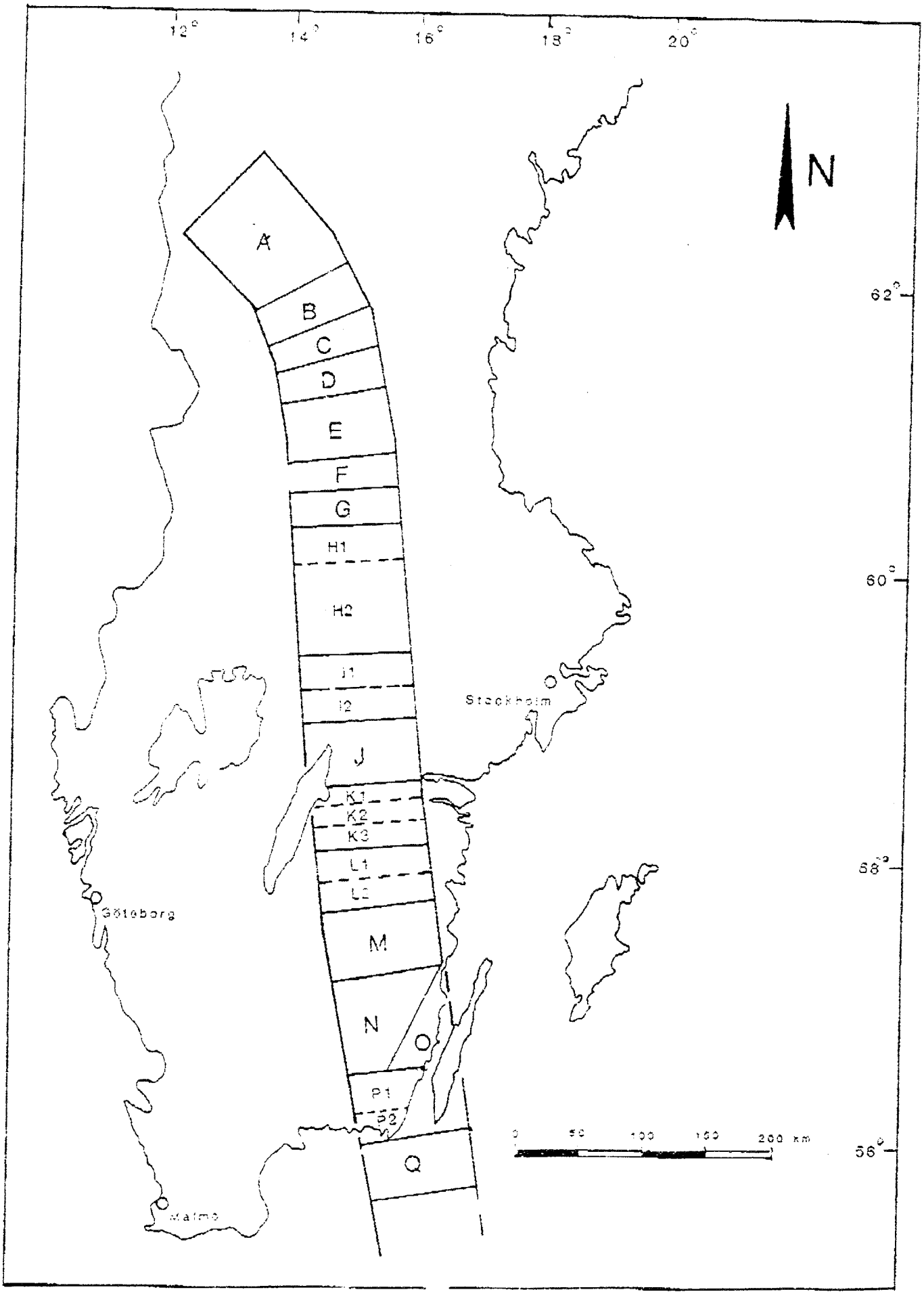

Figure 6.16 The swath along which till thickness data has been collected.

7 PREDICTING FUTURE GLACIATION IN SWEDEN.

Calculations of future Milankovitch-variations are used to calculate future climate, including future N.E. Atlantic SSTs. These are then used to compute future ELA variations and future ice sheet variations, including basal temperatures, melting rates, etc. The probability of sites at different distances from the initial ice divide being glaciated at given future times is estimated. We believe that within the limitations of present knowledge, the ice sheet model is able to satisfactorily simulate the behaviour of the last ice sheet in Europe. Provided therefore that we are able to generate a climate forcing function for the future, we should be able to predict future ice sheet behaviour.

..... ***** .....

7.1 A FUTURE CLIMATE FORCING FUNCTION.

A number of attempts have been made in recent years to predict the future course of climate based on:

- a statistical extrapolation of geological records of past climate trends;

- extrapolation into the future of Milankovitch fluctuations and the inference of future climate, either from statistical correlations of past climate with past Milankovitch fluctuations or by using deterministic models of the climate system forced by future Milankovitch fluctuations.

Calder (1974) produced a simple arithmetic model of climate based on Vernaker's (1972) insolation tables, in which climate was related to summer insolation in the northern hemisphere. Peterson and Larsen (1978) produced a statistical extrapolation from the Emiliani and Shackleton (1974) palaeotemperature series-using an ARIMA model , as did Melice and Berger (1989). Imbrie and Imbrie(1980) produced a parameterisation between past land ice volume and orbital input and used the parameterisation to predict future ice volume from future orbital

changes. Kukla et al. (1981) also used an empirical correlation between orbital parameters and past palaeoenvironment to predict future climate as did Berger et al. (1981). Berger et al. (1989) used a deterministic climate model both to simulate past climate from the orbital input and to predict future climate.

It is reassuring that notwithstanding these varied approaches, essentially similar predictions about the future of the natural climate system are produced. They are summarised below:

	Cold Phases	Warm Phases
Calder (1974)	25ka 54ka 100ka	31ka 73ka
Petersen & Larsen(1978)	30ka 70ka 15ka 60ka 35ka	60ka 85ka 35ka
Melice & Berger (1989)	8ka (10ka limit on model)	
Imbrie & Imbrie (1980)	23ka 63ka	31ka 75ka
Berger et al. (1981)	5ka 22ka 60ka	14ka 30ka 50ka
Kukla et al. (1981)	5ka 23ka 59ka 100ka	14ka 30ka 72ka
Berger et al. (1989)	24ka 56ka	32ka 72ka

Important common elements in all these predictions are major cold phases at between 15-35ka and 54-70ka in the future.

The principal driving function which we have used in our ice sheet reconstructions has been the sea surface temperature in the north-east Atlantic. In order to extrapolate this into the future as a driving function for a future ice sheet, we have used a regression between the N.E. Atlantic SSTs and the Imbrie and Imbrie (1980) model in which computation has been continued to 120ka into the future. We have then used the correlation function described in chapter 4 to generate a future pattern of ELA fluctuation. This is shown in Figure 7.1.

7.2 FUTURE GLACIATION PREDICTIONS

The forcing function derived above, together with an assumed sea level temperature of -5°C at the glacial maximum, have been used as input to the future ice sheet

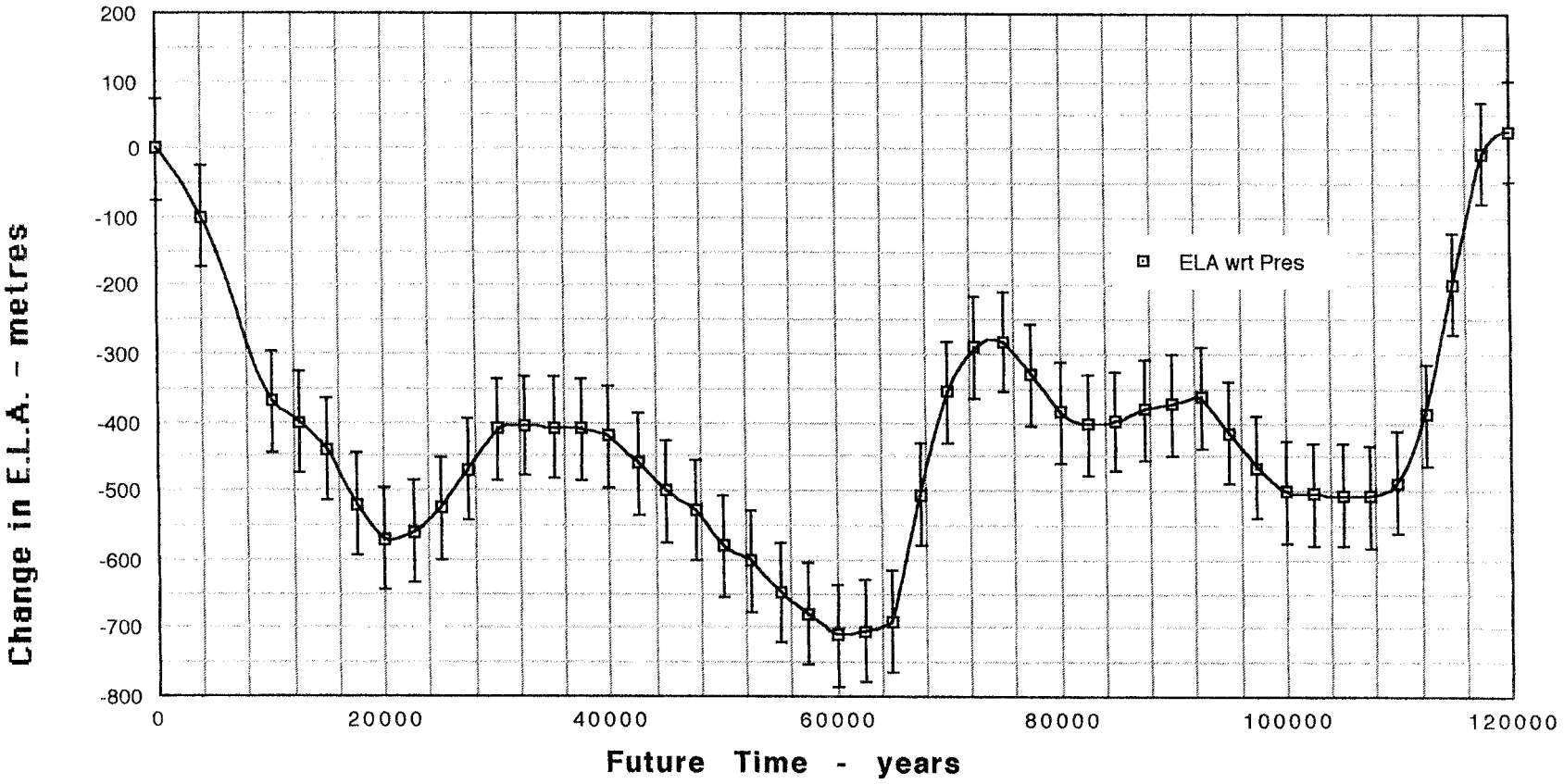

Figure 7.1 Predicted future ELA variation in Europe. Bars show 75% probabilities.

model (sensitivity tests in chapter 4 suggest that the ice sheet characteristics with which we are primarily concerned are relatively insensitive to the normal range of temperatures which are assumed at sea level in Europe during glacial cycles). Ice sheet fluctuations in response to this forcing have been computed using the model established for the Weichselian glacial cycle. The following time/distance fields have been computed along the transect:

Ice thickness (m)	Figure 7.2
Basal velocity (m $year^{-1}$)	Figure 7.3
Basal temperature and proglacial surface temperature for a SLAT air of -10 C	Figure 7.4
Basal temperature and proglacial surface temperature for a SLAT air of -5 C	Figure 7.5
Permafrost thickness for a SLAT air of -10 (m)C	Figure 7.6
Permafrost thickness for a SLAT air of 5 -C (m)	Figure 7.7
Basal melting rate (mm $year^{-1}$)	Figure 7.8

Substantial glacier growth begins in the mountains in about 6000 yrs time. The ice sheet reaches its maximum extent about 70ka into the future, when it extends some 800km to the south of the initial ice divide and reaches as far as Scania. During its initial expansion, the ice sheet is cold-based until it extends some 100km from the initial divide, when basal melting begins. At the maximum the melting zone has a width of about 400km, stretching back from the terminus as far as Dalarna.

Figure 7.9 shows a prediction of the surface and basal melting rate through the glacial cycle.Note that the surface melting rate is two orders of magnitude less than the subglacial melting rate. Surface meltwater is not however regarded as an important source of meltwater for the subglacial bed. Meltwater produced by surface melting is generated during the summer season , and much of it may drain into moulins and crevasses which penetrate to the surface. However, during winter on an ice sheet , any cavities which developed during the previous summer by the action of meltwater would tend to close at a shallow depth of 100m to 150m by the flow of ice . We do not therefore expect any large volumes of surface meltwater to penetrate to the glacier bed in an ice sheet at distances greater than a few 100 metres from the terminus. Valley glaciers are a slightly different case. Here, fast flow may be able to maintain crevasses open to depths beneath which they would normally

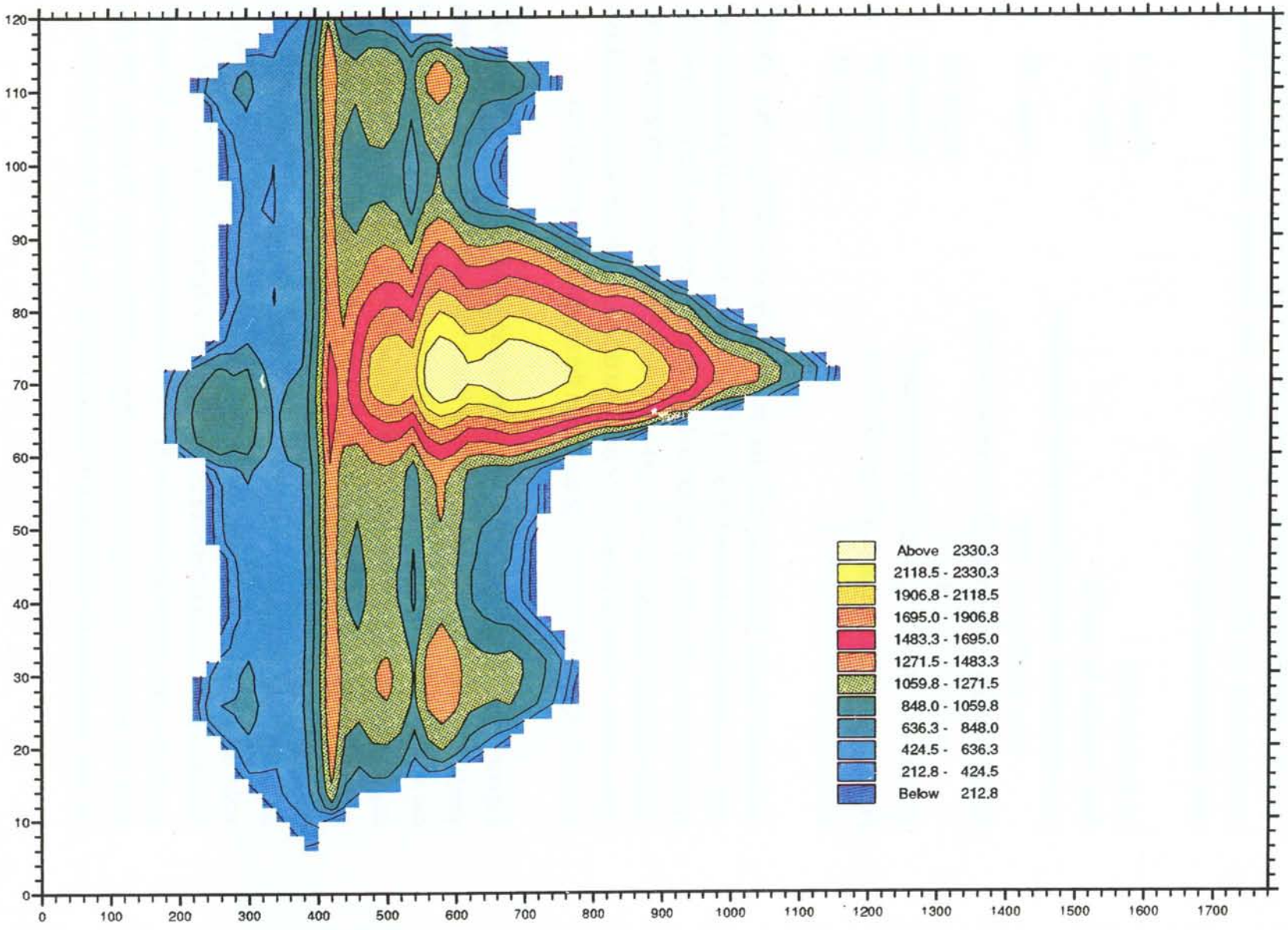

Figure 7.2 Predicted ice sheet thickness along the transect during the next 120ka.

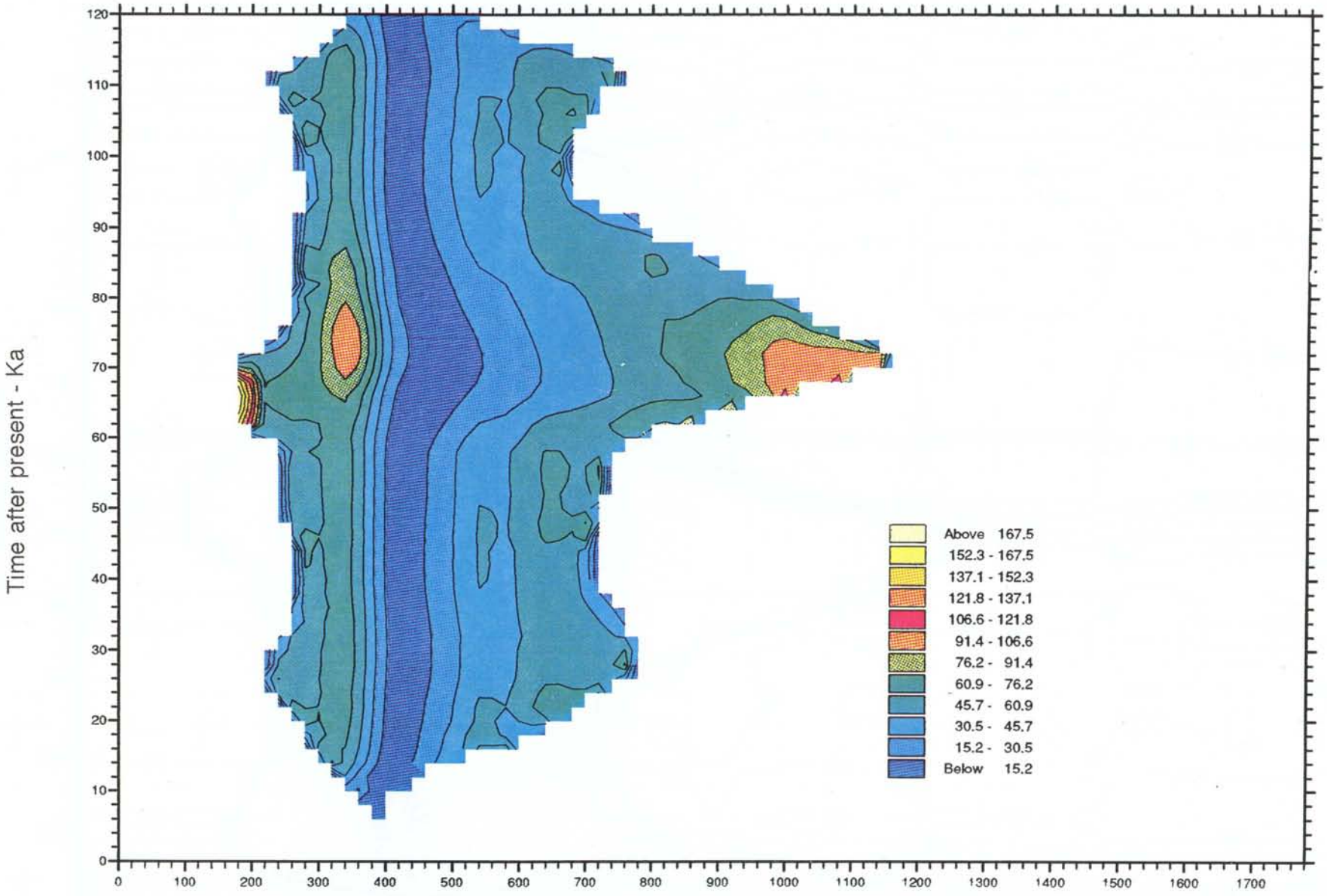

Figure 7.3 Predicted distribution of velocity along the transect through the next glacial cycle.

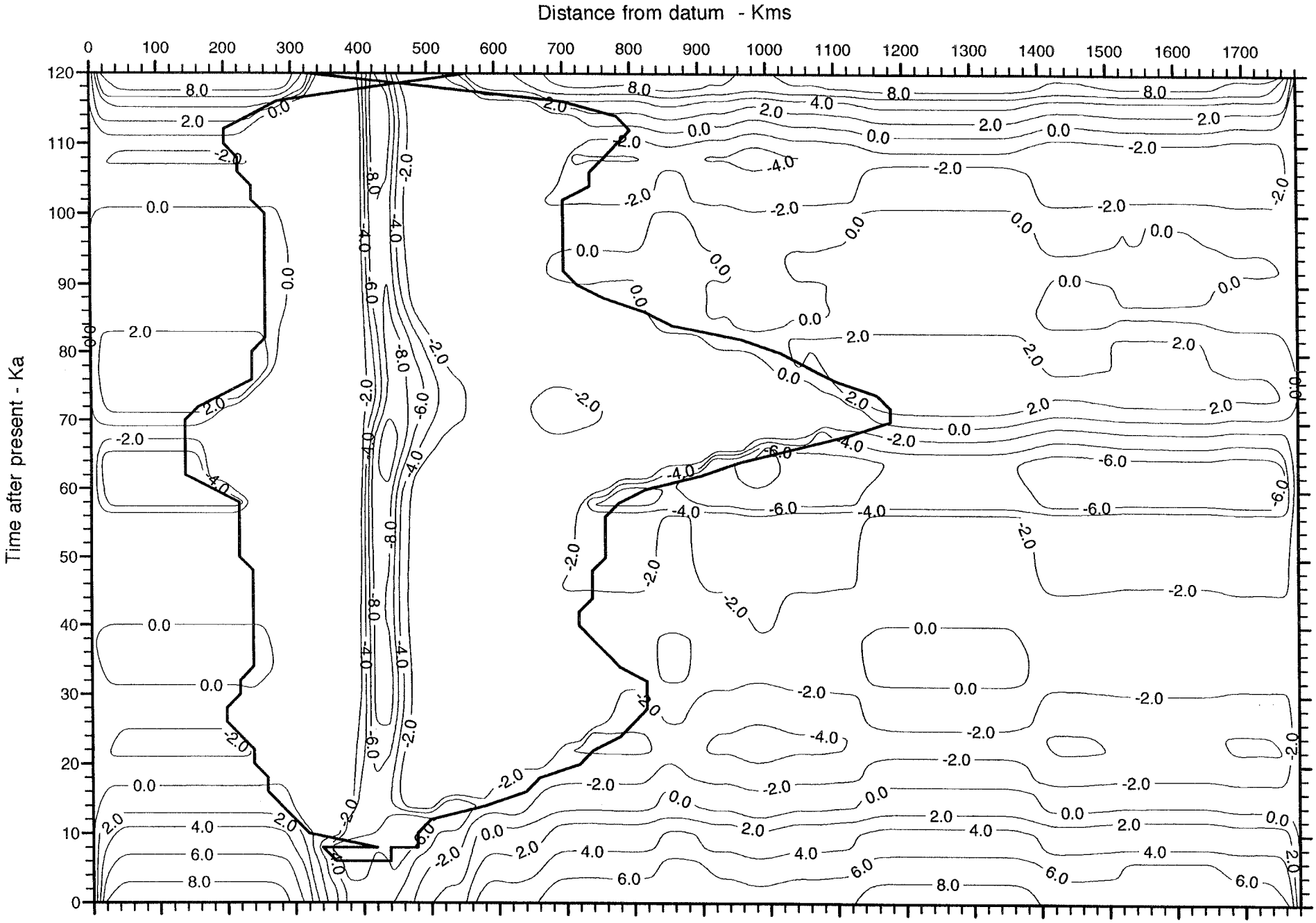

Figure 7.4 Prediction of the time distance variation of an ice sheet along the standard transect (western Norwegian shelf to left, northern Poland to right) during a possible next glacial cycle. It shows the temperature distribution on the subglacial and proglacial surface for a standard sea level temperature of -10°C.

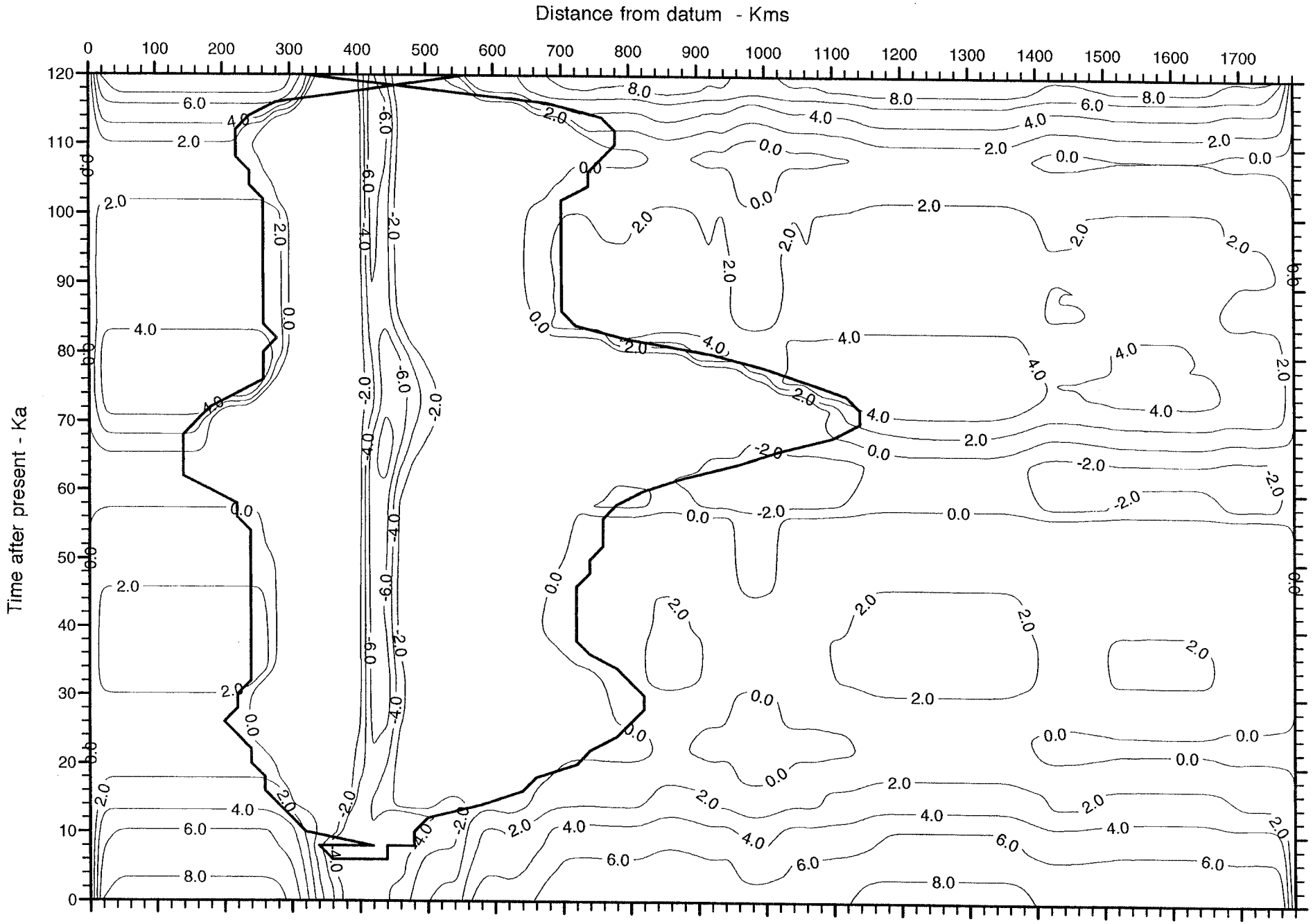

Figure 7.5 As figure 7.4 but for a standard sea level temperature of -5°C.

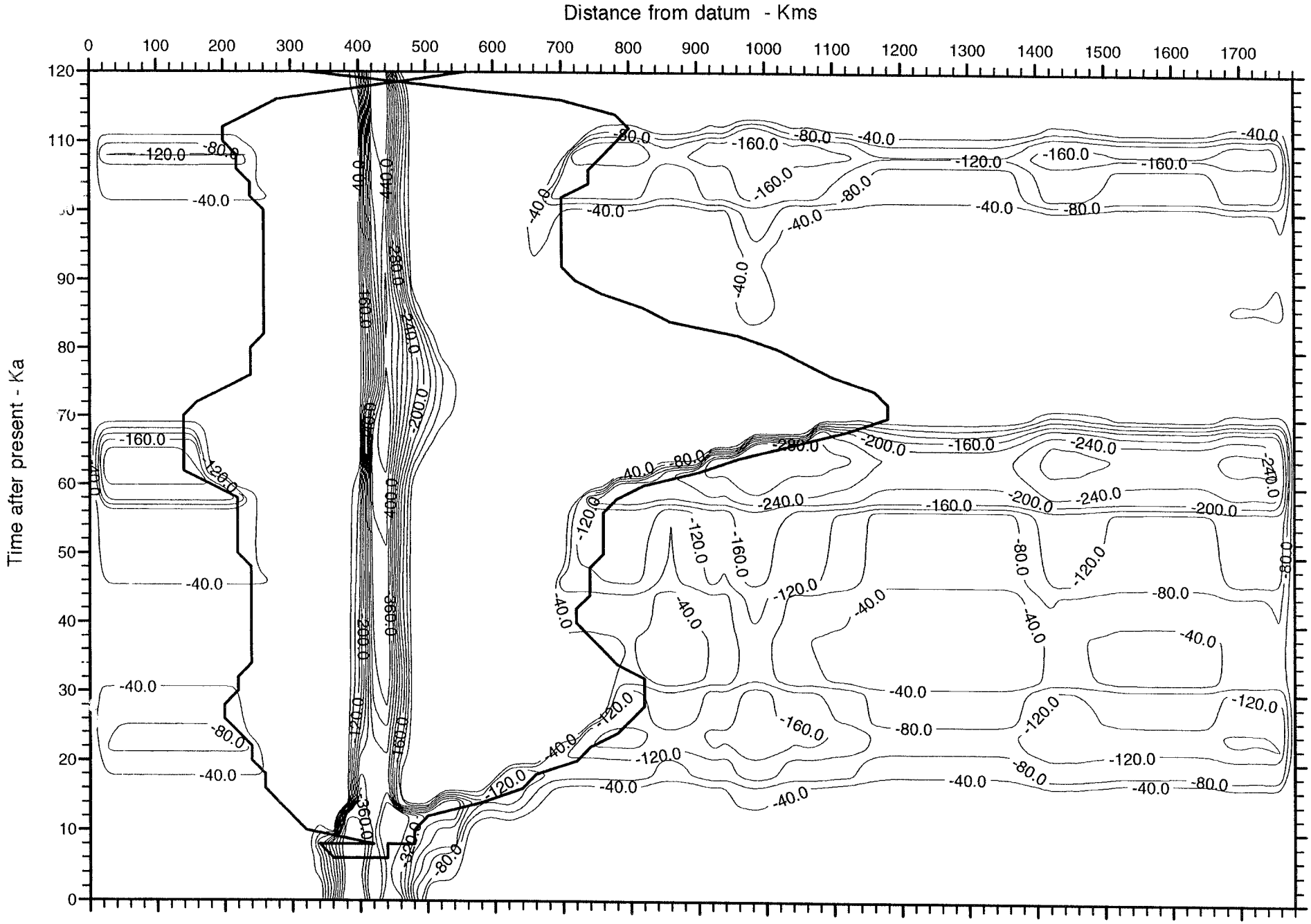

Figure 7.6 Predicted thickness of frozen ground (permafrost) beneath and beyond the ice sheet of a possible next glacial cycle for a standard sea level temperature of -10°C.

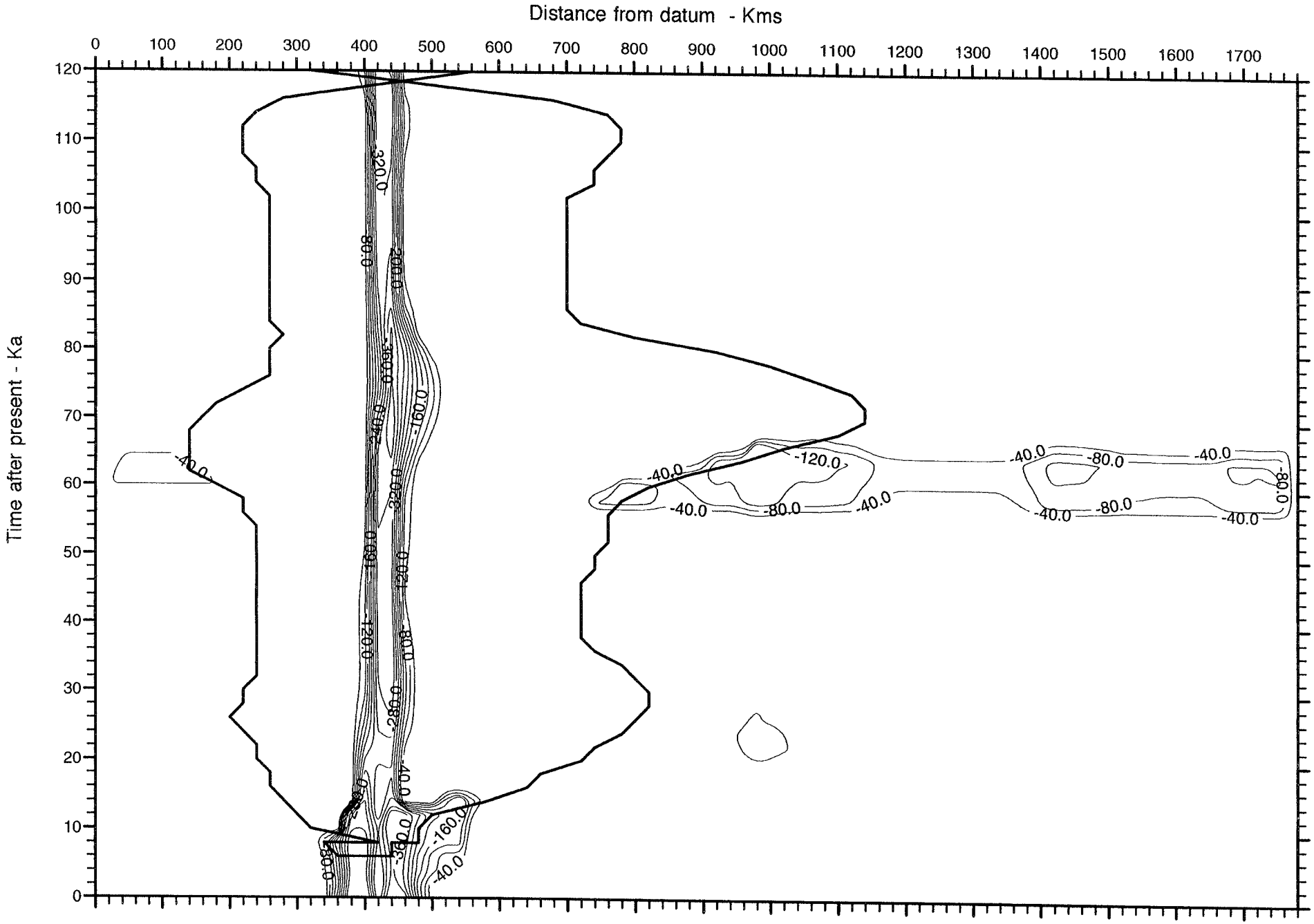

Figure 7.7 As figure 7.6 but for a standard sea level temperature of -5°C.

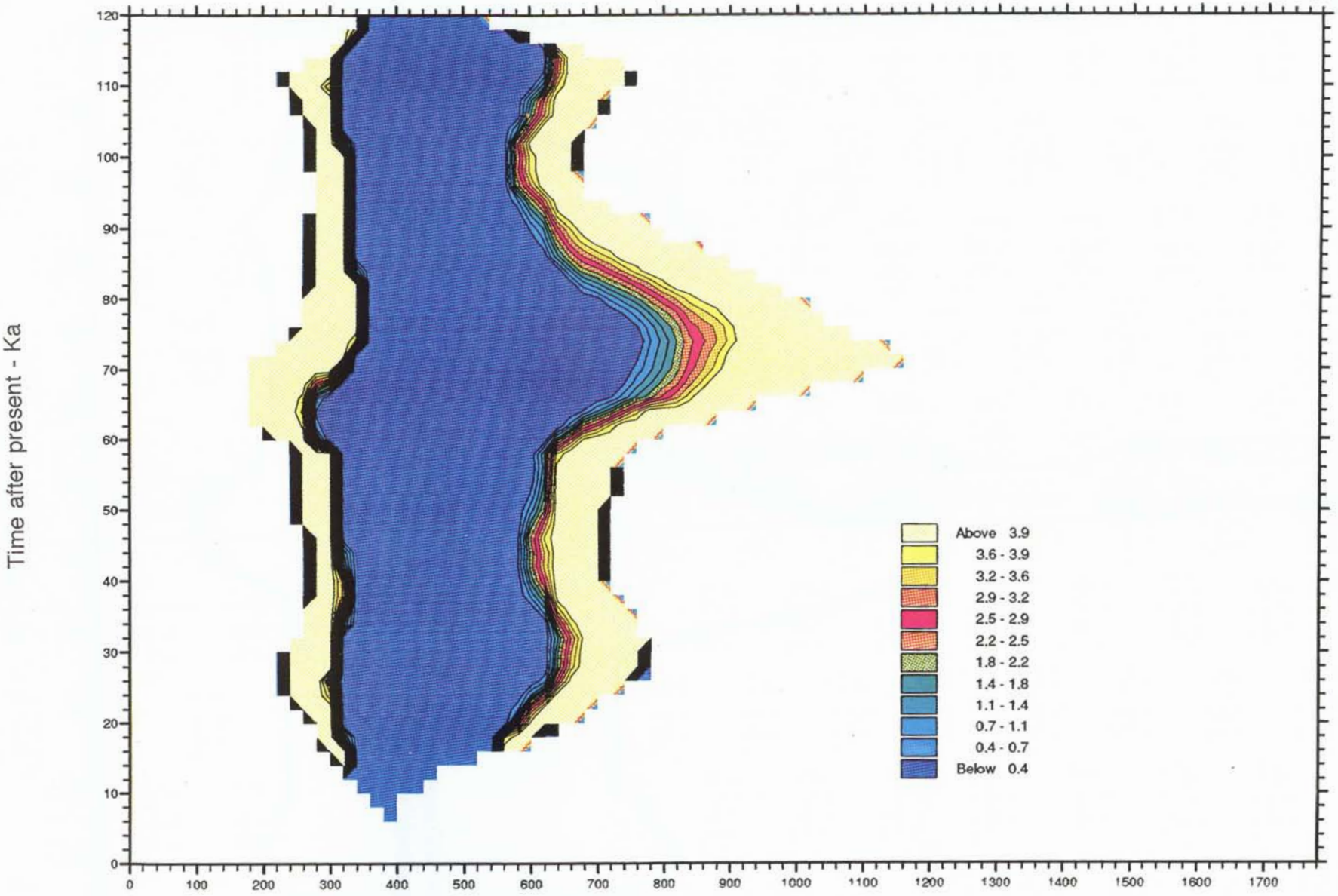

Figure 7.8 Predicted melting rate through time at the base of the ice sheet of the next glacial cycle along the transect.

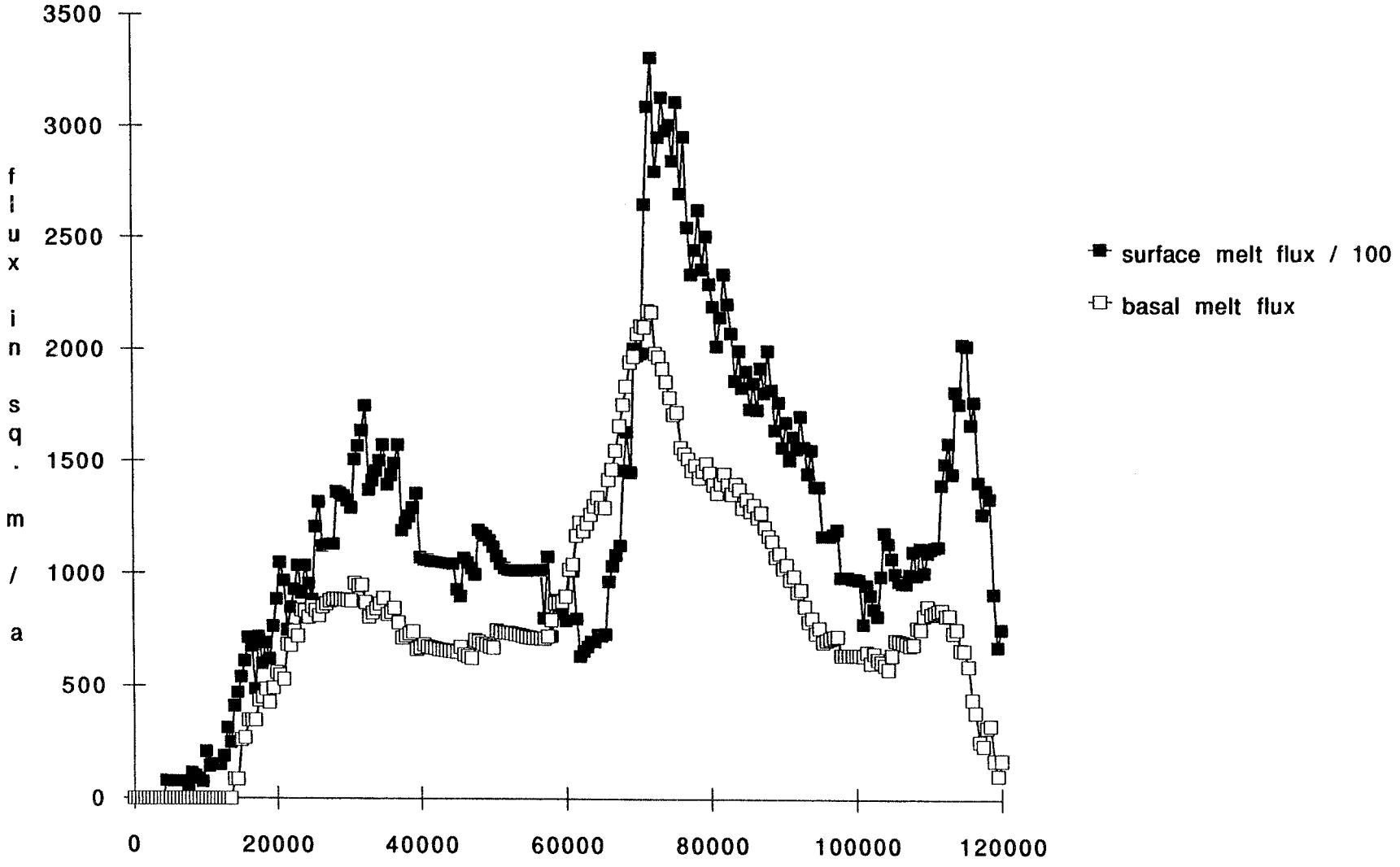

Figure 7.9 Predicted total basal and surface meltwater flux from the ice sheet during the next glacial cycle.

close, and irregularities on the rock bed and valley walls may maintain lee-side cavities, so that surface meltwater may penetrate to greater depths both down valley walls and crevasses.

Subglacial meltwater is however formed continuously, and provided that the groundwater capacity of subglacial beds to absorb water has been exceeded (Boulton and Dobbie, 1993) subglacial meltwater tunnels will form and be relatively permanent.

Figure 7.10 shows the predicted form of a European ice sheet at its maximum extent in about 70,000 years time. This is produced using the central ELA prediction shown in figure 7.1. However there are 2-standard deviation error bars on this prediction. To examine the consequences of this source of uncertainty, we have run a version of the model using the range of ELA predictions shown in figure 7.1. The results are illustrated in figure 7.11, where the probability of the ice sheet reaching a particular distance from the initial ice divide at given times in the future because of uncertainties in ELA prediction is evaluated. It is clear that the ice sheet is very sensitive to relatively small changes in the ELA.

There other sources of uncertainty in modelling exercises such as this, and it is particularly important that they are all evaluated wherever they can be quantified, and scoping calculations are done where only approximate, qualitative indices of uncertainty can be produced.

..... ***** .....

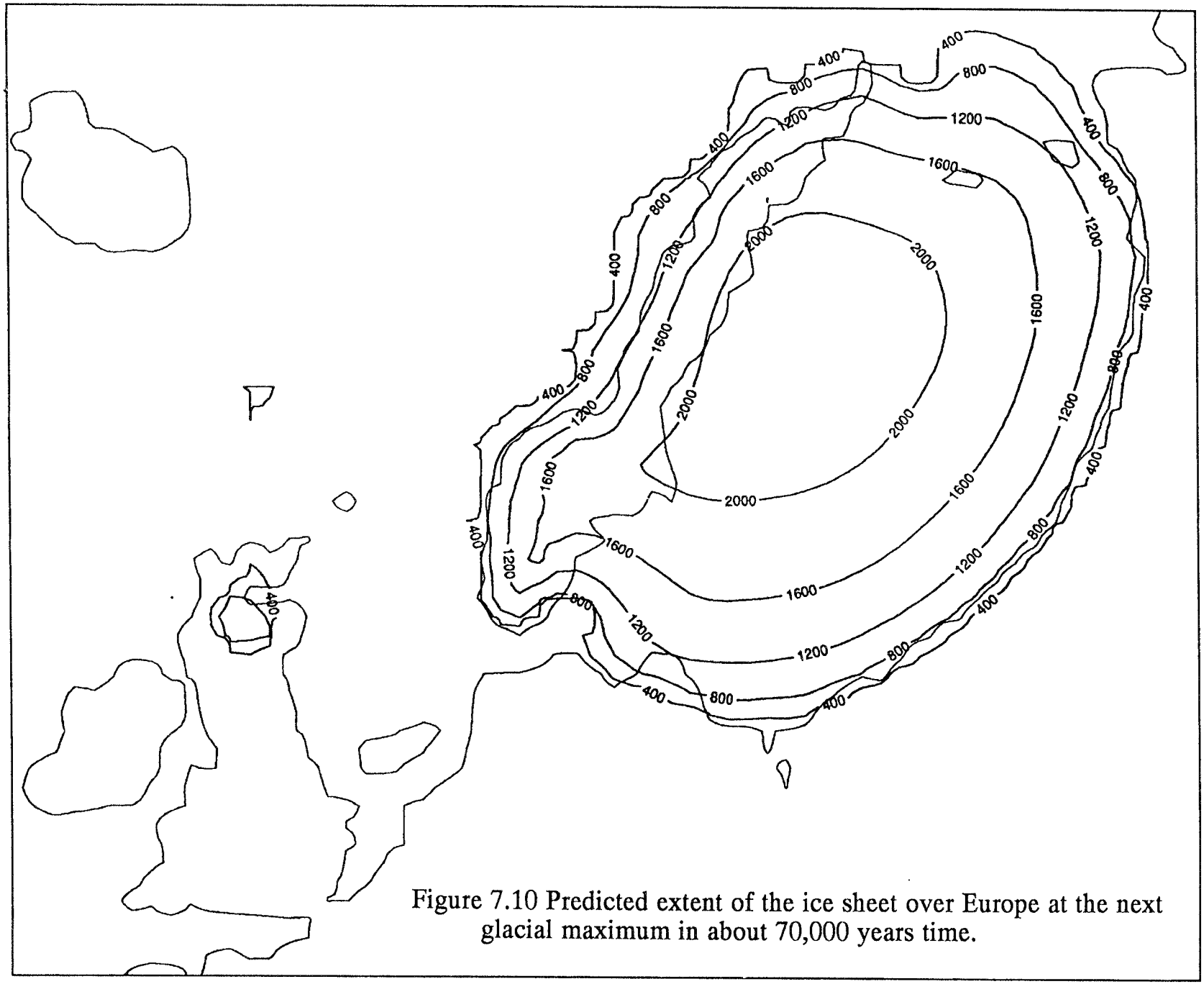

Figure 7.10 Predicted extent of the ice sheet over Europe at the next glacial maximum in about 70,000 years time.

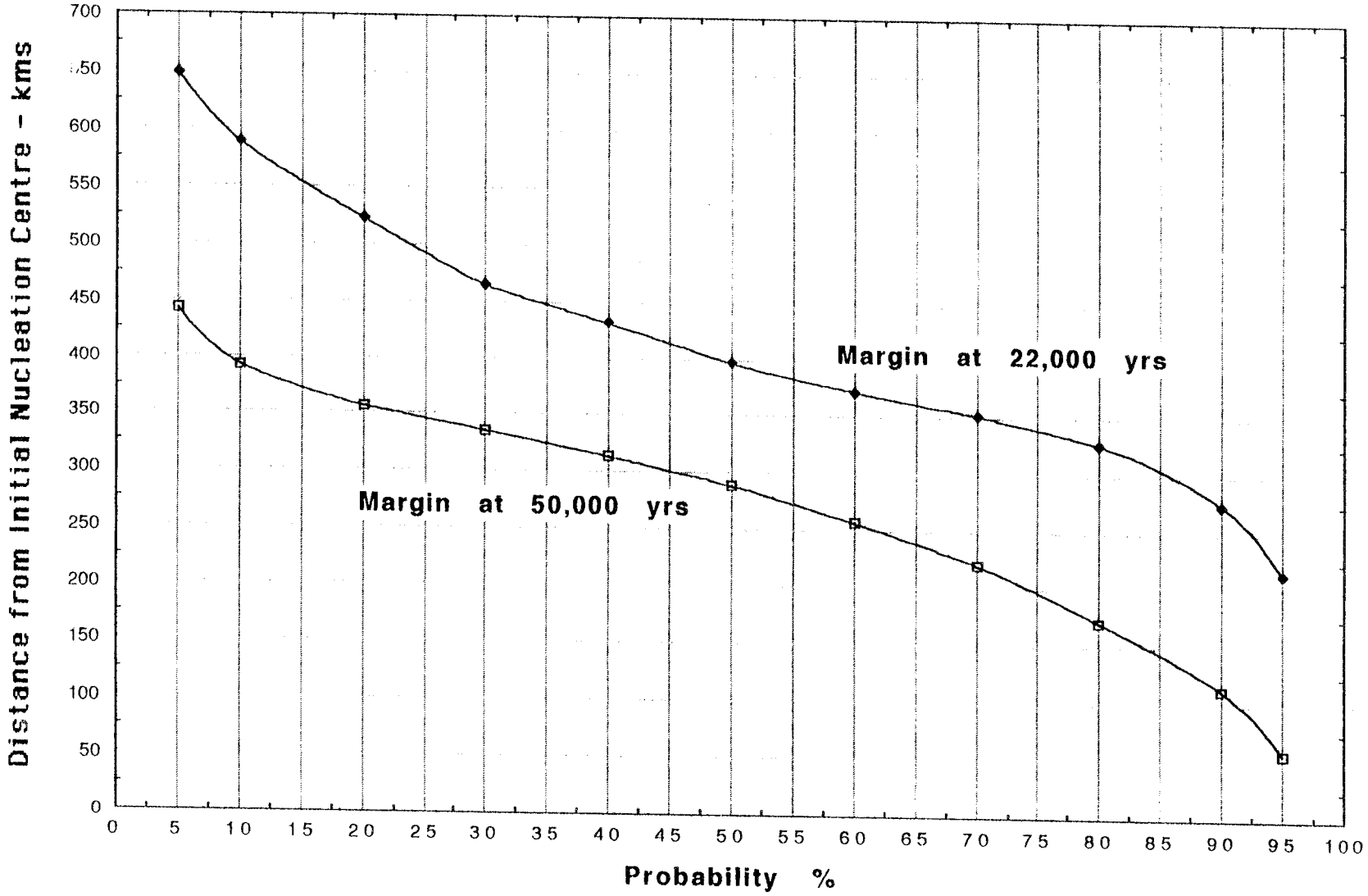

Figure 7.11 The probabilities of future ice sheets reaching given distances from the initial ice divides at 22,000 and 50,000 years in the future.

8 REFERENCES

Alley, R.B. and Whillans, I.M. 1984. Response of the East Antarctic ice sheet to sea-level rise. Journal of Geophysical Research 89, C4, 6487-6493.

Alley, R.B., Blankenship, D.D., Bentley, C.R. and Rooney, S.T. 1987. Till beneath ice stream B. J.of Geophys.Res.92, 8921-8940.

Berger, A. 1978. Long-term variations of caloric insolation resulting from the Earth's orbital elements. Quaternary Research 9, 139-167.

Berger, A., Guiot, J., Kukla, G. and Pestiaux P. 1981. Long term variations of monthly insolation as related to climate change. Geologischen Rundschau Bd. 70(2), 748-758.

Berger, A., Gallée, H., Ficehefet, T. and Tricot, C. 1989. Testing the astronomical theory with a coupled climate-ice sheet model. In. Labeyrie, L. (ed) Glocal & Planetary Change.

Bindschadler, R. 1983. The importance of pressurized subglacial water in separation and sliding at the glacier bed. Journal of Glaciology 29, 3-19.

Boulton G.S. 1987 A theory of drumlin formation by subglacial deformation. In Rose J. and Menzies J. (eds) Drumlins. Balkema, Rotterdam.

Boulton G.S. (in press) A theory of glacier erosion, transport and deposition as a consequence of subglacial sediment deformation.

Boulton G.S. and Dobbie, K. 1993 Consolidation of sediments by glaciers: relations between sediment geotechnics, soft-bed glacier dynamics and subglacial groundwater flow. Journal of Glaciology.

Boulton, G.S. and Hindmarsh, R.C.A. 1987. Sediment deformation beneath glaciers: rheology and geological consequences. Journal of Geophysical Research 92, B9, 059-9082

Boulton, G.S. and Jones, A.S. 1979 Stability of temperate ice caps and ice sheets resting on beds of deformable sediment. Journal of Glaciology 24, 29-43.

Boulton, G.S., Smith, G.D, Jones, A.S. and Newsome, J. 1985. Glacial geology and glaciology of the last mid-latitude ice sheets. Journal of the Geological Society of London 142, 447-474.

Boulton, G.S., Smith, G.D. and Morland, L.W. 1984. The reconstruction of former ice sheets and their mass balance characteristics using a non-linearly viscous flow model. Journal of Glaciology 30, 140-152.

Boulton, G.S., Dongelmans, P., Kelly, R.J. and Pollok, D. 1989. Data and results for TIME4 model of time-dependent environmental processes. Report for Dames and Moore International.

Böse, M. 1990. Reconstruction of ice flow directions south of the Baltic sea during the Weichselian glaciations. Boreas, 19, 217-226.

Braithwaite, R.J. 1981. On glacier energy balance, ablation and air temperature. Journal of Glaciology 27, 381-391.

Budd, W.F. 1970. The longitudinal stress and strain rate gradients in ice masses. Journal of Glaciology 9, 29-48.

Budd, W.F. and Jenssen D. 1975. Numerical modelling of glacier systems.
in Snow and Ice (Proceedings of the Moscow symposium) IASH Publication Number 104, 257-291.

Budd W.F. and Smith, I.N. 1981. The growth and retreat of ice sheets in response to orbital radiation changes. In Sea level, ice and climatic change (Proceedings of the Canberra symposium) IASH Publication Number 131, 369-409.

Budd, W. F., Jenssen, D. and Radok, U. 1971. Derived physical characteristics of the Antarctic ice sheet. ANARE interim reports, 120.

Calder, N. 1974. Arithmetic of ice ages. Nature 252(15), 216-218.

Charlesworth, J.K. 1957. The Quaternary Era.Arnold, London.

Clarke, G.K.C., Nitsan, U. and Paterson, W S.B. 1977. Strain heating and creep instability in glaciers and ice sheets. Reviews of Geophysics and Space Physics 15, 235-247.

Denton, G.H. and Hughes, T.J. 1981. The last great ice sheets. Wiley, New York.

Eismann, L. and Muller, A. 1979. Leitlinien der Quartarentwicklung im Norddeutschen Tiefland. Z. geol. Wiss. Berlin, 7, 57-462.

Ekman, M. 1991. Gravity change, geoid change and remaining postglacial uplift of Fennoscandia. Terra Nova 3, 390-392.

Emiliani, C. and Shackleton, N. 1974. The Bruhnes epoch: isotopic palaeotemperatures and geochronology. Science, 183, 511-514.

Glen, J. W. 1955. The creep of polycrystalline ice. Proceedings of the Royal Society of London, Series A, 228, 519-538.

Guiot, J., Pons, A., Beaulieu, J.L. de and Reille, M. 1989. A 140,000 yr climatic reconstruction from two European pollen records. Nature 338, 309-311.

Haenel, R. (ed) 1980. Atlas of subsurface temperatures in the EC. Publishing Commission of the EC, Luxemburg.

Haltiner, G.J. 1971. Numerical weather prediction. John Wiley and Sons, New York.

Hays, J.D. Imbrie, J. and Shackleton, N. 1976. Variations in the earth's orbit : pacemaker of the ice ages. Science, 194, 1121-1132.

Herterich, K. 1987. On the flow within the transition zone between ice sheet and ice shelf. in van der Veen C.J and Oerlemans J. (eds) Dynamics of the West Antarctic ice sheet, D Reidel, Dordrecht, 85-202.

Hindmarsh, R.C.A., Boulton, G.S. and Hutter, K. 1989. Modes of operation of thermo-mechanically coupled ice sheets. Annals of Glaciology 12, 57-69.

Hirvas, H., and Nenonen, K. 1985. The till stratigraphy of Finland. INQUA Till Symposium, Finland 1985. Geological Survey of Finland, Special Paper 3. 49-63.

Huybrechts, P. 1986. A three-dimensional time-dependent numerical model for polar ice sheets: some basic testing with a stable and efficient finite difference scheme. Report 86-1, Vrije Universiteit, Belgium.

Huybrechts, P. and Oerlemans, H. 1988. Evolution of the East Antarctic ice sheet: a numerical study of thermo-mechanical response patterns with changing climate. Annals of Glaciology 11, 52-59.

Imbrie, J. and Imbrie, J.Z. 1980. Modelling the climatic response to orbital variations. Science 207, 943-953.

Imbrie, J. et al. 1984. The orbital theory of Pleistocene climate: support from a revised chronology of the marine $\delta^{18}O$ frecord. In Berger, A., et al (eds). Milankovitch & Climate, Reidel, Dordrecht.

Jenssen, D, . 1977. A three-dimensional polar ice-sheet model. Journal of Glaciology 18, 373-389.

Kelly, R.J., Morland, L.W. and Boulton, G.S. 1990. Deep penetration of permafrost through saturated ground. Cold Regions Science and Technology 18, 9-27.

Kleman, J. 1990. On the use of glacial striae for reconstruction of palaeo-ice sheet flow patterns. Geogr. Ann. 72A 217-236.

Kukla, G., Berger, A., Lotti, R. and Brown, J.P. 1981. Orbital signature of interglacials. Nature 290, 295-300.

Labeyrie, L.D., Duplessy, J.C., and Blanc P.L. 1988. Norwegian deep sea water variations over the last climatic cycle. In Wanner H. and Siegenthaler U.

(eds) Lecture Notes in Earth Science 16, 83-113. Springer Verlag, New York.

Labeyrie, L.D., Duplessy, J.C., and Blanc P.L. 1987. Variations in mode of formation and temperature of oceanic deep waters over the past 125,000 years. Nature, 327, 477-482.

Lagerbäck, R. 1988. The Veiki moraines in northern Sweden - widesparead evidence of an early Weichselian deglaciation. Boreas, 17, 469-486.

Lambeck K., Johnston, P. and Nakada M. 1990. Holocene glacial rebound and sea level in NW Europe. Geophys. J. Int. 103, 451-468.

Lehman, S.J., Jones, G.A., Keigwin, L.D., Anderson, E.S, Butenko, G. and Ostmo, S.-R. 1991. Initiation of Fennoscandian ice-sheet retreat during the last deglaciation. Nature 349, 513-516

Lliboutry, L. A. 1987. Very slow flow of solids. Martinus Nijhoff Publishers, Dordrecht.

Lundqvist, J. 1981. Weichselian in Sweden before 15,000 B.P., Boreas 10, 395-402.

Lundqvist, J. 1986. Late Weichselian glaciation and deglaciation in Scandinavia. In Sibrava, V. (ed) Quaternary glaciations in the northern hemisphere. Quat. Sci. Revs 5, 269-292.

Mahaffy, M. A. W. 1976. A numerical three dimensional ice flow model. Journal of Geophysical Research 81, 1059-1666.

Mangerud, J. 1981. The Early and Middle Weichselian in Norway: a review. Boreas 10, 381-393.

Mangerud, J. 1991. The Scandinavian ice sheet through the last interglacial/glacial cycle. In. Frenzel, B. (ed). Klimageschichtliche Probleme der Letzten 130,000 fahre. G. Fischer, Stuttgart. 307-330.

Mélice, J. L. and Berger, A. 1989. Modele de prévision statistique du type Box-Jenkins pour la prévision du climat des 10,000 prochaines annees. Scientific Report of the Institut d'Astronomie et de Geophysique . G. Lemaitre, Université Catholique de Louvain-la-Neuve, Belgium.

Milankovitch, M. 1941. Canon of insolation and the ice age problem. K. Serb. Acad. Beorg. Spec. Publ. 132.

Morland, L. W., Smith, G. and Boulton, G. S. 198

Mörner, N-A. 1971. Eustatic changes during the last 20,000 years and a method of separating the isostatic and eustatic factors in an uplifted area. Palaeogeography, Palaeoclimatology, Palaeoecology 9, 153-181.

Muszynski, I. and Birchfield, G.E. 1987. A coupled marine ice-stream - ice-shelf model. Journal of Glaciology 33,3-15.

Nye, J. F. 1959. The motion of ice sheet and glaciers. Journal of Glaciology 3, 493-507.

Oerlemans, J. 1981. Modelling of Pleistocene European ice sheets: some experiments with simple mass-balance parameterizations. Quaternary Research 15, 77-85.

Oerlemans, J. and van der Veen, C.J 1984. Ice sheets and climate. D. Reidel Publishing Company, Dordrecht.

Orvig, S. (ed) 1970. Climates of the polar regions. World Survey of Climatology Volume 14, Elsevier Publishing Company, Amsterdam.

Patankar, S.V. 1980. Numerical heat transfer and fluid flow. Hemisphere Publishing Corporation, Washington.

Paterson, W.S.B. 1981. The physics of glaciers. Pergamon Press Limited, Oxford.

Paterson, W.S.B. and Budd, W.F. 1982. Flow parameters for ice sheet modelling. Cold Regions Science and Technology 6, 175-17

Petersen, E.L. and Larsen, S.E. 1978. A statistical study of a composite palaeotemperature series from the last 700,000 years. Tellus 30, 193-200.

Press, W.H., Flannery, B.P., Teukolsky, S.A. and Vetterling, W.T. 1989. Numerical recipes. Cambridge University Press, Cambridge.

Punkari, M. 1982. Glacial gheomorphology and dynamics in the eastern part of the Baltic Shield interpreted using Landsat imagery. The Photogrammetric Journal of Finland 9, 77-93.

Punkari, M. 1985. Glacial geomorphology and dynamics in Soviet Karelia interpreted by means of satellite imagery. Fennia, 163, 113-153.

Ritz, C. 1987. Time dependent boundary conditions for the calculation of temperature fields in ice sheets. in Waddington E. (ed) The physical basis of ice sheet modelling IASH Publication number 170, 207-216.

Ruddiman, W.F., Shackleton, N.J. and McIntyre, A. 1986. North Atlantic sea-surface temperatures for the last 1.1 million years. In Summerhayes, C.P. and Shackleton, N.J. North Atlantic Palaeoceanography, Geological Society Special Publication 21, 155-173.

Smith, G.D. 1985. Numerical solution of partial differential equations: finite difference methods. Oxford University Press, Oxford.

Sugden, D. E. 1977. Reconstruction of the morphology, dynamics and thermal characteristics of the Laurentide ice sheet at its maximum. Arctic and Alpine Research 9, 21-47.

Turcotte, D. L. and Schubert, G. 1982. Geodynamics: applications of continuum physics in geological problems. John Wiley and Sons Incorporated, Toronto.

Uscinowicz, S., Kramarska,R. and Przezdziecki P. 1988. The Quaternary of the south west area of the Polish Baltic.In The Baltic Sea.Geological Survey of Finland Special Paper 6, 31-37.

van der Veen, C.J. 1987. The West Antarctic ice sheet: he need to understand its dynamics. In van der Veen, C.J. and Oerleman, J. (eds) Dynamics of the West Antarctic ice sheet, D Reidel, Dordrecht, 1-16.

Vernaker, A.E. 1968. Long-period global variations of incoming solar radiation. In Research on the Theory of Climate. Travelers Research Center, Hartford, Conn.

Vernaker, A.D.1972. Long-period global variations of incoming solar radiation. Meteorological Monograph 12(34), 130pp.

Walcott, R.I. 1970. Flexural rigidity, thickness and viscosity of the lithosphere. Journal of Geophysical Research 75, 3941-3954.

Wallen, C.C (ed) 1970. Climates of northern and western Europe. World Survey of Climatology Volume 5, Elsevier Publishing Company, Amsterdam.

Weertman, J. 1979. The unsolved general glacier sliding problem. Journal of Glaciology 23, 97-115.

9. APPENDIX

Table 2.1 Symbols and abbreviations used in the text.

Symbol	Meaning (unit)	Type	Value
H	ice thickness (m)	variable	
h	bedrock elevation (m)	variable	
b	mass balance (m s^{-1})	variable	
u	horizontal velocity (m s^{-1})	variable	
$\bar{u}$	vertically averaged horizontal velocity (m s^{-1})	variable	
w	vertical velocity (m s^{-1})	variable	
w_h	vertical velocity at bed (m s^{-1})	variable	
D	ice sheet flow diffusivity (m^2 s^{-1})	variable	
A	proportionality factor in Glen's flow law (Pa^{-n} s^{-1})	variable	
T	ice= temperature (^oC)	variable	
T^*	ice temperature corrected for variation in the pressure melting point (^oC)	variable	
T_a	air temperature (^oC)	variable	
T_r	rock temperature (^oC)	variable	
S	basal melt rate (m s^{-1})	variable	
ELA	equilibrium line altitude (m)	variable	
SLAT	sea level air temperature (^oC)	forcing	
SST	Sea surface temperature (Rockall trough) (^oC)	forcing	
t	time (years)	dimension	
x	horizontal distance (m)	dimension	
z	vertical distance (m)	dimension	
x	scaled vertical coordinate	scaling	
u_h	horizontal velocity at bed (m $year^{-1}$)	constant	0.00
g	gravity (m s^{-2})	constant	9.81
n	power in Glen's flow law	constant	3.00
Q	activation energy for ice creep (J mol^{-1})	constant	$60x10^3$/ $139x10^3$
R	gas constant (J mol^{-1} $^oC^{-1}$)	constant	8.314
a	a multiplier used in the Arrhenius relation (Pa^{-n} m^{-1})	constant	$7.23x10^{-12}$/ $3.47x10^4$

ρ_i	density of ice (kg m^{-3})	constant	910.0
ρ_m	density of rock (kg m^{-3})	constant	3300.0
c_i	specific heat capacity of ice (J kg^{-1} $^oC^{-1}$)	constant	2009.0
c_r	specific heat capacity of rock (J kg^{-1} $^oC^{-1}$)	constant	1000.0
k_i	thermal conductivity of ice (W m^{-1} $^oC^{-1}$)	constant	2.10
k_r	thermal conductivity of rock (W m^{-1} $^oC^{-1}$)	constant	3.30
L	latent heat capacity of ice (J kg^{-1})	constant	$335x10^3$
G	geothermal heat flux (W m^{-2})	constant	$4.2x10^{-2}$
ϕ	multiplier used in the pressure melting point equation (^oC Pa^{-1})	constant	$9.8x10^{-8}$
D_a	diffusivity of the asthenosphere (m^2 s^{-1})	constant	3.17
ψ	lapse rate (^oC m^{-1})	constant	0.010
a	multiplier used in mass balance equation (s^{-1})	constant	$2.321x10^{-11}$
b	multiplier used in mass balance equation (m^{-1} s^{-1})	constant	$8.498x10^{-15}$
b_{max}	maximum allowed positive mass balance (m s^{-1})	constant	$1.58x10^{-8}$
f_1	multiplier used in equilibrium line depression equation (m $^oC^{-1}$)	constant	88.40
f_2	intercept used in sea level air temperature equation (^oC)	constant	6.000
f_3	multiplier used in sea level air temperature equation	constant	1.222 / 1.777
h_o	relaxed bedrock elevation (m)	constant	
F	a function dependent on x, z, and t		

List of SKB reports

Annual Reports

1977-78
TR 121
KBS Technical Reports 1 – 120
Summaries
Stockholm, May 1979

1979
TR 79-28
The KBS Annual Report 1979
KBS Technical Reports 79-01 – 79-27
Summaries
Stockholm, March 1980

1980
TR 80-26
The KBS Annual Report 1980
KBS Technical Reports 80-01 – 80-25
Summaries
Stockholm, March 1981

1981
TR 81-17
The KBS Annual Report 1981
KBS Technical Reports 81-01 – 81-16
Summaries
Stockholm, April 1982

1982
TR 82-28
The KBS Annual Report 1982
KBS Technical Reports 82-01 – 82-27
Summaries
Stockholm, July 1983

1983
TR 83-77
The KBS Annual Report 1983
KBS Technical Reports 83-01 – 83-76
Summaries
Stockholm, June 1984

1984
TR 85-01
Annual Research and Development Report 1984
Including Summaries of Technical Reports Issued during 1984. (Technical Reports 84-01 – 84-19)
Stockholm, June 1985

1985
TR 85-20
Annual Research and Development Report 1985
Including Summaries of Technical Reports Issued during 1985. (Technical Reports 85-01 – 85-19)
Stockholm, May 1986

1986
TR 86-31
SKB Annual Report 1986
Including Summaries of Technical Reports Issued during 1986
Stockholm, May 1987

1987
TR 87-33
SKB Annual Report 1987
Including Summaries of Technical Reports Issued during 1987
Stockholm, May 1988

1988
TR 88-32
SKB Annual Report 1988
Including Summaries of Technical Reports Issued during 1988
Stockholm, May 1989

1989
TR 89-40
SKB Annual Report 1989
Including Summaries of Technical Reports Issued during 1989
Stockholm, May 1990

1990
TR 90-46
SKB Annual Report 1990
Including Summaries of Technical Reports Issued during 1990
Stockholm, May 1991

1991
TR 91-64
SKB Annual Report 1991
Including Summaries of Technical Reports Issued during 1991
Stockholm, April 1992

1992
TR 92-46
SKB Annual Report 1992
Including Summaries of Technical Reports Issued during 1992
Stockholm, May 1993

Technical Reports
List of SKB Technical Reports 1993

TR 93-01
Stress redistribution and void growth in butt-welded canisters for spent nuclear fuel
B L Josefson[1], L Karlsson[2], H-Å Häggblad[2]
[1] Division of Solid Mechanics, Chalmers University of Technology, Göteborg, Sweden
[2] Division of Computer Aided Design, Luleå University of Technology, Luleå, Sweden
February 1993

TR 93-02
Hydrothermal field test with French candidate clay embedding steel heater in the Stripa mine
R Pusch[1], O Karnland[1], A Lajudie[2], J Lechelle[2], A Bouchet[3]
[1] Clay Technology AB, Sweden
[2] CEA, France
[3] Etude Recherche Materiaux (ERM), France
December 1992

TR 93-03
MX 80 clay exposed to high temperatures and gamma radiation
R Pusch[1], O Karnland[1], A Lajudie[2], A Decarreau[3],
[1] Clay Technology AB, Sweden
[2] CEA, France
[3] Univ. de Poitiers, France
December 1992

TR 93-04
Project on Alternative Systems Study (PASS).
Final report
October 1992

TR 93-05
Studies of natural analogues and geological systems.
Their importance to performance assessment
Fredrik Brandberg[1], Bertil Grundfelt[1], Lars Olof Höglund[1], Fred Karlsson[2], Kristina Skagius[1], John Smellie[3]
[1] KEMAKTA Konsult AB
[2] SKB
[3] Conterra AB
April 1993

TR 93-06
Mineralogy, geochemistry and petrophysics of red coloured granite adjacent to fractures
Thomas Eliasson
Chalmers University of Technology and University of Göteborg, Department of Geology, Göteborg, Sweden
March 1993

TR 93-07
Modelling the redox front movement in a KBS-3 nuclear waste repository
L Romero, L Moreno, I Neretnieks
Department of Chemical Engineering,
Royal Institute of Technology, Stockholm, Sweden
May 1993

TR 93-08
Äspö Hard Rock Laboratory
Annual Report 1992
SKB
April 1993

TR 93-09
Verification of the geostatistical inference code INFERENS, Version 1.1, and demonstration using data from Finnsjön
Joel Geier
Golder Geosystem AB, Uppsala
June 1993

TR 93-10
Mechanisms and consequences of creep in the nearfield rock of a KBS-3 repository
Roland Pusch, Harald Hökmark
Clay Technology AB, Lund, Sweden
December 1992

TR 93-11
Post-glacial faulting in the Lansjärv area, Northern Sweden.
Comments from the expert group on a field visit at the Molberget post-glacial fault area, 1991
Roy Stanfors (ed.)[1], Lars O Ericsson (ed.)[2]
[1] R S Consulting AB
[2] SKB
May 1993

TR 93-12
Possible strategies for geoscientific classification for high-level waste repository site selection
Lars Rosén, Gunnar Gustafson
Department of Geology, Chalmers University of Technology and University of Göteborg
June 1993

TR 93-13
A review of the seismotectonics of Sweden
Robert Muir Wood
EQE International Ltd, Warrington, Cheshire, England
April 1993